

# **Evaluation of Novel Strategies to Address the Challenges of Precision Dosing for Small Molecule Kinase Inhibitors**

by

**Madelé van Dyk**

*Thesis  
Submitted to Flinders University  
for the degree of*

**Doctor of Philosophy**

College of Medicine & Public Health

9 August 2018

---

---

# TABLE OF CONTENTS

---

<b>AWARDS.....</b>	<b>14</b>
<b>PEER REVIEWED JOURNAL MANUSCRIPTS.....</b>	<b>14</b>
<b>MANUSCRIPTS UNDER CONSIDERATION.....</b>	<b>15</b>
<b>PEER REVIEWED CONFERENCE ABSTRACTS.....</b>	<b>16</b>
<b>1.1 PUBLIC SIGNIFICANCE OF CANCER.....</b>	<b>23</b>
<b>1.2 CANCER HALLMARK CHARACTERISTICS.....</b>	<b>23</b>
1.2.1 Sustaining Proliferative Signalling .....	24
1.2.2 Evading Growth Suppressors .....	24
1.2.3 Resisting Cell Death.....	25
1.2.4 Enabling Replicative Immortality .....	26
1.2.5 Inducing Angiogenesis .....	27
1.2.6 Activating Invasion and Metastasis .....	28
1.2.7 Genome Instability and Mutation.....	30
1.2.8 Tumour Promoting Inflammation.....	31
1.2.9 Reprogramming Energy Metabolism.....	31
1.2.10 Evading Immune Destruction .....	32
<b>1.3 TARGETED THERAPIES AND PRECISION MEDICINE.....</b>	<b>33</b>
<b>1.4 SMALL MOLECULE KINASE INHIBITORS .....</b>	<b>35</b>
1.4.1 BCR-ABL Inhibitors.....	38

1.4.2	EGFR Inhibitors .....	39
1.4.3	VEGF Inhibitors .....	41
1.4.4	BRAF / MEK Inhibitors .....	41
1.4.5	Other Kinase Inhibitors.....	41
	Reference.....	58
<b>1.5</b>	<b>PHARMACOKINETICS .....</b>	<b>64</b>
1.5.1	Absorption and Distribution.....	64
1.5.2	Metabolism and Elimination.....	65
1.5.3	Inter-Individual Variability in Absorption.....	66
1.5.4	Inter-Individual Variability in Metabolism and Elimination .....	67
<b>1.6</b>	<b>ADDRESSING INTER-INDIVIDUAL VARIABILITY IN EXPOSURE.....</b>	<b>68</b>
1.6.1	Therapeutic Drug Monitoring .....	69
1.6.2	Other existing strategies .....	73
<b>1.7</b>	<b>HYPOTHESIS AND AIMS .....</b>	<b>79</b>
<b>2.1</b>	<b>INTRODUCTION .....</b>	<b>82</b>
<b>2.2</b>	<b>METHODS .....</b>	<b>84</b>
2.2.1	Chemicals and Reagents.....	84
2.2.2	Enzyme and Substrate Preparations.....	84
2.2.3	Quantification of Substrate Depletion.....	85
2.2.4	Data Analysis .....	85
2.2.5	PBPK Structural Model.....	86

2.2.6 PBPK Population Profile .....	86
2.2.7 PBPK Compound Profiles.....	87
2.2.8 Assessing the Effect of Various Covariates on Exposure .....	91
<b>2.3 RESULTS .....</b>	<b>91</b>
2.3.1 Substrate Depletion by HLM.....	91
2.3.2 Validation of EGFR KI Profiles.....	94
2.3.3 Impact of Covariates on Simulated EGFR KI Exposure .....	95
2.3.4 Application to Optimised EGFR KI Dosing.....	96
<b>2.4 DISCUSSION.....</b>	<b>98</b>
<b>2.5 CONCLUSION.....</b>	<b>102</b>
<b>3.1 INTRODUCTION .....</b>	<b>104</b>
<b>3.2 METHODS .....</b>	<b>105</b>
3.2.1 Study Protocol.....	105
3.2.2 Study Cohort and Medications .....	106
3.2.3 Study Design.....	107
3.2.4 Sample Preparation.....	107
3.2.5 Sample Analysis .....	107
3.2.6 CYP3A Genotype .....	109
3.2.7 Data Analysis .....	109
<b>3.3 RESULTS .....</b>	<b>110</b>
3.3.1 Trial Conduct.....	110
3.3.2 Covariate Assessment.....	111

3.3.3 Baseline CYP3A4 activity in Caucasians and South Asians .....	112
3.3.4 CYP3A4 Inducibility and Inhibition Potential in Caucasians and South Asians.	112
3.4 DISCUSSION.....	117
3.5 CONCLUSION.....	119
4.1 INTRODUCTION .....	121
4.2 MATERIALS AND METHODS.....	122
4.2.1 Study Protocol.....	122
4.2.2 Midazolam Concentrations .....	123
4.2.3 Caffeine Metabolomics.....	123
4.2.4 Caffeine and 1,3,7-trimethyluric Acid Concentrations .....	124
4.2.5 Data and Statistical Analysis.....	124
4.3 RESULTS .....	125
4.3.1 Caffeine Metabolomics.....	125
4.3.2 Study Conduct.....	126
4.3.3 Midazolam Exposure .....	126
4.3.4 Caffeine and TMU Exposure .....	127
4.3.5 Prediction of CYP3A4 Activity Using Caffeine/TMU Ratios.....	129
4.3.6 Impact of Race on Caffeine/TMU Ratio .....	132
4.4 DISCUSSION.....	134
4.5 CONCLUSION.....	137
5.1 INTRODUCTION .....	139
5.2 METHODS AND MATERIALS.....	142

5.2.1 Chemicals and Reagents.....	142
5.2.2 Sample Collection and Preparation .....	142
5.2.3 Chromatography .....	143
5.2.4 Mass Spectrometry.....	144
5.2.5 Calibration .....	145
5.2.6 Method Validation .....	148
<b>5.3. RESULTS.....</b>	<b>155</b>
5.3.1 Sample Collection and Preparation .....	155
5.3.2 Analyte Separation, Detection and Quantification .....	155
5.3.3 Calibration and Validation .....	159
5.3.4 Application to Clinical Trial Samples .....	161
<b>5.4. DISCUSSION.....</b>	<b>164</b>
<b>5.5. CONCLUSION.....</b>	<b>166</b>
<b>6.1 INTRODUCTION .....</b>	<b>168</b>
<b>6.2 METHODS .....</b>	<b>170</b>
6.2.1 Application 1: Identification of physiological and molecular characteristics driving between subject variability in dabrafenib exposure .....	170
6.2.2 Application 2: Use of KI TDM in a ‘real world’ Cohort.....	177
<b>6.3 RESULTS .....</b>	<b>178</b>
6.3.1 Application 1: Identification of physiological and molecular characteristics driving between subject variability in dabrafenib exposure .....	178
6.3.2 Application 2: TDM Patient Population .....	182

<b>6.3.3 Plasma Concentrations.....</b>	<b>184</b>
<b>6.3.4 Therapeutic Drug Monitoring Case Study.....</b>	<b>187</b>
<b>6.4 DISCUSSION.....</b>	<b>189</b>
<b>Appendix 1 – Appendix Table 1 .....</b>	<b>215</b>
<b>Appendix 2 – Rowland A, van Dyk M, et al. <i>Exp Opin Drug Metab Toxicol</i>, 2017, 13: 31-49. ....</b>	<b>Error! Bookmark not defined.</b>
<b>Appendix 3 – van Dyk M, Rowland A. <i>Trans Cancer Res</i>, 2017, 10: 1600-1615.....</b>	<b>Error!</b>
Bookmark not defined.	
<b>Appendix 4 – van Dyk M, et al. <i>Eur J Clin Pharmacol</i>, 2018, 10.1007/s00228-018-2450-4 .....</b>	<b>Error! Bookmark not defined.</b>
<b>Appendix 5 – van Dyk M, et al. <i>J Chroma B</i>, 2016, 1033, 17-25.</b>	<b>Error! Bookmark not defined.</b>
Bookmark not defined.	
<b>Appendix 6 – Rowland A, van Dyk, M, et al. <i>Clin Pharmacol Ther</i>, Accepted 20 Mar 2018 .....</b>	<b>Error! Bookmark not defined.</b>

---

# LIST OF FIGURES

---

Figure 1.1: Therapeutic Targeting of the Hallmarks of Cancer. ....	28
Figure 1.2: Decision tree demonstrating the core aspects of precision oncology and the strategies and tools that underpin these core aspects. ....	34
Figure 1.3: Approved KIs and related target cancers. ....	36
Figure 1.4: Inactive tyrosine kinase (TK) receptor on the left with an activated TK receptor on the right where dimerization took place after ligand binding. ....	38
Figure 1.5: Common mutations found in the EGFR kinase domain in NSCLC. ....	40
Figure 2.1: EGFR KI substrate depletion in the absence and presence of appropriate cofactors and CYP3cide. ....	92
Figure 2.2: Pie charts depicting the contribution of CYP3A4, other CYP and UGT to <i>in vitro</i> EGFR KI metabolism. ....	93
Figure 2.3: Representative concentration-time profile depicting simulated afatinib exposure (solid line), and observed mean and 95% CI afatinib exposure (dotted lines). ....	94
Figure 2.4: Simulated mean and 95% CI concentration time profiles describing exposure to gefitinib (250 mg QD) when dosed for 14 days in cancer patients (n=1,000). ....	96
Figure 3.1: Mean midazolam concentration-time curves for Caucasian (n=19) and South Asian (n=11) cohorts. ....	111
Figure 3.2: Spaghetti plot showing changes in AUC from baseline, following rifampicin and clarithromycin dosing. Panel A; Caucasians, Panel B; South Asians. Dotted lines represent individual participant data, while the solid line represent the cohort means. ....	116
Figure 4.1: Correlation between baseline (blue) and post induction (green) midazolam AUC and caffeine/TMU ratio. ....	130

Figure 4.2: Bland Altman plots for the measurement of CYP3A4 activity by midazolam AUC and caffeine/TMU ratio at 3, 4, and 6 hr post dosing on Day 1 and Day 8.....	131
Figure 5.1: Chemical characteristics for KIs relevant to their detection by mass spectrometry.....	141
Figure 5.2: Representative pooled spiked plasma (100 µg/L) chromatogram (quadrupole acquiring data between m/z 250 and 750).....	157
Figure 5.3: Representative chromatogram for a patient taking a standard combination dose of dabrafenib (150mg BD) and trametinib (2mg OD). ....	162
Figure 5.4: Representative chromatogram for a patient taking a standard dose of sunitinib on a 4 week on and 2 weeks off cycle.....	163
Figure 6.1: Representative [GSK trial ID: 11346] overlay showing the simulated and observed (95% observed range) plasma concentration time curves (0 to 24 hours) for dabrafenib following a single 150 mg oral dose. ....	173
Figure 6.2: Representative [GSK trial ID: 113771 Part D] overlay showing the simulated and observed (95% observed range) plasma concentration time curves (408 to 432 hours) for dabrafenib when dosed for 14 days (150 mg BD). ....	174
Figure 6.4: Computed tomography (CT) scan showing primary tumour.....	187

---

# LIST OF TABLES

---

Table 1.1: Overview of kinase inhibitor pharmacology .....	42
Table 1.2: Summary of kinase inhibitor physiochemical properties.....	45
Table 1.3: Summary of kinase inhibitor pharmacokinetics.....	54
Table 1.4: Metabolic enzymes and transporters involved in kinase inhibitor disposition.....	58
Table 1.5: Kinase inhibitor pharmacokinetics associated with superior clinical outcomes.....	72
Table 2.1: Substrate and inhibitor parameter values used for KI substrate profile .....	88
Table 2.2: Comparison of geometric mean ( $\pm$ 95 % CI) simulated pharmacokinetic parameters with those observed in clinical studies.....	89
Table 2.3: Comparison of mean simulated AUC and $C_{max}$ ratios with those observed in clinical studies.....	90
Table 2.4: Impact of covariates on mean simulated EGFR KI exposure.....	97
Table 3.1: Participant characteristics.....	106
Table 3.2: Pharmacokinetic parameters describing midazolam exposure.....	114
Table 3.3: Coefficients defining differences in midazolam exposure between Caucasian and South Asian healthy males .....	115
Table 4.1: Midazolam AUC and $C_{max}$ values at baseline and following rifampin induction .....	127
Table 4.2: Caffeine/TMU ratios at baseline and following rifampin induction .....	127
Table 4.3: Bias in CYP3A activity measured by the caffeine/TMU ratio and midazolam AUC.....	128
Table 4.4: Impact of ethnicity on the caffeine/TMU ratio and midazolam AUC. ....	132
Table 5.1: Mass spectrometer instrument settings.....	144
Table 5.2: Analyte quantification characteristics.....	146
Table 5.3: Assay precision and recovery.....	150

Table 5.4: Assay accuracy.....	152
Table 6.1: Input parameters for the dabrafenib compound file. ....	171
Table 6.2: Characteristics describing the core simulated cancer patient cohort (n = 1,000).....	175
Table 6.3: Univariate logistic regression analysis of physiological and molecular characteristic associated with a dabrafenib C <sub>ss_trough</sub> > 48 mg/mL .....	178
Figure 6.3: Receiver operating characteristic curves demonstrating multivariate model performance in the training set (Panel A) and verification sets (Panel B and C).....	181
Table 6.4: Participant demographics by drug.....	183
Table 6.5: Variability in KI exposure relative to target concentration .....	186

---

# DECLARATION

---

I certify that this thesis does not incorporate without acknowledgment any material previously submitted for a degree or diploma in any university and that to the best of my knowledge and belief, it does not contain any material previously published or written by another person except where due reference is made in the text.

Maldele van Dyk

March 2018

---

# ACKNOWLEDGEMENTS

---

I would like to express my sincere gratitude to my principle supervisor, Dr Andrew Rowland, for his continuous guidance and mentorship throughout the journey of my PhD studies. I thank him for always encouraging me to use my own initiative and develop my own ideas but still steer me in the right direction. His friendship, patience, immense knowledge and the expertise he has shared with me will always be appreciated.

I thank my co-supervisors, Professor John Miners, Professor Ross McKinnon, Professor Michael Sorich and Dr Ganessan Kichenadasse for their valuable assistance and advice, Ms Heather Bailey and Ms Karli Goodwin for their clerical and friendly support, and the past and present staff and students of the Department of Clinical Pharmacology, Flinders University for their friendship and support. I would also like to thank the co-authors of the manuscripts that resulted from this thesis for their valuable advice and contributions.

Finally, I would like to thank my Father who always taught me to aim high and to give everything I attempt a 100% and my Mother who encouraged me to follow my passion and dreams with an ambitious and positive attitude. Without this, this PhD would not have been as enjoyable as it has been.

I could not have completed this work without the help and support of the aforementioned people. I am sincerely grateful to them all.

---

# PUBLICATIONS AND AWARDS

---

## Awards

- 2014-2017 Flinders University Research Scholarship, Flinders University, Adelaide, Australia
- 2015 Drug Disposition & Response Special Interest group prize, Australian Society of Clinical and Experimental Pharmacologists and Toxicologists (ASCEPT), Hobart, Australia

## Peer Reviewed Journal Manuscripts

1. **van Dyk M**, Miners JO, Kichenadasse G, McKinnon RA and Rowland A (2016). A novel approach for the simultaneous quantification of 18 small molecule kinase inhibitors in human plasma: A platform for optimised KI dosing. *Journal of Chromatography B*, 1033: 17-26.
2. Rowland A, **van Dyk M**, Mangoni AA, Miners JO, McKinnon RA, Wiese MD, Rowland A, Kichenadasse G, Gurney G and Sorich MJ (2017). Kinase inhibitor pharmacokinetics: comprehensive summary and roadmap for addressing inter-individual variability in exposure. *Expert Opinion on Drug Metabolism & Toxicology*, 13: 31-49
3. **van Dyk M**, Rowland A (2017). Physiologically based pharmacokinetic modelling as an approach to evaluate the effect of covariates and drug-drug interactions on variability

- in EGFR kinase inhibitor exposure. *Translational Cancer Research*, 6: 1600-1612.
4. **van Dyk M**, Marshall JC, Sorich MJ, Wood LS, Rowland A (2018) Assessment of inter-racial variability in CYP3A4 activity and inducibility among healthy adult males of Caucasian and South Asian ancestries. *European Journal of Clinical Pharmacology*, DOI: 10.1007/s00228-018-2450-4.
  5. Rowland A, **van Dyk, M**, Hopkins AM, Mounzer R, Polasek TM, Rostami A, Sorich MJ (2018) Physiologically-based pharmacokinetic modelling to identify physiological and molecular characteristics driving variability in drug exposure. *Clinical Pharmacology and Therapeutics*, In press (Accepted 20<sup>th</sup> March 2018).

## Manuscripts Under Consideration

6. **van Dyk M**, Miners JO, Marshall JC, Wood LS, Sorich MJ, Rowland A (2018) Assessment of the caffeine to trimethyluric acid ratio as a dietary marker of variability in cytochrome P450 3A4 activity, *Drug Metabolism and Disposition*.

## Peer Reviewed Conference Abstracts

National conference: Australian Society of Clinical and Experimental Pharmacologists and Toxicologists (ASCEPT) – Melbourne, December 2016. Publication: Abstract/poster presentation – Assessing the substrate depletion of EGFR kinase inhibitor metabolism. Madelé Van Dyk, Michael J Sorich, Andrew Rowland. Department of Clin Pharmacol, Flinders Univ School of Medicine, Adelaide SA, 5042

International conference: Australian Society of Clinical and Experimental Pharmacologists and Toxicologists (ASCEPT) – Hong Kong, May 2015. Oral presentation: The development of an UPLC-MS assay for 18 TKIs.

National conference: Australian Society of Clinical and Experimental Pharmacologists and Toxicologists (ASCEPT) – Hobart, November 2015. Publication: Abstract/poster presentation assessing the contribution of cyp3a4 to total cytochrome p450 mediated tyrosine kinase inhibitor metabolism. Madelé Van Dyk, John O Miners, Michael J Sorich, Andrew Rowland. Department of Clin Pharmacol, Flinders Univ School of Medicine, Adelaide SA, 5042

---

# ABSTRACT

---

Small molecule protein kinase inhibitors (KIs) are a key class of oral antineoplastic drugs that are effective at treating numerous malignancies, including previously difficult to treat forms of cancers. However, variability in KI absorption and disposition causes variability in KI exposure that is inadequately addressed by the standard fixed-dose schedule of administration. Accordingly, it is proposed that the optimisation of KI dosing has great potential to maximise therapeutic response, minimise adverse drug reactions (ADRs), and improve cost-effectiveness of these expensive drugs. To facilitate this, a more comprehensive understanding of the sources of variability in KI exposure is required.

Results presented in Chapters II and III elucidate sources of variability in KI exposure using physiologically based pharmacokinetic (PBPK) modelling and a healthy volunteer study. Specifically, in Chapter II, robust mechanistic models with the capacity to describe epidermal growth factor receptor (EGFR) KI exposure and the impact of covariates on exposure are developed and verified. These models may be applied to inform the impact of different dosing regimens on EGFR KI exposure, the potential impact of poor compliance on EGFR KI efficacy, the need to perform bridging studies when introducing EGFR KIs to new international markets, and the potential impact of DDIs on EGFR KI exposure. In Chapter III inter-racial variability in midazolam exposure was assessed in a cohort of healthy males with Caucasian and South Asian ancestries. This study demonstrated significantly higher midazolam clearance in healthy age-matched males of South Asian compared to Caucasian ancestry that was not explained by differences in the frequency of CYP3A genotypes.

Given the limitations in terms of evidence generation, novel and practical strategies are required to facilitate the clinical application of dose optimisation. Such strategies may facilitate

earlier dose optimisation and identify patients for whom TDM is most critical. In this regard, pathway phenotyping (PP) involves monitoring the blood for a rapidly cleared surrogate probe, or cocktail of probes (typically exogenous), that are substrates for pathways involved in the disposition of the drug of interest. Chapter IV describes the development of a novel phenotyping approach based on dietary markers of CYP3A4 activity to optimise KI dosing from a limited number of blood samples without a requirement to administer prescription drugs.

Studies have demonstrated the benefit of using therapeutic drug monitoring (TDM) to individualise KI dosing on the basis of plasma-KI concentration, and therapeutic concentration ranges have been established for dasatinib, erlotinib, gefitinib, imatinib, nilotinib, pazopanib and sunitinib. However, the broader clinical uptake of TDM is hindered by the requirement to:

- (i) establish and validate separate analytical methods for each KI as they enter clinical practice,
- and (ii) generate sufficiently powered evidence to support the clinical validity of the benefit of concentration guided dosing.

Chapter V describes the development and verification of a panel based approach to facilitate the efficient assessment of KI plasma concentrations. This approach was developed, validated and reported in accordance with the 2015 version of the FDA guidance for industry on ‘analytical procedures and methods validation for drugs and biologics’ facilitating direct application as a clinical trials platform.

---

# ABBREVIATIONS

---

ADAM	advanced dissolution, absorption and metabolism
ADR	adverse drug reactions
ATP	adenosine triphosphate
AUC	concentration time curve
BCR-ABL	break point cluster – Abelson
BCS	biopharmaceutics classification system
BD	twice daily
C	concentration
CAF	caffeine
CDK	cyclin-dependent kinases
CL	clearance
CL <sub>int</sub>	intrinsic clearance
CL <sub>H</sub>	hepatic clearance
C <sub>max</sub>	maximum concentration
CL <sub>S</sub>	systemic clearance
C <sub>ss_trough</sub>	steady-state trough concentration
CYP	cytochrome P450
DDI	drug-drug interactions
DNA	deoxyribonucleic acid
EDTA	ethylenediamine tetraacetic acid
EGFR	epidermal growth factor receptor
EMT	epithelial-mesenchymal transition
ERK	extracellular signal-regulated kinase
ESI	electron spray ionisation

FDA	Food and Drug Administration
$f_u$	fraction unbound
HER2	human epidermal growth factor receptor 2
HLM	human liver microsomes
HPLC	high performance liquid chromatography
HR	homologous repair
IV	intravenously
IVP	<i>In vivo</i> pathway phenotyping
KI	kinase inhibitors
KR	kinase receptor
LLOD	lower limit of detection
LLOQ	lower limit of quantification
MAP	mitogen-activated protein
MAPK	mitogen-activated protein kinase
MEC	minimum effective concentrations
MS	mass spectrometry
MTC	minimum toxic concentrations
MTD	maximum tolerated dose
NADP	nicotinamide adenine dinucleotide phosphate
NSCLC	non-small cell lung cancer
NTID	narrow therapeutic index drugs
OATP1B1	organic anion transport peptide 1B1
PBPK	physiologically based pharmacokinetic
PDGFR	platelet-derived growth factor receptor
P-gp	p-glycoprotein
PGx	pharmacogenomics
PK	pharmacokinetic

PO	orally administered
PPI	proton pump inhibitor
QC	quality control
QD	once daily
Q-ToF-MS	quadrupole, orthogonal acceleration time-of-flight tandem mass spectrometer
RB	retinoblastoma-associated
RCT	randomised control trial
RT	retention time
SD	standard deviation
TAD	toxicity-adjusted dosing
$t_{1/2}$	half-life
TBL	tracheal, bronchus and lung
TDM	therapeutic drug monitoring
TIC	total ion count
$t_{max}$	time to maximum concentration
TTP	total time to progression
UDPGA	UDP-glucuronic acid
UGT	UDP-glucuronosyltransferase
UPLC-MS	ultra performance liquid chromatography mass spectrometry
UV	ultraviolet
$V_d$	volume of distribution
VEGF	vascular endothelial growth factor
VEGFR	vascular endothelial growth factor receptor
$V_{max}$	maximum velocity

---

# CHAPTER I: GENERAL

## INTRODUCTION

---

*The results presented in this chapter  
contributed substantially to the manuscript:*

Rowland A, van Dyk M, Mangoni AA, Miners JO, McKinnon RA, Wiese MD, Rowland A, Kichenadasse G, Gurney G and Sorich MJ (2017). Kinase inhibitor pharmacokinetics: comprehensive summary and roadmap for addressing inter-individual variability in exposure. *Expert Opinion on Drug Metabolism & Toxicology*, 13: 31-49.

## 1.1 Public Significance of Cancer

Cancer is one of the most feared and deadliest diseases (1) and rightly so, as cancer is now the leading cause of death and disease burden in the developed world (2). The most common cancers are prostate, breast, TBL (tracheal, bronchus and lung) and colorectal, with the most deaths due to TBL, liver, breast and colorectal cancer. A significant increase in incidence has been observed worldwide, however, population growth accounted for the majority of this observation, along with a contribution from advances in modern screening, detection and diagnosis (3). Although incidence rates have increased with time, mortality rates have decreased for the majority of cancers including some of the world's most common and deadliest forms. The development of multidisciplinary treatment approaches and the more recent discoveries in terms of targeted anticancer therapies are largely responsible for these improved mortality rates (4). Cancer is not a single disease but rather a collection of genetic and metabolic changes that alter the function of normal cells. Because of this cancer is considered a heterogeneous disease as these changes present differently in various tissues and individuals.

## 1.2 Cancer Hallmark Characteristics

The capabilities acquired by cells during the development of cancer have been termed 'cancer hallmarks'. Six hallmark capabilities were initially summarised by Hanahan and Weinberg (2000); two emerging hallmark capabilities and two enabling characteristics were subsequently added (5). These hallmark characteristics are based on the aspects of tumour biology and serve as key targets for many drugs used in the treatment of cancer (**Figure 1.1**). Understanding these key components of tumour biology provides an important basis for understanding the

mechanisms of antineoplastic drugs.

### **1.2.1 Sustaining Proliferative Signalling**

One of the key capabilities of cancer is the ability to chronically proliferate. Normally cell growth and proliferation is highly regulated, however, once these cells become cancerous, the regulation is disrupted and the growth is controlled in a very complex manner. Interestingly, a more comprehensive understanding exists for cancer mitogenic signalling in comparison to normal cell signalling and growth (6). There are several ways that cancer cells manipulate normal growth and proliferation systems; cancer cells can upregulate cell growth by increasing their own growth factor receptors making them hyper-responsive to such growth factors. Cancer cells can stimulate normal cells to produce growth factors and can also produce growth factor themselves which results in autocrine proliferation. Growth factor itself can be stimulated from further downstream proteins such as RAF or MAP, while negative-feedback loops required to slow down signalling can be dysregulated by the oncogene, RAS, resulting in uncontrolled signal transduction. Many other mutations present in cancer cells that result in uncontrolled signal transduction may lead to dysregulated cell growth. The observations that growth factors play a critical role in the various mechanisms around sustaining proliferative signalling make epidermal growth factor receptor (EGFR) kinase inhibitors an ideal therapeutic target to reduce such proliferative signalling and will be discussed further in section 1.6.

### **1.2.2 Evading Growth Suppressors**

Another characteristic that cancer cells manifest is the ability to interfere with processes such as senescence or apoptosis as part of the cell cycle (5). Tumour suppressors encode for the RB (retinoblastoma-associated) and TP53 proteins which function as the gatekeeper proteins which

control or 'decides' whether a cell will deteriorate or undergo apoptosis. Both these proteins function in part with a larger network of cell redundancy but the way RB functions is from the extracellular environments where cell growth signals are inhibited; TP53 functions from the intracellular environment where it can detect stressors such as suboptimal oxygenation, glucose or cell growth promoting signals, which will be actioned by putting cell proliferation signals on hold until the abnormal intracellular environments return to normal (7). In cancer cells these proteins are defected and cancer cells essentially 'skip' this process and continue to grow uncontrollably regardless of the environments. The RB proteins are also substrates to the cyclin-dependent kinases (CDKs) which play an important role in cell cycle divisions and transcription and often become mutated in cancer, with loss of cell cycle control. CDKs also control the activity of the transcription factor E2F, which is over expressed in cancer cells. Therefore targeting CDKs by inhibition can have anti-cancer effects (8). Additionally, in cancer the *MYC* gene becomes mutated and over expresses resulting in unregulated cell proliferation due to repression of cell senescence. However, MYC requires activation of CDK2, making CDK inhibitors a further eligible anticancer agent (8, 9). As a result a number of CDK inhibitors have been approved by the US food and drug administration (FDA) as cancer therapy when individuals present with specific tumour genetics.

### **1.2.3 Resisting Cell Death**

Necrosis is a form of cell death which has protective mechanisms against tumour development, but it has recently been shown to be tumour promoting as necrotic cells can release growth factors into the microenvironment to stimulate proliferation (10). Another form of cell death, apoptosis, is triggered by stressors such as increased levels of oncogene signalling and DNA damage that results in excessive cell proliferation, however, the process of apoptosis is

weakened in tumours found in high grade malignancies (11). The Bcl-2 protein family play an important role in apoptosis and consists of anti-apoptotic Bcl-2 proteins, pro-apoptotic Bak and Bax proteins, and pro-apoptotic BH3 only proteins. One of the key tumour suppressors, TP53, detects damaged DNA and induces apoptosis. However, TP53 suppression function is lost during carcinogenesis (11). There are a variety of strategies adopted by cancer cells to avoid apoptosis, contributing to the diversity and complexity of malignancies. One of these processes, autophagy, often presents in nutrient deficient cancer cells. Autophagosomes engulf such cells and bind to lysosomes for degradation, creating a recycled source for biosynthesis and energy metabolism; this ensures the survival of small molecule metabolites found in cancer environments (5). BH3 proteins that regulate anti-apoptotic programming can trigger autophagy by binding to Bcl-2 proteins, which blocks apoptosis. BH3-mimetics are anti-cancer agents designed to target and inhibit the anti-apoptotic Bcl-2 proteins resulting in cell death (12). It has also been observed that BCR-ABL (break point cluster – Abelson) signalling promotes cell survival by increasing expression of anti-apoptotic Bcl-2 proteins therefore, BH3-mimetics can be used in combination with inhibitors of oncogenic kinases such as BCR-ABL (13).

#### **1.2.4 Enabling Replicative Immortality**

To ensure cell proliferation, growth and division cycles need to be successful. However, two processes, senescence and apoptosis, can curtail these cycles and typically act as control mechanisms to prevent unnecessary cell proliferation (5). These processes occur in normal cell function in response to shortened telomeric DNA as a part of a complex controlled cell life. However, in cancer cells, these processes are absent and the cells can become immortal (14). In cancer, telomeric DNA is mechanistically maintained or telomerase expression is upregulated by adding DNA repeats to the ends of chromosomes, which protects the ends of

the chromosomes for long enough to avoid senescence and apoptosis, ensuring unlimited cell proliferation. Cell senescence plays a protective role against cancer when abnormalities such as excessive oncogene signalling or critically shortened telomeric DNA ends are detected (5). Additionally, it has been shown that telomerase has the ability to promote tumorigenesis independent of its enzymatic activity for telomere elongation; instead it can act as a transcriptional cofactor by modulating the Wnt signalling pathway which results in the accumulation of the  $\beta$ -catenin protein which activates transcription factors, thus promoting cell proliferation (15). Given that telomerases are barely found in normal cells but upregulated in cancer cells, telomerase inhibitors make great candidates for targeted anticancer therapy (16).

### **1.2.5 Inducing Angiogenesis**

Typically in normal physiological states, angiogenesis is required to supply cells with nutrients and oxygen, and facilitate waste removal, and is regulated by induction and inhibitor signalling factors such as VEGF-A (vascular endothelial growth factor-A) and TSP-1 (thrombospondin-1), respectively. These signalling factors respond according to a 'switch' as required. In contrast, during tumorigenesis, this 'switch' is permanently turned on and thus the tumour has a supply of nutrients and oxygen to grow uncontrolled (17). VEGF (vascular endothelial growth factor) can be upregulated in response to hypoxia or oncogene signalling, promoting angiogenesis, while in contrast TSP-1 can suppress angiogenesis when binding to transmembrane receptors on the endothelial cells (18). Angiogenesis can present in diverse ways depending on tumour type; in some cancers such as pancreatic ductal adenocarcinomas, angiogenesis is down regulated (19) and in others, such as renal and pancreatic neuroendocrine carcinomas, it is upregulated (20). VEGF kinases play a significant role in promoting angiogenesis, therefore a number of VEGF kinase inhibitors have been approved to reduce this hallmark characteristic involved in cancer development.

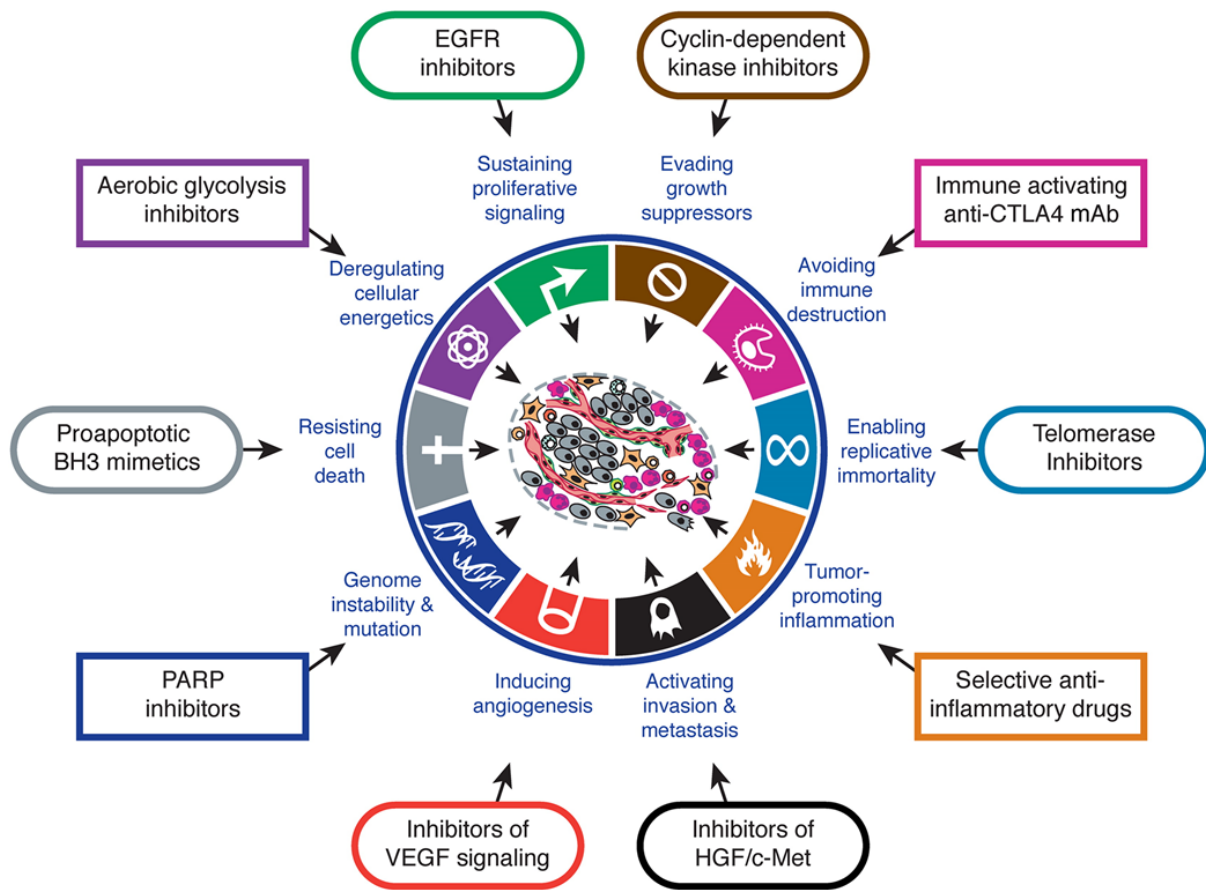


**Figure 1.1: Therapeutic Targeting of the Hallmarks of Cancer.**

*Source: Hanahan and Weinberg (5)*

### 1.2.6 Activating Invasion and Metastasis

During activation of cancer invasion and metastasis, cancer cells travel from local cells through the lymphatic and haematological systems to functional tissue in distant organs. The EMT (epithelial-mesenchymal transition) program plays a role in activating the ability of cancer cells to become invasive and the expression of EMT-induced cells has been observed on the margins of the tumours, rather than in the middle of the tumour (5, 21). It has also been suggested that heterotypic contributions of stromal cells are involved with invasion and metastasis; signalling between cancer cells and non-malignant stromal cells result in the stromal cells releasing

signalling proteins such as chemokine ligand 5, which stimulate the cancer cells to become invasive (22). During local invasion cancer cells release interleukin 4 to stimulate macrophage proteases to degrade matrices of cells, thereby promoting invasion (23). Cancer cells have also shown ability to revert back to a non-invasive state once they are residing in the new location and no longer being exposed to the signalling that facilitates the transition from epithelial cells to mesenchymal cells, hence some cells express both mesenchymal and residual epithelial cells (24). EMT invasion results in metastasis whereas collective and amoeboid invasion does not. Collective invasion relies on 'lumps' of cancer cells to migrate to adjacent tissues, whereas amoeboid invasion relies on individual cells that move through the extracellular matrix instead of making its own pathway like the other two types of invasion (25). Inflammatory cells have also been suggested to facilitate cancer cell invasion by releasing extracellular matrix degrading proteins (26). Some cancer cells have the ability to move to distant tissues and adapt to the new microenvironment where they colonise to form macroscopic tumours. However, in some types of cancers (breast cancers and melanomas), micrometastatic tumours remain dormant for a period of time before becoming macroscopic. A number of factors such as nutrient starvation, antigrowth signals from healthy extracellular matrix and tumour suppressing signals from the immune system have been shown to contribute to this dormancy and reversibility of micro metastatic cells (27-29). Therefore surgical treatments can both benefit and disadvantage tumour growth in different ways (30). Tyrosine kinase cMET and hepatocyte growth factor (HGF) play a crucial role in cellular proliferation, invasion and metastasis and have been shown to be upregulated in many malignancies. When the active form of HGF binds to cMET several signalling cascades associated with invasion and metastasis are activated. EGFR kinases also play a role in the activating cMET, making EGFR kinase inhibitors and cMET inhibitors an encouraging combination targeted therapy (31).

### 1.2.7 Genome Instability and Mutation

In healthy conditions, genomic 'care taker' systems are in place to regulate damaged DNA to ensure low rates of mutations (32). In contrast, increased rates of mutations occur in cancer (33). This increased rate of mutations may be due to changes in the tumour suppressor protein, TP53, which controls cell regulatory circuits, resulting in decreased ability to search, detect and program damaged cells into a senescent or apoptotic state (34). Generally telomeres protect chromosomal ends and shorten over time. However, it has been demonstrated that telomerases play an important role in producing telomeres during cancer development and promote cancer growth, therefore telomerases can now be included as a genome 'care takers'. The telomeric chromosomal ends are normally at risk each time DNA replication occurs and are therefore susceptible to DNA instability, which is one of the newer enabling characteristics of cancer (35). BRCA1 and BCRA2 are tumour suppressor genes and play a role in repairing damaged DNA, however, these genes are mutated in some forms of breast and ovarian cancers and lack the homologous repair (HR) pathway which normally repairs lesions in the double-strand breaks. When this repair pathway is dysfunctional, the cell is susceptible to cell death given that both DNA strands are damaged and have no template to work from. The poly (ADP-ribose) polymerase (PARP) repair pathway can aid in DNA repair by correcting lesions in the single-strand breaks which can still allow for double-strand formation given that there is a template to work from. In cancers where repair mechanisms are affected and cells are already vulnerable to cell death, targeting such cells can be effective in reducing cancer cell survival. Therefore, targeting the PARP pathway by blocking this enzyme with PARP inhibitors, single-strand breaks are unable to be corrected to facilitate double-strand DNA formation thus becoming unstable and promoting cell death (36, 37).

### **1.2.8 Tumour Promoting Inflammation**

It has long been known that the immune system plays a role in tumour development whereby leukocytes infiltrate the area of developing cancers with the aim to destroy the cancer cells. However, in recent years it has been demonstrated that the immune responses can be both tumour suppressing and tumour promoting depending on the cancer type and conditions of the microenvironment (38). The immune responses found in various cancer types are similar to that during the process of wound healing; however, in cancer development this response does not stop due to innate immune cells such as granulocytes, macrophages, natural killer cells, and dendritic cells releasing tumour promoting molecules such as growth factors, extracellular matrix degrading enzymes, cytokines, chemokines and other bioactive mediators which can facilitate proliferation signalling, cell survival, angiogenesis, invasion, activation of EMT and metastasis (39). The immune system can also release reactive oxygen species which can further promote active mutations in neighbouring cancer cells thus increasing mutation rates, which is a key issue in advanced malignancies (10). Based on these more recent discoveries about the roles of the immune system during tumour development, it is evident that inflammation is another enabling characteristic of cancer making selective anti-inflammatory drugs a promising anti-cancer agent.

### **1.2.9 Reprogramming Energy Metabolism**

Another emerging hallmark of cancer is the understanding of the adjustment of energy metabolism within cancer cells to enable continuous cell division and growth, which can be demanding given that cell content has to double during each cell cycle (5). In contrast to non-cancerous cells, it has been demonstrated that cancer cells rely on 'aerobic glycolysis' and skip mitochondrial oxidative phosphorylation to obtain energy from glucose (40). This change in energy metabolism results in a far less effective ATP production when compared to non-

cancerous cells which normally rely on glycolysis (formation of glucose to pyruvate) and mitochondrial oxidative phosphorylation (pyruvate to carbon dioxide in the mitochondria) (40). Instead, cancer cells rely on upregulation of glucose transporters which allows for more cytoplasmic glucose which is then converted to pyruvate and then to lactate by the enzyme lactate dehydrogenase A (LDH-A) resulting in the upregulation of LDH-A (41). This increase in glycolysis and upregulation of LDH-A has been observed to be linked with the oncogenes, RAS, MYC, and mutant tumour suppressors such as TP53 (41, 42), thus making aerobic glycolysis inhibitors potential effective anti-cancer agents. Interestingly, two types of energy metabolism have been observed within the same tumour depending on the state of the cell; the one being dependant on aerobic glycolysis where oxygen levels are low as described above, and the second being neighbouring cells with sufficient oxygen levels dependant on the lactate formed by the former system as an energy source (5). These observations of energy metabolism reprogramming suggests that it plays a significant role in increased cell proliferation present in tumours, but this phenomenon requires further investigation to be established as an independent hallmark of cancer.

### **1.2.10 Evading Immune Destruction**

It is well established that the immune system acts as a surveillance operation ready to attack cancerous cells with the aim to eradicate them as a protection measure against the development of tumours (29). However, it is clear that some cancers not only bypass or escape this surveillance/destruction system but also have the ability to employ immune cells supportive of cancer (5). The mechanisms behind this evasion is still somewhat unclear as some confounding results have been noted. For example, it has been demonstrated that when cancerous cells from immune deficient mice are transplanted into another immune deficient animal, secondary cancers were unable to form. By contrast, when cancerous cells from immune proficient mice

were transplanted into either immune proficient or deficient mice, secondary cancers were able to form (29). This observation suggests that a defective immune system may play a role in the evasion of cancer eradication. However, the incidence of non-viral cancers was not significantly increased, suggesting that defective immune systems may not play a critical role in evading immune destruction, indicating the need for further investigation. Cytotoxic T lymphocytes have the ability to destroy cancerous cells, but cytotoxic T lymphocyte-associated antigen 4 can turn this response off by interfering with the T-cell activation required for the immune response required for anti-cancer effects. By blocking CTLA-4, the regulatory T-cells can function normally to signal for additional immune cells to upregulate the immune response (43).

This understanding of the characteristics that distinguish cancer cells from normal cells is central to selectively targeting tumours using various pharmacological agents and is largely responsible for the paradigm shift that has occurred over the last decade in terms of how anticancer medicines work. As depicted in **Figure 1.1**, ‘targeted therapies’ have now been developed to selectively interfere with each of the hallmark characteristics.

### **1.3 Targeted Therapies and Precision Medicine**

The principle underpinning anti-cancer targeted therapies is that by selectively interfering with neoplastic pathways (i.e. pathways involved in cancer development), it is possible to administer a sufficiently high dose of the drug to routinely achieve therapeutic effect, while maintaining an acceptable toxicity profile (i.e. applying the principle of ‘selective toxicity’). Over the past decade a number of targeted therapies have been developed that effectively treat solid organ malignancies, including many previously difficult to treat forms of cancers.

The development of targeted therapies for cancer has evolved in parallel with individualised health care, now termed ‘precision medicine’. While the concept of the ‘right drug at the right dose for the right patient’ is not new, the application of the concept to cancer medicines has gained considerable momentum over the past decade. The concept of precision medicine in oncology (‘Precision Oncology’) involves two aspects: (i) the selection of the optimal drug for the patient based on characteristics of the cancer and the patient, and (ii) the selection of the optimal dose of that drug for the patient. As show in **Figure 1.2**, there are several factors that need to be considered when selecting both the optimal drug and the optimal dose of the drug, and there are multiple strategies and tools that can be applied to inform each of these decisions.

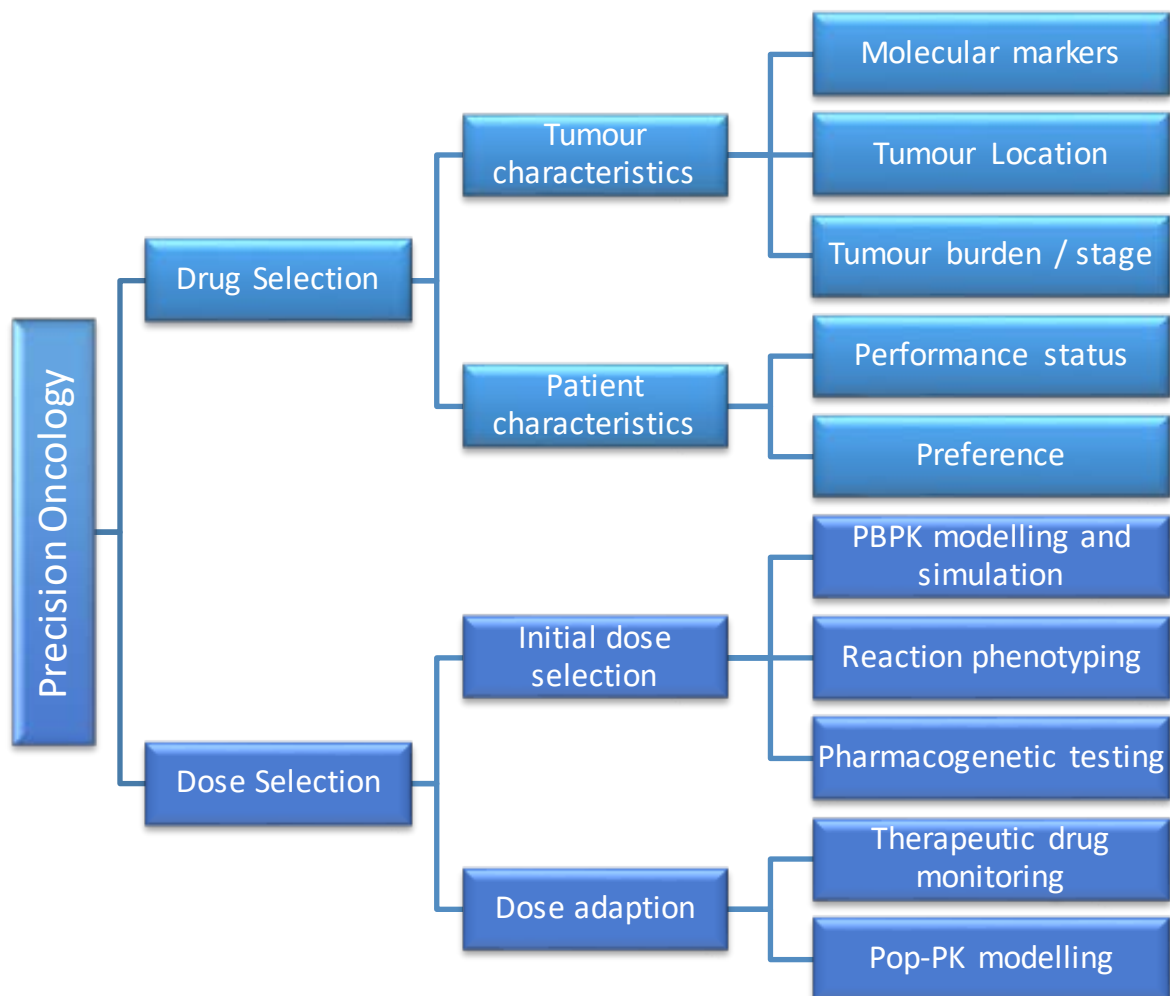


**Figure 1.2: Decision tree demonstrating the core aspects of precision oncology and the strategies and tools that underpin these core aspects.**

In practice, the application of precision oncology to date has typically focussed on the use of molecular markers to guide drug selection, with comparatively little emphasis on the selection of the optimal dose. This is largely because of the greater capacity to develop evidence of clinical validity for drug selection using routinely collected samples from clinical trials.

## 1.4 Small Molecule Kinase Inhibitors

Small molecule protein kinase inhibitors (KIs) are a novel and rapidly expanding class of targeted oral antineoplastic drugs that have demonstrated widespread success, often first-line, for the treatment of numerous malignancies, including previously difficult to treat forms of cancer. In addition, nintedanib and tofacitinib have recently been approved for the non-neoplastic indications idiopathic pulmonary fibrosis and rheumatoid arthritis, respectively (**Table 1.1**). However, inter-individual variability in absorption and disposition manifesting as variability in exposure is inadequately addressed by fixed-dose prescribing practices, resulting in unpredictable and potentially sub-optimal outcomes (44, 45). While fixed-dose prescribing is routinely used for orally administered drugs with a wide therapeutic index and limited inter-individual variability in exposure, it is rarely used for narrow therapeutic index drugs (NTIDs) (e.g. warfarin, digoxin, anticonvulsants and immunosuppressants) or for drugs that exhibit substantial inter-individual variability in exposure. As with many antineoplastic drugs, KIs are NTIDs (46), whereby the difference between the minimum toxic concentrations (MTC) and minimum effective concentrations (MEC) is small (typically < 2-fold). Indeed, for several KIs, e.g. bosutinib, erlotinib, ponatinib, pazopanib and sunitinib, the recommended starting dose required to achieve therapeutic efficacy is the reported maximum tolerated dose (MTD) from dose-escalation studies (46). Accordingly, the extent and duration of exposure to a KI are important determinant of therapeutic efficacy and tolerability.

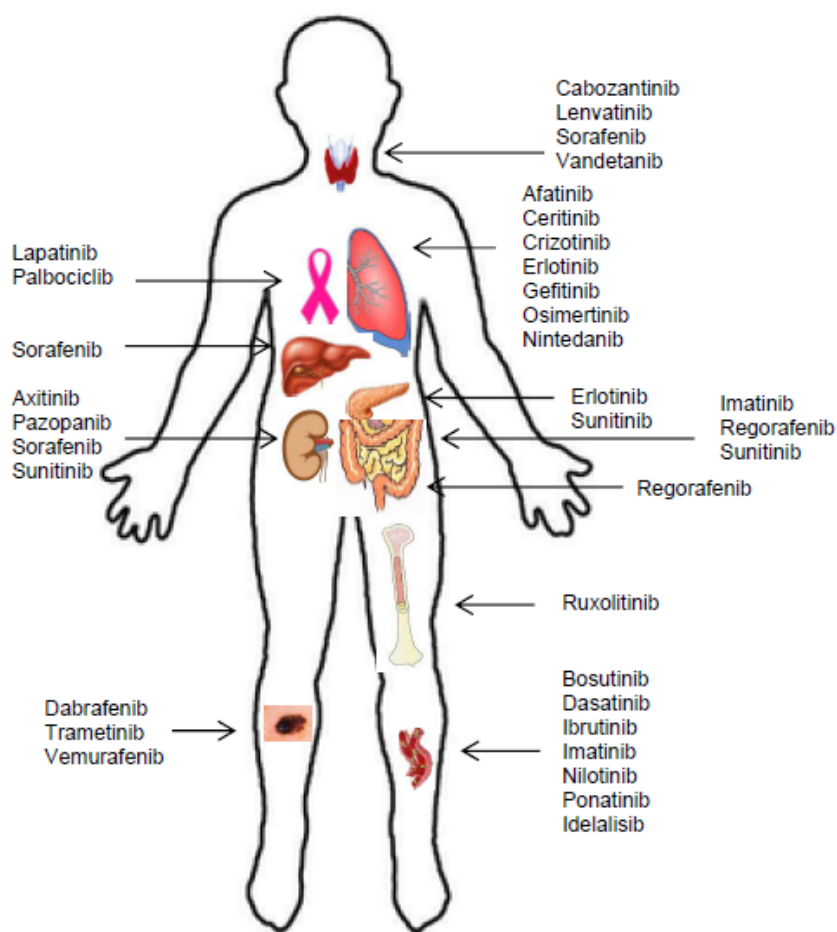


**Figure 1.3: Approved KIs and related target cancers.**

*Thyroid cancers are treated with cabozantenib, lenvatenib, sorafenib and vandetinib; lung cancers are treated with afatinib, ceritinib, crizotinib, erlotinib, gefitinib, osimertinib and nintedanib; breast cancers are treated with palbociclib and lapatinib; liver cancer is treated with sorafenib; kidney cancers are treated with axitinib, pazopanib, sorafenib and sunitinib; gastrointestinal cancer is treated with sunitinib, imatinib and regorafenib; regorafenib is also used to treat colorectal cancer; pancreatic cancers are treated with erlotinib and sunitinib; myelofibrosis and polycythemia vera are treated with ruxolitinib; metastatic melanoma is treated with vemurafenib, dabrafenib, trametinib or dabrafenib and trametinib in combination; blood cancers are treated with bosutinib, dasatinib, ibrutinib, imatinib, nilotinib, ponatinib and idelalisib. Tofacitinib is not displayed as it is used to treat rheumatoid arthritis and not cancer.*

Imatinib was the first KI to be approved in 2001. Since then a further 29 KIs have been approved for the treatment of various malignancies, 21 of these in the past five years (**Figure 1.3; Table 1.1**). KIs are potent inhibitors of pathways that regulate cellular functions such as growth, differentiation and survival (47). These pathways are activated by the membrane bound cell surface kinase receptor (KR) superfamily, which comprises more than 500 members. KR families of particular importance to the development of malignancy are the EGFR, platelet-derived growth factor receptor (PDGFR), and vascular endothelial growth factor receptor (VEGFR) families and their associated signalling pathways such as the mitogen-activated protein kinase (MAPK) pathway, which incorporate families of signalling proteins such as RAS, RAF, MEK, MAPK, extracellular signal-regulated kinase (ERK) and c-KIT (48). Impaired regulation of kinase activity either through mutation of the KR or downstream proteins leads to constitutive pathway activation, uncontrolled cell proliferation and malignancy. Many KIs such as EGFR and VEGFR inhibitors act directly on the membrane bound cell surface KR, while other KIs such as BRAF and MEK inhibitors act on downstream proteins (**Figure 1.4**). At a molecular level KIs interact with the ATP binding site of the intracellular kinase domain. As such most drugs in this class share a common planar heterocycle as the core structure. Accordingly there are similarities in the physicochemical properties between most, but not all KIs that also translate to common pharmacokinetic characteristics. KIs differ in terms of their target selectivities and mechanism of inhibition, and as such are effective in treating a variety of malignancies, with some KIs effective in treating multiple malignancies. Crystallographic analyses performed to elucidate molecular conformations and interactions have demonstrated that the potency and clinical efficacy of VEGF inhibitors such as axitinib relate to the conformation of the protein that is bound by ligand (49). Each KI is briefly described below with approval details, physicochemical properties and pharmacokinetic properties summarised in **Table 1.1, 1.2** and **1.3**, respectively.

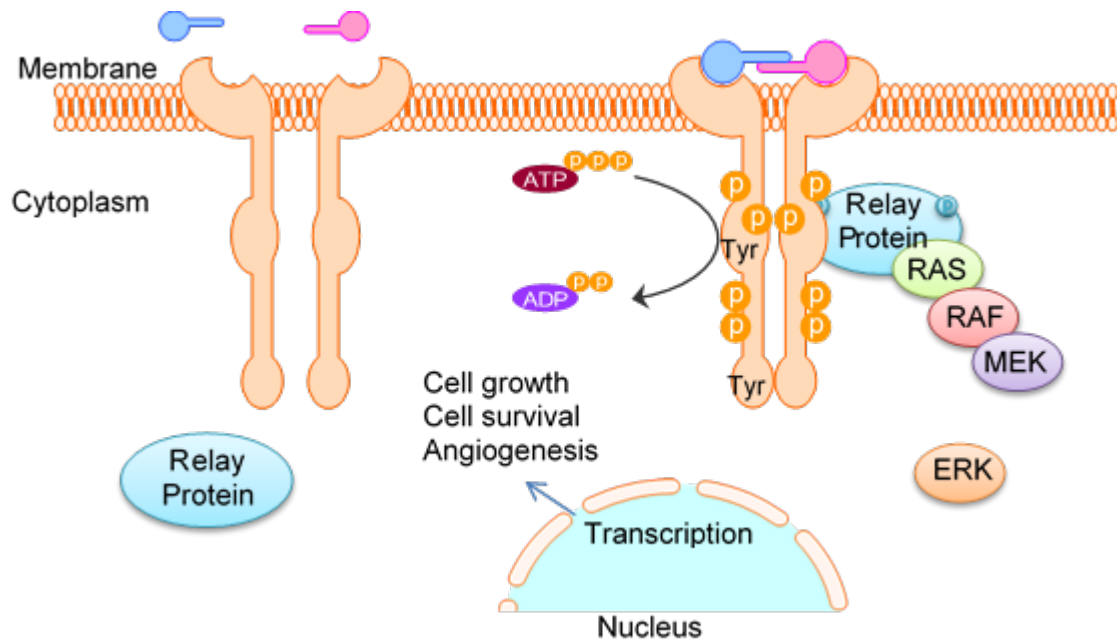


**Figure 1.4: Inactive tyrosine kinase (TK) receptor on the left with an activated TK receptor on the right where dimerization took place after ligand binding.**

*Cell signal transduction is tightly controlled by TKs which add phosphate groups from ATP to the amino acid tyrosine in the tail of the receptor for activation, and by phosphatases for removal of phosphate groups for deactivation. TKIs exert their physiological effect by inhibiting the TKs resulting in no phosphorylation resulting in deactivation of proteins involved in cancer growth such as ALK, RAS, RAF, MEK and ERK further downstream and can no longer cause conformational change that would lead to transcription to code for cellular processes required for cancer growth. In other words KIs turn the ‘on switch’ back to ‘off’ when TKs becomes stuck in ‘on mode’.*

### 1.4.1 BCR-ABL Inhibitors

The BCR-ABL fusion gene results from a rearrangement of genetic material between chromosomes 9 and 22 (the Philadelphia chromosome). This fusion gene, which is the ABL1

gene from chromosome 9 translocation onto the BCR gene from chromosome 22, codes for a hybrid BCR-ABL tyrosine kinase that is always 'switched on', causing cells to divide uncontrollably. BCR-ABL is highly prevalent in chronic myeloid and acute lymphoblastic leukaemias, and targeting of BCR-ABL by the prototypic KI, imatinib, is widely regarded as one of the greatest advances in the treatment of cancer. Dasatinib and Nilotinib is effective against point mutations such as BCR – ABL and Src. It targets both the active (unsuccessful binding of imatinib) and inactive form of the BCR – ABL gene, however, it is not effective against the T3151 resistant mutation. Ponatinib is, however, effective against the native form of the BCR-ABL gene, multiple other mutations and most importantly, against the T3151 mutation. Pharmacokinetic parameters describing exposure to BCR-ABL inhibitors are reported in [Table 1.3](#).

#### **1.4.2 EGFR Inhibitors**

Epidermal growth factor receptor (EGFR) small molecule KIs have made a significant improvement in the treatment of advanced non-small cell lung cancer (NSCLC). Currently, there are four EGFR inhibitors approved for the treatment of EGFR activating mutation positive NSCLC; afatinib, erlotinib and gefitinib are first-line options, while osimertinib is a second line option for tumours that develop resistance to afatinib, erlotinib and gefitinib (50). In approximately 50% of patients resistance to first line EGFR inhibitors occurs through acquisition of the T790M mutation in exon 20 of EGFR; unlike first line options, osimertinib retains activity against T790M positive tumours. The use of EGFR KIs for the treatment of this cancer is particularly interesting and has become a prominent example of personalized medicine where treatment is determined based on the mutation status of the individual's tumour (51). EGFR activating mutations occur at a high frequency in NSCLC with 10 to 50% of tumours being positive for a mutation. It has been established that the outcome for NSCLC

patients treated with KIs are superior for tumours harbouring an activating mutation compared to those without (52, 53). Common mutations that confer either sensitivity or resistance to EGFR KIs are shown in **Figure 1.5** and include alterations at exon 18, 19, 20 and 21 (54).

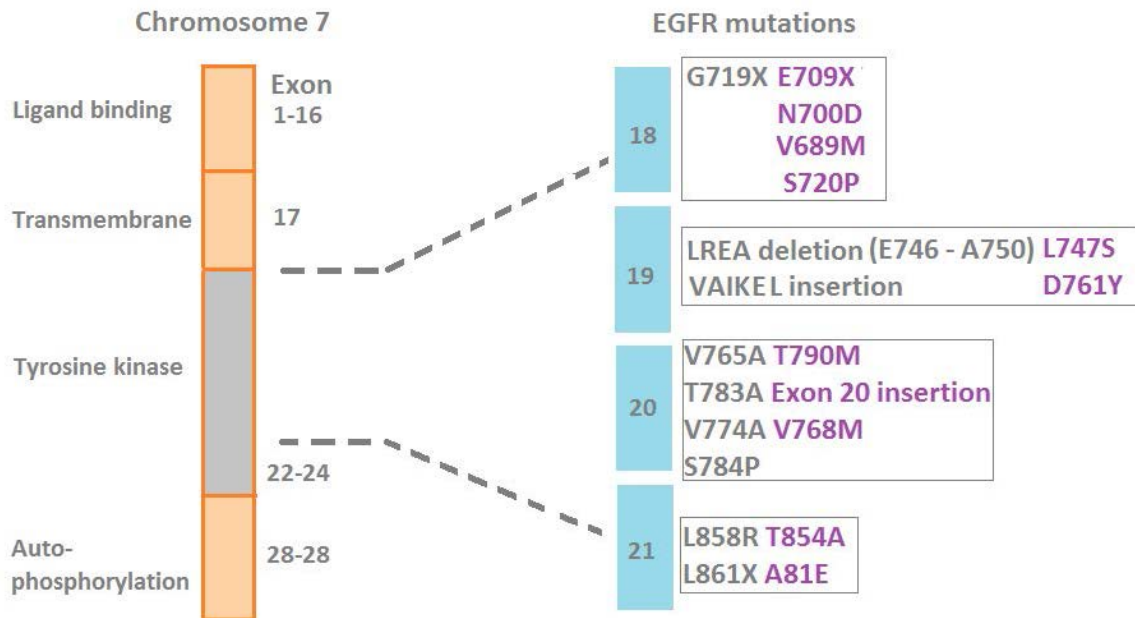


**Figure 1.5: Common mutations found in the EGFR kinase domain in NSCLC.**

*Mutations in grey generally respond to EGFR KIs and mutations in purple are typically resistant. Abbreviations: LREA (leucine, arginine, glutamine and alanine) and VAIKEL (valine, alanine, isoleucine, lysine, glutamate, and leucine).*

Activating mutations in exons 18, 19 and 21 of the EGFR are present in approximately 30% of NSCLC tumours. These mutations confer sensitivity to EGFR inhibitors (**Table 1.1**). Lapatinib is a dual kinase inhibitor with activity against human epidermal growth factor receptor 2 (HER2) and EGFR pathways. Unlike other EGFR inhibitors, it is mainly used in the treatment of HER2-positive breast cancer. Pharmacokinetic parameters describing exposure to EGFR inhibitors are reported in **Table 1.3**.

### 1.4.3 VEGF Inhibitors

In cancers including hepatocellular, renal cell and thyroid carcinomas, activation of VEGF-mediated angiogenesis plays a critical role in tumour growth and metastasis. By inhibiting the intracellular catalytic domain of VEGF receptors, small molecule VEGFR inhibitors block VEGF-mediated angiogenesis and impair the tumour's capacity to access the nutrients required for growth. Pharmacokinetic parameters describing exposure to VEGFR inhibitors are reported in **Table 1.3**.

### 1.4.4 BRAF / MEK Inhibitors

BRAF is a member of the RAF family of serine/threonine kinases that are related to retroviral oncogenes. Mitogen-activated protein kinase kinase (MEK) is the protein that phosphorylates MAPK. BRAF and MEK are key regulatory proteins in MAPK / ERK signalling cascade, which affects cell division and differentiation. When BRAF and/or MEK is inhibited, cell proliferation is blocked and apoptosis is induced. Mutations in the *BRAF* gene, particularly at residue 600 are associated with various cancers including colorectal, lung, melanoma and thyroid. Vemurafenib and dabrafenib are BRAF inhibitors approved for treatment of unresectable or metastatic BRAF V600E-positive melanoma. In order to maximize therapeutic effect, BRAF inhibitors are often used combination with a MEK inhibitor; cobimetinib (with vemurafenib) or trametinib (with dabrafenib). Pharmacokinetic parameters describing exposure to these inhibitors are reported in **Table 1.3**.

### 1.4.5 Other Kinase Inhibitors

In addition to VEGFR, EGFR, BRAF/MEK and BCR-ABL, a number of additional kinases have been implicated in the development and progression of cancer. In recent years, inhibitors of anaplastic lymphoma kinase (ALK; alectinib, ceritinib, crizotinib), Bruton's tyrosine kinase

(BTK; ibrutinib), phosphoinositide 3-kinase (PI3K; idelalisib), and CDK (palbociclib), have emerged as effective drugs for the treatment of solid organ tumours including breast and non-small cell lung cancer, and various forms of leukaemia.

**Table 1.1: Overview of kinase inhibitor pharmacology**

<b>Class</b>	<b>Agent</b>	<b>Approved Indication(s)</b>	<b>Molecular Target(s)</b>	<b>First Approval <sup>a</sup></b>
VEGF inhibitors	axitinib	RCC	KIT, PDGFR $\beta$ , VEGFR1-3	27 Jan 2012 (FDA)
	cabozantinib	MTC	FLT3, c- KIT, c-MET, RET, VEGFR2	29 Nov 2012 (FDA)
	lenvatinib	TC	VEGFR1-3, FGFR1-4, RET, KIT, PDGFR $\alpha$	13 Feb 2015 (FDA)
	Nintedanib	IPF	PDGFR $\alpha/\beta$ , FGFR1-3, VEGFR1-3, FLT3,	15 October 2014 (FDA)
	pazopanib	RCC	VEGFR1-3, PDGFR $\alpha/\beta$ , c-KIT, FGFR2	19 Oct 2009 (FDA)
	regorafenib	CRC, GIST	c-KIT, PDGFR $\beta$ , RAF, RET, VEGFR1-3	27 Sept 2012 (CRC; FDA)
	sorafenib	HCC, RCC, TC	VEGFR2/3, PDGFR $\beta$ , FLT3, FGFR1, c-KIT, RAF, RET	20 Dec 2005 (RCC; FDA)
	sunitinib	GIST, pNET, RCC	VEGFR1-3, c-KIT, PDGFR $\alpha/\beta$ , FLT3, RET	26 Jan 2006 (RCC; FDA)
	vandetanib	MTC	EGFR, RET, VEGFR2	6 Apr 2011 (FDA)
EGFR inhibitors	afatinib	NSCLC (EGFR MUT)	EGFR, HER2 , HER4	12 Jul 2013 (FDA)
	erlotinib	NSCLC, PC	EGFR	18 Nov 2004 (NSCLC; FDA)
	gefitinib	NSCLC	EGFR	1 May 2003

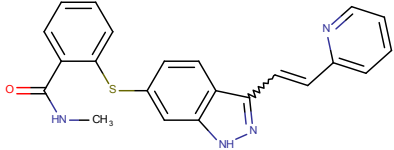
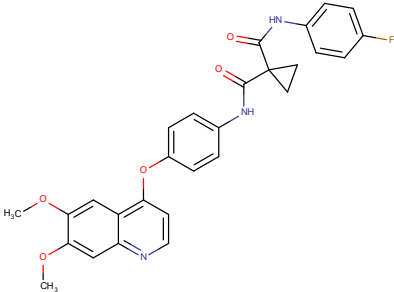
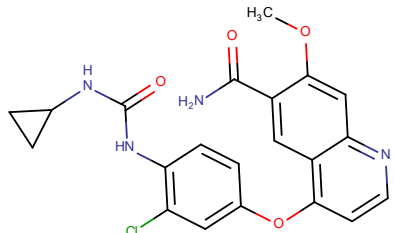
		(EGFR MUT)		(FDA)
	lapatinib	BC (HER2+)	EGFR, HER2	13 May 2007 (FDA)
	osimertinib	NSCLC (EGFR MUT)	EGFR	13 Nov 2015 (FDA)
ALK inhibitors	alectinib	NSCLC (ALK MUT)	ALK	11 Dec 2015 (FDA)
	ceritinib	NSCLC (ALK MUT)	ALK, IGF-1, ROS1, InsR	29 Apr 2014 (FDA)
	crizotinib	NSCLC (ALK MUT)	ALK, c-MET	26 Aug 2011 (FDA)
BRAF / MEK inhibitors	cobimetinib	MEL (BRAF MUT)	MEK1-2	10 Nov 2015 (FDA)
	dabrafenib	MEL (BRAF MUT)	BRAF	10 Jan 2014 (FDA)
	trametinib	MEL (BRAF MUT)	MEK1-2	29 May 2013 (FDA)
	vemurafenib	MEL (BRAF MUT)	BRAF	17 Aug 2011 (FDA)
BCR-ABL inhibitors	bosutinib	CML (Ph+)	ABL, SRC	4 Sept 2012 (FDA)
	dasatinib	ALL(Ph+), CML (Ph+)	BCR-ABL, SRC, c-KIT, PDGFR $\alpha/\beta$ , EphA2	23 Dec 2005 (ALL; EMA)
	imatinib	ALL (Ph+), CML (Ph+), DFSP, GIST (KIT+)	c-KIT, PDGFR $\alpha/\beta$ , BCR-ABL	11 May 2001 (CML; FDA)
	nilotinib	CML (Ph+)	KIT, PDGFR $\alpha/\beta$ , BCR-ABL	29 Oct 2007 (FDA)
	ponatinib	ALL (Ph+), CML (Ph+)	BCR-ABL, FGFR1-3, FLT3, VEGFR2, c- KIT, RET, PDGFR $\alpha$	14 Dec 2012 (FDA)
BTK inhibitor	ibrutinib	CLL, MCL, WM	BTK	13 Nov 2013 (MCL; FDA)

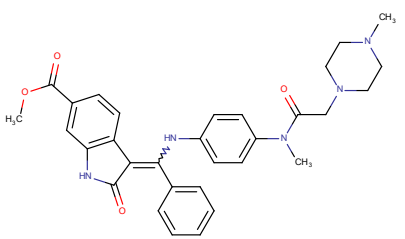
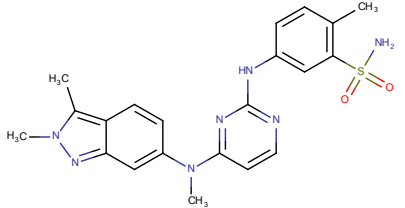
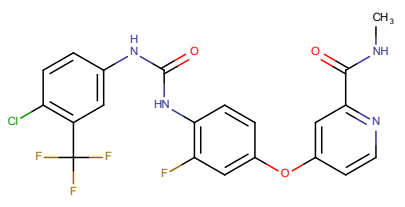
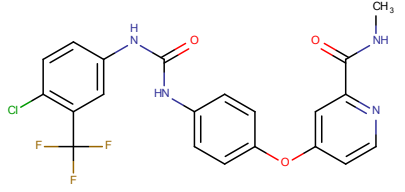
PI3K inhibitor	idelalisib	CLL, FNHL, SLL	PI3K $\delta$	23 Jul 2014 (FDA)
JAK inhibitors	ruxolitinib	MF, PV	JAK1/2	16 Nov 2011 (PV; FDA)
	tofacitinib	RA	JAK3	6 Nov 2012 (FDA)
CDK inhibitor	palbociclib	BC (ER+, HER2-)	CDK4/6	3 Feb 2015 (FDA)

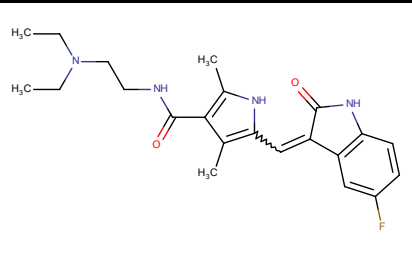
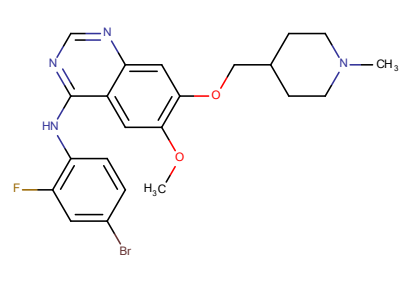
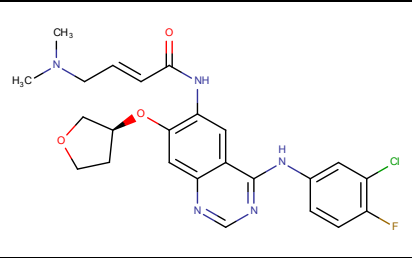
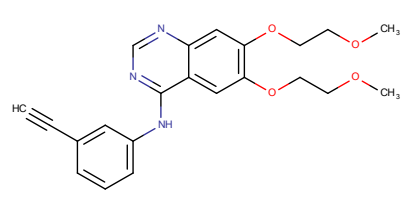
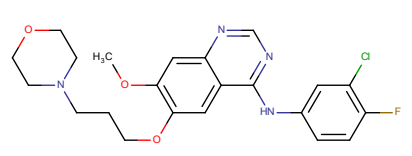
<sup>a</sup> where indications were approved separately, the first approved indication is noted, some KIs received simultaneous approval for multiple indications.

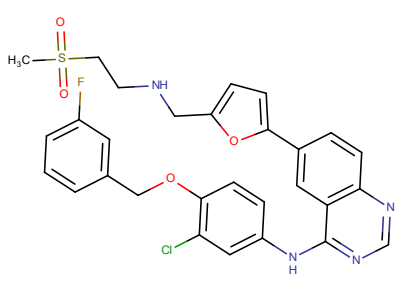
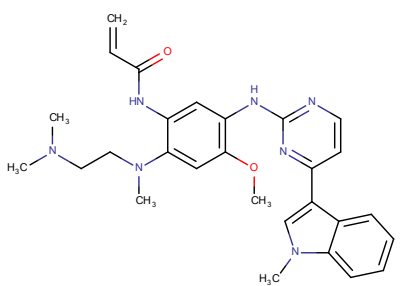
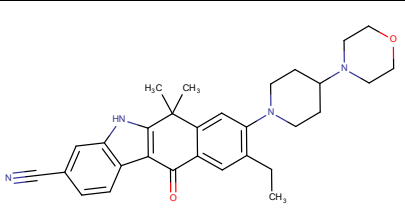
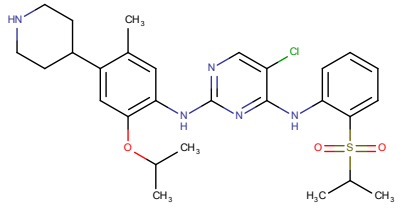
**Abbreviations:** ALL; acute lymphoblastic leukemia, BC; breast cancer, CLL; chronic lymphocytic leukemia, CML, chronic myelogenous leukemia, CRC; colorectal cancer, DFSP; dermatofibrosarcoma protuberans, FNHL; follicular B-cell non-Hodgkin lymphoma, GIST; gastrointestinal stromal tumors, HCC; hepatocellular carcinoma, IPF; idiopathic pulmonary fibrosis, MCL; mantle cell lymphoma, MEL; melanoma, MF; myelofibrosis, MTC; medullary thyroid cancer, NSCLC; non-small cell lung cancer, PC; pancreatic cancer, Ph+; Philadelphia chromosome positive, pNET; pancreatic neuroendocrine tumors, PV; polycythemia vera, RA; rheumatoid arthritis, RCC; renal cell carcinoma, SLL; small lymphocytic lymphoma, TC; thyroid cancer, WM; Waldenstrom's macroglobulinemia.

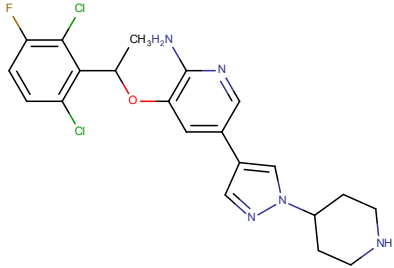
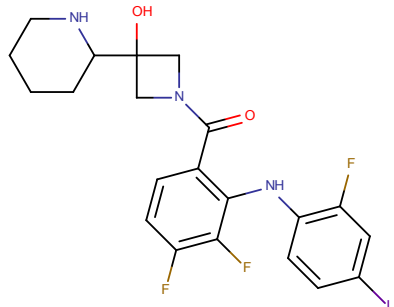
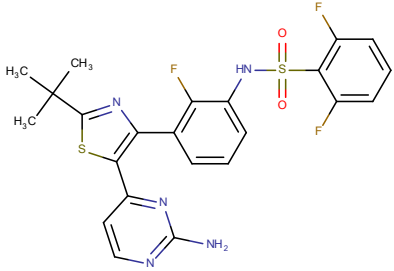
**Table 1.2: Summary of kinase inhibitor physiochemical properties**

Class	Agents	Structure	BCS Class	Physiochemical Properties						
				MW (Da)	ApKa / BpKa	Log P <sub>o:w</sub>	HBD	HBA	PSA (Å <sup>2</sup> )	Species
VEGF inhibitors	axitinib		II	386.47	12.7 / 4.3	4.2	2	4	96.0	N
	cabozantinib		II	501.51	- / -	5.4	2	7	98.8	N
	lenvatinib		IV	426.85	3.1 / -	2.8	3	5	115.6	A

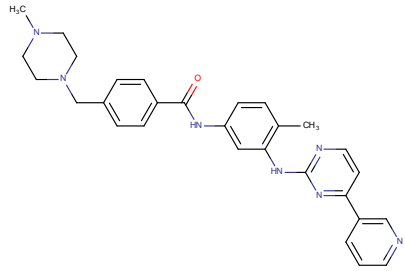
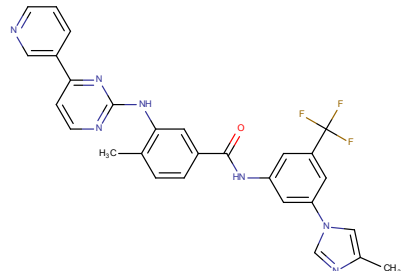
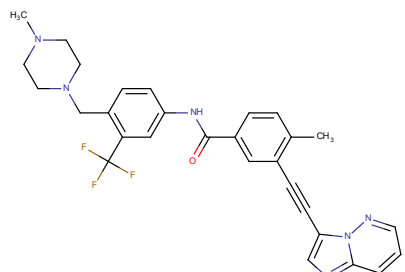
nintedanib		II or IV	539.62	- / 10.5	3.3	2	7	94.2	B
pazopanib		II	437.51	11.1 / -	3.1	2	8	127.4	N
regorafenib		II	482.82	12.0 / 2.3	4.2	3	8	92.4	N
sorafenib		II	464.82	9.5 / 9.6	4.1	3	7	92.4	B

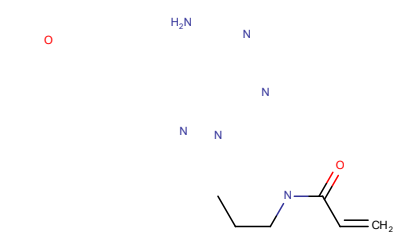
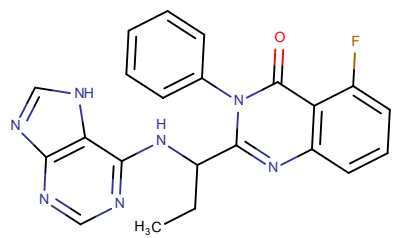
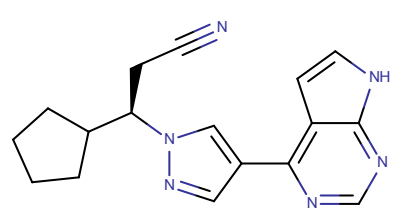
	sunitinib		II	398.47	- / 11.3	2.6	3	4	77.2	B
	vandetanib		II	475.35	- / 8.9	4.9	1	7	59.5	B
EGFR inhibitors	afatinib		IV	485.94	- / 0.6	3.6	2	8	88.6	N
	erlotinib		II	393.44	- / 5.3	3.3	1	7	74.7	N
	gefitinib		II	446.90	- / 7.0	4.1	1	8	68.7	N

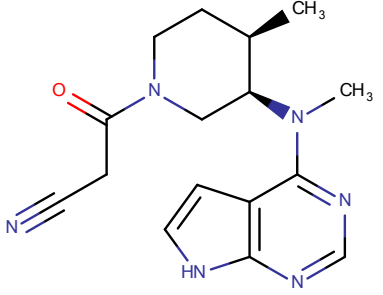
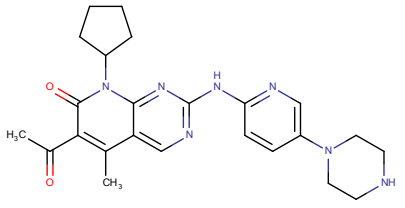
	lapatinib		IV	581.06	- / 6.3	5.1	2	9	114.7	N
	osimertinib		II	499.61	- / 8.9	3.7	2	7	87.5	B
ALK inhibitors	alectinib		IV	482.62	13.7 / 7.5	5.2	1	5	72.4	N
	ceritinib		IV	558.14	8.7 / -	6.4	3	8	113.6	N

	crizotinib		II	450.34	- / 9.8	3.7	2	6	78.0	B
BRAF / MEK inhibitors	cobimetinib		I	531.31	7.6 / 9.7	3.9	3	7	64.6	B
	dabrafenib		II	519.56	- / -	4.8	2	11	147.5	N



	imatinib		II	493.60	13.3 / 7.6	3.5	2	7	86.3	N
	nilotinib		IV	529.52	6.7 / 10.2	4.9	2	9	97.6	B
	ponatinib		II	532.56	- / 11.5	4.1	1	8	65.8	B

BTK inhibitors	ibrutinib		IV	440.50	- / 7.8	3.6	1	6	99.2	N
PI3K inhibitors	idelalisib		II	415.42	- / 6.3	3.7	2	7	99.2	N
JAK inhibitor	ruxolitinib		I	306.37	13.9 / 3.9	2.1	1	4	83.2	N

	tofacitinib		III	312.37	10.0 / 7.9	1.5	1	5	88.9	N
CDK inhibitor	palbociclib		IV	447.53	- / 8.7	1.8	2	8	103.4	B

**Abbreviations:** HBA; hydrogen bond acceptors, HBD; hydrogen bond donors, Log  $P_{o:w}$ ; octanol/water partition coefficient, MW; molecular weight, PSA; polar surface area.

**Table 1.3: Summary of kinase inhibitor pharmacokinetics**

Class	Agents	Standard Dose (mg)	BCS Class	PK Parameters							References
				F (%)	$f_{u,p}$	$C_{max}$ (ng/mL)	$t_{max}$ (hr)	$t_{1/2}$ (hr)	$V_d / F$ (L)	$CL / F$ (L/hr)	
VEGF inhibitors	axitinib	5 mg BD	II	58	< 0.01	28	2 - 6	3.3	180	38	(55, 56)
	cabozantinib	140 mg QD	II		< 0.003	608	2 - 5	28	349	11	(57)
	lenvatinib	24 mg QD	IV		0.02	655	1 - 4	35	336	6.7	(58)
	nintedanib	150 mg BD	II or IV	4.7	0.025	14	2-4	9.5	1050	83.4	OFEV (nintedanib) FDA prescribing information
	pazopanib	800 mg QD	II	21	< 0.01	44000	2 - 4	31	25	0.6	(59, 60)
	regorafenib	160 mg QD	II	69 - 83	0.005	3.45	4	14 - 58	88		(61)
	sorafenib	400 mg BD	II	< 50	< 0.005		3	25 - 48		8.1	(62, 63)
	sunitinib	50 mg QD <sup>a</sup>	II		0.05		6 - 12	60	2230	34	(64, 65)
	vandetanib	300 mg QD	II		0.06	130	6	220	4048	14	(66)
EGFR inhibitors	afatinib	40 mg QD	IV		0.054	25	4-6	34	2520	83	(67, 68)
	erlotinib	150 mg QD <sup>b</sup>	II	60 <sup>c</sup>	0.07	1760	4	36	232	5.3	(69, 70)

	gefitinib	250 mg QD	II	57	0.09		3 - 7	48	1400	36	(71, 72)
	lapatinib	1500 mg QD	IV		0.01		3 - 4	24	>2200	28	(73, 74)
	osimertinib	80 mg QD	II		"Low"		4	48	986	14	TAGRISSO (osimertinib) FDA prescribing information
ALK inhibitors	alectinib	600 mg BD	IV	37	< 0.01	665	4	33	4016	82	ALECENSA (alectinib) FDA prescribing information
	ceritinib	750 mg QD	IV	≥ 25		800	4 - 6	40	1916	33	(75)
	crizotinib	250 mg BD	II	43	0.09	100	4	42	1772	65	(76, 77)
BRAF / MEK inhibitors	cobimetinib	60 mg QD	I	46	0.05	273	2.5	44	806	14	(78) COTELLIC (cobimetinib) FDA prescribing information
	dabrafenib	150 mg BD	II	95	0.003	1324	2	6.5	70	17	(79) TAFINLAR (dabrafenib) FDA prescribing information
	trametinib	2 mg QD	II	72	0.026	22	1.5	115	214	4.9	(80) MEKINIST

											(trametinib) FDA prescribing information
	vemurafenib	960 mg BD	IV		< 0.01	42000	3	57	106	1.3	(81)
BCR-ABL inhibitors	bosutinib	500 mg QD	IV	18	0.05	114	6	23	6080	189	(82)
	dasatinib	100 mg QD <sup>d</sup>	II	< 34	0.04		3	3 - 5	2505	578	(83)
	imatinib	400 mg QD <sup>e</sup>	II	98	0.05		2 - 4	18	295	12	(84)
	nilotinib	300 mg BD <sup>f</sup>	IV	30	0.02	2260	3	17	579	29	(85)
	ponatinib	45 mg QD	II		0.01	45	< 6	36	1433	28	(86) ICLUSIG (ponatinib) FDA prescribing information
BTK inhibitors	ibrutinib	560 mg QD	IV	60	0.027	128	1 - 2	4 - 6	10000	62	(87) IMBRUVICA (ibrutinib) FDA prescribing information
PI3K inhibitors	idelalisib	150 mg BD	II		< 0.16	2168	2	8.2	216	15	(88) ZYDELIG (idelalisib) FDA prescribing information

JAK inhibitor	ruxolitinib	20 mg BD	I	95	0.03		1 - 2	3.0	65	< 22	JAKAFI (ruxolitinib) FDA prescribing information
	tofacitinib	5 mg BD	III	74	0.6	397	1.1	3.2	87	18.8	(89)
CDK inhibitor	palbociclib	125 mg QD	IV	46	0.15	116	6 - 12	29	2583	63	IBRANCE (palbociclib) FDA prescribing information

<sup>a</sup> standard dose for schedule 4/2 in GIST and RCC; lower dose of 37.5 mg QD for schedule 2/1 and pNET, <sup>b</sup> standard dose for NSCLC; lower dose of 100 mg QD for PC, <sup>c</sup> increases to ~100 % when taken with food, <sup>d</sup> standard dose for CML and ALL; higher dose of 140 mg QD for accelerated phase (AP) ALL or CML, <sup>e</sup> standard dose for ALL, CML and GIST; higher doses of 600 mg QD for AP ALL or CML, and 400 mg BD for DFSP, <sup>f</sup> standard dose for CML; higher dose of 400 mg BD for resistant or intolerant CML and AP CML.

**Abbreviations:** BD; twice daily,  $C_{max}$ ; maximum plasma concentration, CL/F; oral clearance, F; bioavailability,  $f_{u,p}$ ; fraction unbound in plasma, QD; once daily,  $t_{max}$ ; time to maximum plasma concentration,  $t_{1/2}$ ; elimination half-life,  $V_D/F$ ; apparent volume of distribution.

**Table 1.4: Metabolic enzymes and transporters involved in kinase inhibitor disposition**

Class	Agents	Metabolic enzymes			Transporters	FDA Guidance Regarding Use of Concomitant Medications Altering CYP3A4 Activity <sup>a</sup>		Reference
		Functionalisation	Conjugation	Active Metabolites		Strong Inducers	Strong Inhibitors	
VEGF inhibitors	axitinib	CYP3A4, CYP1A2	UGT	No			Avoid; reduce axitinib dose by 50%	(90)
	cabozantinib	Major: CYP3A4, Minor: CYP2C9		No		Avoid	Avoid	(57)
	lenvatinib	CYP3A4, aldehyde oxidase		Yes	P-gp, BCRP			(58)
	nintedanib	CYP3A4	UGT1A1, UGT1A7, UGT1A8, UGT1A10	No	P-gp	Avoid	Monitor	(91)
	pazopanib	Major: CYP3A4, CYP1A2, Minor:		No	P-gp, BCRP	Alterna	Avoid; reduce	(92)

		CYP2C8				te	pazopanib dose to 400 mg QD	
	regorafenib	CYP3A4	UGT1A9	Yes	MRP2, OATP1B1	Avoid	Avoid	(82)
	sorafenib	CYP3A4	UGT1A9	Yes	P-gp	Caution ; increase sorafenib dose, monitor		(90)
	sunitinib	CYP3A4		Yes	P-gp, BCRP	Increase sunitinib dose to 87.5 mg QD <sub>b</sub>	Reduce sunitinib dose to 37.5 mg QD <sup>c</sup>	(90)
	vandetanib	CYP3A4	FMO1, FMO3	Yes		Avoid		(66)
EGFR inhibitors	afatinib	CYP3A4	FMO3	No	P-gp, BCRP	<sup>d</sup> [P-gp: increase afatinib dose by 10 mg	<sup>d</sup> [P-gp: reduce afatinib dose by 10 mg until	(93)

						as tolerated]	tolerated ]	
	erlotinib	Major: CYP3A4, CYP3A5, Minor: CYP2C8, CYP2D6, CYP1A1, CYP1A2		Yes	P-gp, BCRP	Increase erlotinib dose	Reduce erlotinib dose	(90)
	gefitinib	CYP3A4, CYP3A5, CYP2D6, CYP1A1		Yes	BCRP	Increase gefitinib dose to 500 mg QD	Monitor	(90)
	lapatinib	Major: CYP3A4, CYP3A5, Minor: CYP2C19, CYP2C8		Yes	P-gp, BCRP, HOCT1, OATP1B1	Avoid	Avoid	(90)
	osimertinib	CYP3A		Yes	P-gp, BCRP	Avoid	Avoid	(94)
ALK inhibitors	alectinib	CYP3A4		Yes				(95)
	ceritinib	CYP3A4		No	P-gp	Avoid	Avoid; reduce ceritinib dose to 150 mg QD	(75)

	crizotinib	CYP3A4, CYP3A5		Yes		Avoid	Avoid	(96)
BRAF / MEK inhibitors	cobimetinib	CYP3A4	UGT2B7	No	P-gp	Avoid	Avoid	(78)
	dabrafenib	CYP3A4, CYP2C8		Yes		Avoid <sup>e</sup>	Avoid <sup>e</sup>	(97)
	trametinib	CYP3A4	UGT	No		Avoid <sup>e</sup>	Avoid <sup>e</sup>	(80)
	vemurafenib	CYP3A4		No	P-gp	Caution	Caution	(81)
BCR-ABL inhibitors	bosutinib	CYP3A4, CYP3A5		No		Avoid <sup>f</sup>	Avoid <sup>f</sup>	(82)
	dasatinib	CYP3A4	Minor: FMO-3 and UGT	Yes	P-gp, BCRP	Avoid; increase dasatinib dose	Avoid; reduce dasatinib dose to 20 mg QD <sup>g</sup> , monitor	(90)
	imatinib	Major: CYP3A4, CYP3A5, Minor: CYP1A2, CYP2D6, CYP2C9, CYP2C19, CYP1A1, CYP1B1	Minor: FMO-3	Yes	P-gp, BCRP, MRP4, OATP1A2, HOCT1	Avoid; increase imatinib dose by 50%, monitor clinical respons		(90)

						e		
	nilotinib	CYP3A4, CYP3A5, CYP2C8		No	P-gp, BCRP	Avoid	Avoid; reduce nilotinib dose, monitor QTc	(90)
	ponatinib	CYP3A4		Yes	P-gp		Reduce ponatinib dose to 30 mg QD	(86)
BTK inhibitors	ibrutinib	Major: CYP3A4 Minor: CYP2D6		Yes		Avoid	Avoid; reduce ibrutinib dose to 140 mg QD, monitor	(98)
PI3K inhibitors	idelalisib	Major: aldehyde oxidase Minor: CYP3A4	UGT1A4	Yes	P-gp	Avoid	Avoid	(88)
JAK inhibitor	ruxolitinib	CYP3A4		Yes			Reduce ruxoliti nib dose to 10 mg BD,	(99)

							monitor <sup>h</sup>	
	tofacitinib	Major: CYP3A4, Minor: CYP2C19		No			Reduce tofacitinib dose to 5 mg QD	(89)
CDK inhibitor	palbociclib	CYP3A	SULT2A1	No		Avoid	Avoid; reduce palbociclib dose to 75 mg QD	(100)

<sup>a</sup> **Descriptors regarding FDA labelling:** Alternate: Consider an alternate concomitant medication, Avoid: Avoid use of concomitant medication, Caution: Continuous concomitant administration, Monitor: monitor closely for tolerability (unless specified otherwise). <sup>b</sup> Dose escalation for standard 50mg dose, for lower dose of 37.5 mg dose escalation to 62.5 mg recommended. <sup>c</sup> Dose reduction for standard 50mg dose, for lower dose of 37.5 mg dose reduction to 25 mg recommended. <sup>d</sup> No advise specified regarding concomitant administration of drugs affecting CYP3A4 activity. <sup>e</sup> Advice specified for concomitant use of strong inducers or inhibitors of CYP3A4 and CYP2C8. <sup>f</sup> Advice specified for concomitant use of moderate and strong inducers or inhibitors of CYP3A4/5. <sup>g</sup> Dose reduction for standard 100mg dose, for higher dose of 140 mg dose reduction to 40 mg recommended. <sup>h</sup> In patients with a platelet count greater than or equal to  $100 \times 10^9 /L$ ; avoid in patients with platelet counts less than  $100 \times 10^9 /L$ .

## 1.5 Pharmacokinetics

For many KIs disposition is directly linked to the physicochemical properties of the drug. By way of example, most KIs are either neutral or weak basic compounds and pKa is strongly associated with pH dependent solubility (discussed in section 1.5.3). The physicochemical properties of individual KIs are summarised in **Table 1.2**. SMILES strings obtained from the PubChem database (<https://pubchem.ncbi.nlm.nih.gov/>) were used to generate 2-dimensional structures in Marvin. Calculator Plugins were then used to calculate structural properties (Marvin 16.4.18.0, 2016, ChemAxon, <http://www.chemaxon.com>). Mean pharmacokinetic (PK) parameters describing patient exposure to individual KIs (bioavailability; F, fraction unbound in plasma;  $f_u$ , maximum plasma concentration;  $C_{max}$ , time to maximum plasma concentration;  $t_{max}$ , elimination half-life;  $t_{1/2}$ , apparent volume of distribution;  $V_D/F$ , and oral clearance;  $CL/F$ ) are summarised in **Table 1.3**.

### 1.5.1 Absorption and Distribution

With the exception of sunitinib (6 – 12 hrs), KIs achieve a peak plasma concentration within 6 hrs of oral dosing (46, 101, 102). Oral bioavailability differs between KIs, ranging from 20 % for pazopanib up to 95 % for dabrafenib, primarily due to differences in the rate and extent of gastrointestinal absorption. In addition to differing between KIs, gastrointestinal absorption for individual KIs is affected by multiple environmental and physiological factors (discussed in section 1.5.3) resulting in substantial inter- and intra- individual variability in exposure (103). As KIs are typically ‘low clearance’ substrates for metabolic pathways (i.e.  $E_H < 0.2$  or  $CL_H < 18$  L/hr) factors affecting gastrointestinal and first-pass metabolism such as drug-drug interactions (DDIs) have a minor effect on bioavailability (104). Multiple KIs including nilotinib and sorafenib exhibit non-proportional increases in exposure with dose escalation, which may be due to factors such as saturation of absorption sites or transporter (p-

glycoprotein; P-gp) mediated interactions (105, 106). KIs are highly protein bound ( $f_u < 0.1$ ) and distribute extensively into tissue. As such, KIs are characterised by a volume of distribution ( $V_d$ ) in excess of total body water, typically in the order of 100s to 1,000s of litres, but in some cases as high as 10,000 L (ibrutinib), and a prolonged terminal half-life, frequently ranging from 24 to 48 hrs. Notably, the  $V_d$  for more basic KIs tends to be higher than that of neutral KIs.

### 1.5.2 Metabolism and Elimination

KIs are primarily cleared from the systemic circulation through hepatic metabolism and biliary excretion, with elimination of unchanged drug in urine accounting for  $< 10\%$  of total systemic clearance (90, 101, 102). As such, inter-individual variability in hepatic and biliary, but not renal, clearance pathways are potential sources of variability in KI exposure. The key enzymes and transporters involved in the elimination of individual KIs are summarised in (**Table 1.4**). Many KIs including axitinib, bosutinib, dasatinib, erlotinib, gefitinib, imatinib, lapatinib, nilotinib, sorafenib and sunitinib primarily undergo cytochrome P450 (CYP) 3A4-catalysed oxidative metabolism. This serves as both a metabolic activation and clearance pathway, with other CYP (primarily 2C sub-family and 2D6) and UDP-glucuronosyltransferases (primarily UGT1A9) playing lesser roles (90). A notable exception being idelalisib, which is primarily metabolised by aldehyde oxidase, with lesser contributions from CYP3A4 and UGT1A4. With the exception of dasatinib, KIs are also substrates and/or inhibitors for the efflux and influx transporters P-gp and organic anion transport peptide 1B1 (OATP1B1). KI elimination is primarily determined by hepatic clearance via CYP3A4-mediated oxidative pathways, and P-gp-mediated biliary excretion (90, 102).

However, in addition to being substrates for CYP3A4, multiple KIs are also potent competitive inhibitors of this enzyme with  $K_i$  values in the sub- to low- micromolar range (107). As such,

these KIs have the potential to inhibit their own metabolism resulting in low  $k_m$  / saturable metabolism (108). Additionally, multiple KIs including crizotinib cause time dependent inhibition of CYP3A4, and as such have the capacity to cause auto-inhibition. Accordingly, it is postulated that with chronic dosing metabolism via alternate CYP pathways may contribute significantly to systemic clearance. Notable in this regard is evidence demonstrating a minimal effect of ritonavir, a potent inhibitor of CYP3A4, on the steady-state PK of imatinib (109). Limited recent complementary *in vitro* data support a potential role of CYP2C8 interactions and polymorphisms as a source of inter-individual variability in steady-state imatinib elimination (110)

### 1.5.3 Inter-Individual Variability in Absorption

As lipophilic organic bases (111) KIs are typically Biopharmaceutics Classification System (BCS) class II or class IV drugs that exhibit either low solubility and high permeability (class II) or low solubility and low permeability (class IV) (**Table 1.4**). Many KIs including axitinib, crizotinib, dasatinib, erlotinib, gefitinib, lapatinib, nilotinib, pazopanib, sunitinib and vandetanib exhibit pH-sensitive solubility (105), with a rapid and marked reduction in solubility above a pH of 2.0 (112). As such, co-administration of acid-suppressing agents (e.g. antacids, proton-pump inhibitors and H<sub>2</sub>-antagonists), which increase gastrointestinal pH from approximately 1.0 to 4.0, is postulated to impair gastrointestinal KI absorption leading to a reduction in exposure and potential failure of therapy (105). This interaction is supported by evidence of reduced  $C_{max}$  and area under the plasma concentration time curve (AUC) for axitinib, dasatinib, erlotinib, gefitinib and nilotinib when administered with, or shortly after, acid-suppressing agents (105). Recent evidence suggest that the effect of concomitant proton pump inhibitor (PPI; esomeprazole) use on erlotinib bioavailability may be overcome by co-administration of erlotinib with an acidic beverage (cola) (113). Co-administration of cola with

erlotinib in patients not treated with a PPI had a marginal effect on erlotinib bioavailability.

Since many KIs are both highly lipophilic and exhibit pH-dependant solubility, the impact of food consumption on absorption is complex and dependent on a number of variables including meal volume and timing, caloric, liquid, fat and carbohydrate content, temperature, and physical composition (114). Consistent with this complexity there are variable reports regarding the impact of food consumption on KI absorption. Differences in bioavailability between fed- and fasting- states have been reported for at least six KIs (115, 116). However, despite exhibiting pH-sensitive solubility, sunitinib bioavailability is apparently not influenced by food consumption (117). When considering evidence for the impact of food consumption on KI absorption it is important to acknowledge the challenges associated with characterising these complex effects even under controlled conditions. By way of example lapatinib bioavailability, which does differ between fed- and fasting- states, may be increased between 2.7- and 4.3- fold depending on the fat content of the meal (118). Given the inconsistent impact of food consumption on KI absorption, recommendations for dosing in the fasted state in order to achieve consistent therapeutic exposure are supported. As KIs are typically low hepatic clearance drugs ( $E_H < 0.2$ ,  $CL_H < 18$  L/hr), factors affecting gastrointestinal and first-pass metabolism such as drug-drug interactions (DDIs) have a minor effect on bioavailability (104).

#### **1.5.4 Inter-Individual Variability in Metabolism and Elimination**

As KIs are primarily 'low  $CL_H$ ' CYP substrates the rate of clearance is affected by  $f_u$  and intrinsic enzyme activity ( $CL_{int}$ ) (104). Clinically relevant inter-individual variability in CYP3A4, P-gp and OATP1B1 activities due to inherent (age, gender, pharmacogenetic) and environmental (diet, disease, polypharmacy) factors is well established (119, 120). Multiple covariates may lead to inter- and intra- individual variability in KI exposure. Given the broad and inter-related substrate, inducer and inhibitor profiles of CYP3A4 and P-gp (121, 122), and

the high prevalence of polypharmacy in older cancer patients to address multiple comorbidities and KI related toxicities (123), DDIs involving weak / moderate inducers or inhibitors of CYP3A4 and P-gp represent potential sources of inter-individual variability in KI exposure. This variability in KI exposure is frequently clinically relevant and can manifest as therapeutic failure due to reduced tumour exposure resulting from enhanced clearance or impaired uptake, or toxicity due to increased systemic exposure resulting from impaired clearance or enhanced uptake (122). Notably, with the exception of alectinib and lenvatinib, FDA labelling for all approved KIs advise avoiding concomitant use of strong CYP3A4 inducer and or inhibitors, and specify dose modifications where concomitant use cannot be avoided typically with monitoring of tolerability and/or efficacy. Indeed, multiple medications including verapamil, erythromycin, clarithromycin, fluconazole and itraconazole have been reported to increase KI exposure, predisposing patients to toxicity and reducing tolerability, by reducing CYP3A4 and P-gp activities (69).

## **1.6 Addressing Inter-Individual Variability in Exposure**

The use of KIs is commonly associated with a lack of treatment response (i.e. therapeutic failure). As ‘targeted therapies’, despite limiting clinical trials to individuals on the basis of pharmacodynamic characteristics (e.g. tumour histology and genotype) associated with efficacy, response rates in the range 36 to 78 % are routinely reported (90). Similarly, KI therapy is commonly associated with severe adverse drug reactions (ADRs), in particular Grade 3 fatigue, hypertension, gastrointestinal, hepatobiliary and skin toxicities. The frequency of severe ADRs that necessitate cessation of therapy or modification of dosing regimens differs between individual KIs and classes, but is typically clinically relevant. By way of example, KIs that inhibit VEGFR, such as axitinib, pazopanib, sorafenib and sunitinib are associated with

cardiovascular toxicities such as grade 3 hypertension, thromboembolism and bleeding (124).

While a proportion of the therapeutic failures and ADRs associated with KI use are unavoidable, by addressing inter-individual variability in KI exposure and ensuring optimal exposure through precision KI dosing, it is plausible that the incidence of sub-optimal outcomes may be minimised. Multiple approaches have been proposed to facilitate precision KI dosing, each with potential advantages and limitations. When selecting a precision dosing strategy for KIs, the criteria that are likely to be associated with the greatest clinical benefit include the capacity to (i) identify patients at greatest risk of significant under- or over- dosing from fixed-dose prescribing, (ii) account for all potential sources of inter-individual variability in exposure in a cohort of clinically complex patients, and (iii) minimise impact on compliance due to increased complexity of dosing instructions. Additionally, when evaluating the potential utility of precision KI dosing strategies broader considerations such as the strength of evidence, capacity to generate evidence of suitable quality, clinical judgement and patient preferences must also be addressed.

### 1.6.1 Therapeutic Drug Monitoring

A benefit from individualising KI dosing on the basis of plasma-KI concentration has been reported for a panel of KIs (44, 79, 80) and target PK parameters, typically steady-state trough concentration ( $C_{ss\_trough}$ ), have been proposed for multiple KIs and indications (125) (**Table 1.5**). When considering the evidence underpinning therapeutic drug monitoring (TDM) guided KI dosing it is important to acknowledge that proposed target  $C_{trough}$  values are often derived by secondary analysis of data from clinical trials, generally Phase-I dose escalation studies. By definition, these studies are not fundamentally designed to address questions regarding precision dosing as they are often conducted in unselected patient cohorts including terminally ill patients and do not accurately represent the intended patient population. Additionally, the

sample size of Phase I studies is usually very low compared to later trials. These observational analyses involve correlation of markers of exposure ( $C_{\text{trough}}$  or AUC) and efficacy (including response, response rate, progression free and overall survival). Furthermore, many associations between KI exposure and efficacy (126-128) are characterised by ‘continuous’ rather than ‘quantal’ (clearly discriminated) relationships. As such, in the absence of pre-specified assessment criteria, target  $C_{\text{trough}}$  values are subject to arbitrary determination with a substantial risk of bias. This does not entirely negate the value of this evidence but, rather, means that caution must be applied when interpreting established targets. Indeed, acknowledging these limitations, de Wit et al. (125) propose that there is currently sufficient evidence to apply target  $C_{\text{trough}}$  for three KIs; imatinib (1,100  $\mu\text{g/L}$ ), sunitinib (37.5  $\mu\text{g/L}$  with continuous dosing, 50  $\mu\text{g/L}$  with intermittent dosing) and pazopanib (20,000  $\mu\text{g/L}$ ). Notably, in contrast to the traditional application of TDM where target concentrations are determined for both minimal (ensuring efficacy) and maximal (avoiding toxicity) exposure, despite reported associations between exposure and toxicity for many KIs (125), TDM-guided KI dosing currently focusses on ensuring exposure above a minimal target  $C_{\text{trough}}$ . The role of maximal exposure targets remains to be addressed for these drugs.

When considering the feasibility of definitively characterising robust target PK parameters logistical and financial considerations must also be considered. Based on published data, it was reported that in order to achieve 80 % power to demonstrate improved clinical outcomes associated with TDM-guided sunitinib dosing for gastrointestinal stromal tumours (GIST), a prospective trial would require at least 600 subjects with a 2-year follow-up (129). As sample size is inversely related to the effect size, considering that this calculation was performed in a context of a large observational effect, whereby a much small effect may still be considered significant, it is likely that the actual sample size required to justify a benefit and cost-effectiveness for TDM-guided KI dosing may, in fact, be even larger than has been reported.

The universal implementation of TDM-guided KI dosing also requires substantial development in terms of analytical platforms with the capacity to quantify plasma concentrations for this rapidly expanding class of drugs. Liquid chromatography (LC) based approaches with detection by ultra violet (UV) absorbance or mass spectrometry (MS) have been reported for the quantification of plasma concentrations of many KIs. However, these approaches are typically designed to facilitate the analytical requirements of a specific study. Approaches utilising UV detection normally facilitate the measurement of only a single KI, and as such are of limited utility in terms of TDM platforms. Recently, a number of multi-analyte LC-MS based approaches with the capacity to quantify between 3 and 9 KIs have been reported. Continued development and expansion of these analytical platforms is critical to facilitate this approach. Additionally, with routine analytical platforms achieving much higher sensitivity the potential use of micro-sampling techniques such as blood spot analysis warrant attention as these techniques facilitate less invasive sample collection for cancer patients, particularly in paediatric patients. The comparative merits of quantifying total versus unbound plasma KI concentrations remains to be considered. Analytical approaches such as MS may have the capacity to accurately quantify unbound KI concentrations despite their low total plasma concentration and extensive protein binding. However, given the analytical challenges demonstrated when determining  $f_u$  for KIs by standard approaches such as equilibrium dialysis (111) due to the low aqueous solubility of these drugs, determination of absolute unbound plasma KI concentration is likely to be equally challenging.

**Table 1.5: Kinase inhibitor pharmacokinetics associated with superior clinical outcomes**

KI	Indication	Sample size	PK Parameter	Reference
axitinib	RCC	168	$AUC_{0-24} > 300 \mu\text{g/L/hr}$	(128)
		109	$AUC_{SS} > 605 \mu\text{g/L/hr}$	(130)
erlotinib	NSCLC	56	$C_{\text{trough}} > 1,810 \mu\text{g/L}$	(131)
gefitinib	NSCLC	30	$C_{\text{trough}} > 200 \mu\text{g/L}$	(132)
imatinib	CML	605 <sup>a</sup>	$C_{\text{trough}} > 1,000 \mu\text{g/L}$	(133, 134)
	GIST	73	$C_{\text{trough}} > 1,100 \mu\text{g/L}$	(126)
nilotinib	CML <sup>b</sup>	30	$C_{\text{trough}} > 761 \mu\text{g/L}$	(135)
	CML <sup>c</sup>	455	$C_{\text{trough}} > 829 \mu\text{g/L}$	(136)
pazopanib	RCC	10	$C_{\text{trough}} > 15,000 \mu\text{g/L}$	(92)
		205	$C_{\text{trough}} > 20,500 \mu\text{g/L}$	(137)
	HCC	28	$C_{\text{trough}} > 20,000 \mu\text{g/L}$	(138)
sorafenib	HCC	36	$C_{\text{max}} > 4,780 \mu\text{g/L}$	(139)
sunitinib	RCC	146	$AUC_{SS} > 800 \mu\text{g/L}$ <sup>d</sup>	(140)
	GIST	278	$AUC_{SS} > 600 \mu\text{g/L}$ <sup>e</sup>	(140)

<sup>a</sup> total sample size across two studies, individual study samples sizes of 351 and 254 patients,

<sup>b</sup> imatinib pre-treated CML <sup>c</sup> untreated (newly diagnosed CML) <sup>d</sup> intermittent dosing

extrapolated to combine  $C_{\text{trough}}$  for sunitinib and desethyl-sunitinib (active metabolite) of  $> 50$

$\mu\text{g/L}$ , <sup>e</sup> continuous dosing, extrapolated to combine  $C_{\text{trough}}$  for sunitinib and desethyl-sunitinib

(active metabolite) of  $> 37.5 \mu\text{g/L}$

## 1.6.2 Other existing strategies

### 1.6.2.1 Toxicity Guided Dosing

Toxicity based KI dosing strategies have recently been considered as simple and practical alternatives to TDM-guided KI dosing (141, 142). In broad terms these approaches are used to optimise KI dosing based on the presence (or absence) of particular toxicities. There are subtle nuances in the potential application of these strategies. Firstly, in a similar manner to the application of target  $C_{\text{trough}}$  for TDM-guided KI dosing, efficacy-related toxicities (e.g. increases in blood pressure with VEGFR inhibitors (143)) may be targeted as predictive indicators of efficacy (toxicity-guided dosing). Alternatively, in a more crude approach, KI dose may be commenced at a threshold of unacceptable toxicity then adjusted in order to maximise the exposure and hence efficacy (toxicity-adjusted dosing; section 1.6.2.2).

Recent studies have evaluated the feasibility of utilizing on-target toxicities as surrogate indicators of efficacy for multiple classes of KIs (144). Foremost amongst these associations is increasing evidence that induction of hypertension resulting from disruption of VEGFR-mediated angiogenesis reflects adequate pharmacological activity of VEGFR inhibitors (143). However alternate mechanisms of KI-induced hypertension cannot be discounted (145) and may confound associations. As such, additional studies are required to characterise VEGFR inhibitor induced hypertension and the potential impact of confounding factors before this marker can be used in routine practice. Similarly mechanistic, albeit complex, evidence linking VEGFR inhibition with proteinuria indicates that the efficacy of VEGFR inhibitors may correlate with the incidence of on-therapy proteinuria. However, there is limited clinical evidence to substantiate this association. Notably, a recent pooled analysis of phase III studies involving metastatic renal cell carcinoma (mRCC) patients treated with pazopanib or sunitinib demonstrated that a number of covariates including Asian ethnicity, history of diabetes, blood

pressure, pre-existing proteinuria and prior nephrectomy were independent predictors of on-therapy proteinuria. The latter was associated with improved survival (146). Conversely, while the precise mechanism of KI induced hypothyroidism is poorly understood, associations between clinical outcomes and the incidence of hypothyroidism have been reported for multiple VEGFR inhibitors including axitinib, sorafenib and sunitinib (147-149). As for hypertension, additional studies are required to characterise associations with proteinuria and hypothyroidism, the potential impact of confounding factors and survival outcomes before these markers can be used in routine practice. There is extensive literature evaluating associations between the presence and severity of skin rash and clinical efficacy in patients treated with EGFR inhibitors such as erlotinib and gefitinib across a range of malignancies (150-154), although the impact of external factors on the predictive value of skin reactions remains to be addressed. Notably a phase II 'dosing-to-rash' dose escalation study with erlotinib failed to demonstrate correlations between exposure and either rash severity or response (155). In evaluating the role of toxicity-guided KI dosing strategies, it is critical to note that individual KIs exhibit distinct toxicity profiles, and that associations with exposure and / or efficacy have been evaluated for a limited panel of KIs.

### **1.6.2.2 Toxicity Adjusted Dosing**

Toxicity-adjusted dosing (TAD) has been used in medical oncology for many years, where severe toxicity (e.g. myelosuppression, peripheral neuropathy) is a common limiting determinant of dose intensity for many intravenously (IV) administered systemic cytotoxic anticancer drugs (156). For systemic cytotoxic anticancer drugs there is a strong association between dose intensity and the efficacy of a regimen whereby reductions in dose intensity have been shown to compromise both the effectiveness of a regimen and patient survival, leading to a negative perception of this approach. However, the continuous nature of the relationship between KI exposure and efficacy (126-128, 140, 157), which underpins an implication that

maximising exposure will maximise efficacy, supports the concept that maximising KI exposure to a point of unacceptable toxicity via TAD may be associated with optimal efficacy outcomes.

When considering the application of TAD (typically involving dose reduction), the negative perception regarding a potential loss of efficacy (158) must be addressed. Notably, for multiple KIs in contrast to this perceived negative impact of dose reduction of efficacy, studies have demonstrated either minimal impact or paradoxical improvement in efficacy among patients requiring dose reduction (159, 160). Significant in this regard, a retrospective analysis of two studies of mRCC with sunitinib indicates that, despite exhibiting comparable exposures (measured as  $C_{\text{trough}}$ ), patients who required dose reduction due to toxicity had superior PFS compared to patients who could tolerate the recommended dose. Similarly, it has been demonstrated that the use of a modified sunitinib dosing schedule for mRCC (i.e. 2 wks treatment / 1 wks break) in patients who are unable to tolerate the standard dosing schedule (i.e. 4 wks treatment / 2 wks break) due to severe toxicity is not associated with inferior outcomes (161, 162). Furthermore, a retrospective analysis demonstrated that patients who tolerated the standard sunitinib dosing schedule with minimal or no toxicity had inferior survival outcomes compared to those who experienced  $\geq$  grade 2 toxicity (161).

An additional consideration for KI TAD strategies that is not an issue for IV systemic cytotoxic anticancer drugs is the potential negative impact on treatment compliance. Any negative impact would need to be addressed given that improving compliance to KI dosing is already an emerging issue in oncology practice, with adherence rates as low as 16 % reported for some KIs (163). Furthermore, in addition to considerations regarding compliance in the presence of severe toxicity, it is necessary to consider the potential risk of underreporting of toxicity due to patient concerns regarding treatment interruption, which is estimated to occur in up to 66 %

of cases (164). In order to address these issues, patient engagement and education must be a core component of any TAD approach.

Given the comparable time-course of TDM and TAD strategies, it is plausible that these approaches may be applied in either an alternative or complementary manner to achieve precision KI dosing. While TAD has an established role in oncology practice, there is limited specific evidence for KI TAD strategies. The strongest evidence for this approach comes from a longitudinal study of TAD for sunitinib in patients (n =27) with mRCC, which did demonstrate a significant reduction in inter-patient variability in exposure, with 89 % of patients achieving target exposure ( $C_{\text{trough}} > 50 \text{ ng/mL}$ ) (142). Substantial additional trials to evaluate the comparative benefit of TDM and TAD strategies are warranted.

### **1.6.2.3 Target Concentration Intervention**

The approach of TDM and TAD can also be used in combination and is referred to as Target Concentration Intervention (TCI). This approach allows optimisation of efficacy and toxicity simultaneously on an individual basis rather than a population approach like TDM. The TCI approach finds the ideal concentration for an individual patient where efficacy is maximum and toxicity is acceptable or negligible. Thus when any interacting drug is added to therapy or a significant covariate changes, measuring a concentration and then dose adjusted can be used to ensure the patient returns back to their ideal (target) concentration (165).

### **1.6.2.4 Pharmacogenetic Testing**

Pharmacogenomics (PGx) is generally considered among the best established and most important approaches to facilitate personalised medicine. Indeed, when considering targeted anti-cancer drugs, there are numerous examples where PGx is used to guide treatment decisions, such as selection of mAb therapy for the treatment of metastatic colorectal cancer (mCRC) (166-168). While substantial efforts have been made to elucidate direct CYP3A4

genotypes associated with increased or decreased catalytic activity, there has been limited success. Of the reported CYP3A4 genotypes associated with altered substrate turnover only the CYP3A4\*22 allele is considered clinically relevant and given the low frequency of this allele (5-7% in Caucasian populations) (169), testing is unlikely to account for much of the observed inter-individual variability in CYP3A4 activity. Intriguingly, emerging data suggest that PGx testing for transcription factors involved in the regulation of CYP3A4 may be a more promising PGx approach for this enzyme (170), although quantitative data are currently lacking. While there is some evidence that the contribution of CYP3A4 decreases with chronic dosing, there is currently no evidence demonstrating that pharmacogenetic testing for other CYP accounts for variability in KI exposure. Given the major role of CYP3A4 in determining KI exposure, while potentially useful as an adjunct, it is unlikely that PGx alone will be sufficient to guide KI dosing.

#### **1.6.2.5 *In vivo* Pathway Phenotyping**

*In vivo* pathway phenotyping (IVP) has been proposed as a novel approach to account for inter-individual variability in KI exposure (171). While routinely used in drug development, in particular in the evaluation of drug-drug interactions, with the exception of creatinine clearance as a marker of renal function, IVP is not routinely used to evaluate drug exposure in clinical practice. IVP typically involves administering a sub-therapeutic dose of a rapidly cleared surrogate probe drug or cocktail of probe drugs that are substrates for the pathways involved in the disposition of the drug of interest, with the collection of a series of timed blood samples, typically over a 4 to 8 hr period (172). For KIs, in a research setting IVP for CYP3A4 and P-gp has been demonstrated to correlate with sunitinib clearance and risk of toxicity, but did not fully account for inter-individual variability in exposure (171). This observation is consistent with a contribution of variability in sunitinib gastrointestinal absorption, which cannot be accounted for using this approach. As such, while potentially useful for facilitating initial dose

stratification and identifying patients at the highest risk of sub-optimal outcomes requiring robust TDM follow-up, like PGx, IVP is unlikely to yield sufficient insights to independently guide KI dosing (171).

Furthermore, while IVP may assist in predicting KI exposure, the application of this approach to oncology practice is likely to be hindered by financial implications, logistical complexity and potential adverse consequences associated with administering additional drugs and blood sampling over several hours. In particular, while safe and feasible in healthy volunteers, the process of administering probe drugs and collecting blood samples via cannulation typically over a period of 6 to 12 hrs may result in complications in frail cancer patients. A more desirable approach may be to utilise phenotypes based on endogenous markers of the key pathways involved in KI disposition, in much the same way that plasma-creatinine concentration is used as a marker of renal function, and hence the dosing of renally cleared drugs. While a number of endogenous compounds have been demonstrated to reflect changes in CYP3A4 activity resulting from inhibition or induction (173), there are currently no established endogenous markers of absolute activity for CYP3A4. Coproporphyrins I and III have been proposed as potential endogenous functional markers of OATP1B activity based on the findings of *in vitro* (cell line, human and monkey hepatocytes) and pre-clinical animal (oatp1a/1b knock-out mice and cynomolgus monkey) studies (174). There are no human data to support the use of coproporphyrins I and III or any other endogenous compound as a marker of absolute activity for P-gp or OATP1B1. Given the potential application in terms of guiding drug dosing further studies to elucidate endogenous markers of CYP3A4, P-gp and OATP activities are warranted.

## 1.7 Hypothesis and Aims

The general hypothesis underpinning this thesis is that precision dosing strategies can be used to optimise KI dosing in order to maximise efficacy and minimise toxicity. In order to address this overarching hypothesis, a series of complementary studies were performed to address sub-hypotheses. These sub-hypotheses were addressed with the following specific aims:

**Hypothesis 1:** Physiologically based pharmacokinetic (PBPK) models built using *in vitro* data trained on clinical trial reports may be used to identify drivers of variability in KI exposure.

**Aim 1:** Investigate the *in vitro* substrate depletion kinetics for a panel of EGFR inhibitors in the presence of mixed CYP and UGT cofactors, specific and non-selective inhibitors to characterise the kinetics and enzyme involvement in hepatic clearance for these drugs.

**Aim 2:** Evaluate PBPK modelling as a strategy to characterise the impact of physiological covariates and drug-drug interactions as sources of variability in EGFR inhibitor exposure.

The studies performed to address Aim 1 identified CYP3A4 as a key protein involved in determining KI exposure, and identified ethnicity as potential, currently uncharacterised, source of variability in KI exposure.

**Hypothesis 2:** Development of strategies that provide the capacity to characterise variability in CYP3A4 will facilitate marked advances in the ability to define KI exposure.

**Aim 3:** Assess inter-racial variability in CYP3A4 activity and inducibility among healthy adult males of Caucasian and South Asian ancestry using an *in vivo* pathway reaction phenotyping trial.

**Aim 4:** Investigate dietary markers of CYP3A4 as a means of phenotyping individuals to characterise variability in the activity of this enzyme.

**Hypothesis 3:** It is possible to address the limitations of existing analytical platforms and precision dosing strategies by applying advances in analytical platforms and technologies.

**Aim 5:** Apply an ultra-performance liquid chromatography (UPLC) – mass spectrometry (MS) based assay for the quantification of TKIs as a platform for TDM

**Aim 6:** Apply the PBPK modelling and TDM precision dosing strategies developed in Chapter II and IV to case studies to demonstrate the potential clinical application of these techniques

Taken together, the studies undertaken through this thesis have developed, verified and demonstrated the application of two strategies to facilitate precision dosing of KIs in a manner that overcomes limitations of existing strategies.

---

# CHAPTER II: ASSESS PBPK MODELLING AS AN APPROACH TO EVALUATE VARIABILITY IN EGFR KI EXPOSURE

---

*The results presented in this chapter have*

*been reported in:*

van Dyk M, Rowland A (2017) Physiologically-based pharmacokinetic modelling as an approach to evaluate the effect of covariates and drug-drug interactions on variability in epidermal growth factor receptor kinase inhibitor exposure. *Translational Cancer Research*, 10: 1600-1615.

## 2.1 Introduction

As described in Chapter I environmental, demographic, and genetic factors can affect exposure to kinase inhibitors, resulting in inconsistencies in clinical response to these drugs in patients (175, 176). In particular, inter-individual variability in drug exposure has been widely reported in a number of studies where a large proportion of patients experience either a lack of efficacy due to sub-therapeutic dosing or toxicity as a result of excessive dosing (122, 177).

As NSCLC is responsible for the highest number of cancer related deaths globally, EGFR KIs are frequently prescribed to terminally ill patients at high doses therefore a number of EGFR KIs were selected to develop models to characterise exposure and to examine covariates likely to predict differences in exposure between populations. It is well established that afatinib, erlotinib and gefitinib are extensively metabolised by CYP 3A4. Wide inter- and intra-individual variability in the activity of this enzyme due to factors effecting expression is widely reported. In addition, these EGFR KIs are also substrates for various transporters, OATP1B1 P-gp, in the intestinal tract and liver, which are all known to impact on exposure (90, 125, 178, 179).

In addition to the many physiological factors, that influence exposure to EGFR KIs, given the environment that they are prescribed in, it is very likely that patients are co-administered other medications. Many commonly prescribed medications such as antibiotics (e.g. clarithromycin) and antifungals (e.g. fluconazole) are also metabolised by CYP3A4 and are known to alter the activity of this enzyme, and consequently may alter EGFR KI exposure. Given that patients receive a standard fixed dosing regimen, it is no surprise that significant inter-individual variability is an issue. Although, many clinicians recognise this, and research toward optimal EGFR KI dosing has received significant attention, the solution is still unclear and currently unaddressed in clinical practice due to a lack of prospective evidence. Therefore, to assist in

optimised EGFR KI dosing, the pharmacokinetics and hence exposure to these drugs is a key research focus.

Physiologically based pharmacokinetic (PBPK) modelling, is a mechanistic ‘bottom up’ approach, whereby the concentration-time profile for a drug in a particular patient cohort is simulated based on the physiochemical and *in vitro* kinetics of the drug and the physiological characteristics of the patient cohort. PBPK modelling is routinely utilised for the prediction of pharmacokinetic behaviour of new chemical entities during drug development, where it can be applied to investigate the potential impact of covariates such as age, gender, and metabolic drug-drug interactions (DDIs) on drug exposure in various population groups (180-182). While, it has been recognised that CYP3A4 is the major enzyme responsible for the metabolic clearance of afatinib, erlotinib and gefitinib, the exact contribution of CYP3A4 to the clearance of these drugs is less clear (177). EGFR KIs exhibit complex pharmacokinetic behaviour with permeability and or solubility limited absorption, variable distribution profiles, complex metabolism, typically resulting in the formation of multiple metabolites and substantial transporter mediated clearance resulting in enterohepatic recirculation.

This chapter describes a series of experiments performed to assess the *in vitro* human liver microsomal metabolism of afatinib, erlotinib and gefitinib using a substrate depletion approach that allowed for the total CYP, total UDP-glucuronosyltransferase (UGT), and specific CYP3A4 mediated metabolism to be quantified without the necessity to individually quantify the formation of each metabolite. The *in vitro* intrinsic clearance for afatinib, erlotinib and gefitinib determined by substrate depletion were used to develop PBPK modelling profiles for each compound. These profiles were validated using data from healthy volunteer trials. The capacity to predict the impact of covariates such as age, gender, and ethnicity reported in clinical trials, and the impact of co-administration with strong CYP3A4 inhibitors and inducers

on *in vivo* clearance were assessed using the Simcyp simulator (version 15.1).

## **2.2 Methods**

### **2.2.1 Chemicals and Reagents**

Afatinib, erlotinib and gefitinib were purchased from Selleckchem (Boston, MA). Alamethicin, glucose-6-phosphate (G-6-P), G-6-P dehydrogenase, nicotinamide adenine dinucleotide phosphate (NADP), NADPH reductase, and UDP-glucuronic acid (UDP-GlcUA) were purchased from Sigma-Aldrich (St Louis, MO). Acetonitrile, ammonium acetate, formic acid and methanol were purchased from Merck Millipore (Melbourne, Australia). High purity water was obtained using a MilliQ Synergy UV Ultrapure water system (Merck Millipore, Sydney, Australia). All other solvents and reagents were of analytical grade or higher.

### **2.2.2 Enzyme and Substrate Preparations**

Human liver microsomes (HLMs) were pooled from five individual livers (H7, H10, H12, H13, H40) obtained from the human liver bank of the Department of Clinical Pharmacology, Flinders University (Adelaide, Australia). Microsomes were prepared according to the method of Bowalgaha et al. (183). Approval was obtained from the Southern Adelaide Clinical Research Ethics Committee for the use of human liver tissue in drug disposition studies *in vitro*. HLMs were activated by pre-incubation with alamethicin (50 mg/mg microsomal protein), as described by Boase and Miners (184). HLM protein content was assessed according to standard measures (185). Afatinib, erlotinib and gefitinib were prepared in methanol such that the final solvent concentration in microsomal incubations was 1%.

### 2.2.3 Quantification of Substrate Depletion

The rate of microsomal KI metabolism was quantified in incubation samples (2,000  $\mu\text{L}$ ) containing HLM (0.5 mg/mL), phosphate buffer (0.1 M; pH 7.4) and substrate (1  $\mu\text{M}$ ) in the presence and absence of CYP (1mM NADPH generating system) and/or UGT (5mM UDP-GlcUA) cofactors (186, 187). The contribution of non-CYP3A4 metabolism was quantified in the presence of the selective CYP3A4 inhibitor (CYP3Cide; 0.5  $\mu\text{M}$ ). Following a 10 minute pre-incubation, reactions were initiated by the addition of substrate and the rate of depletion was assessed over three hours. Reactions were terminated with 4% acetic acid in methanol and samples were kept on ice. The supernatant fraction was isolated by centrifugation (5,000 g 10 min, 10  $^{\circ}\text{C}$ ). Substrate concentrations quantified in aliquots (200  $\mu\text{L}$ ) collected at 0, 30, 45, 60, 90, 120, 150, 180, 240, 300 and 360 minutes were used to calculate the rate of KI clearance for incubations performed in the presence of the appropriate cofactors and inhibitor (CYP3A4).

Substrate concentrations were quantified by high performance liquid chromatography (HPLC) (Agilent 1100 series instrument; Agilent Technologies, Sydney, Australia) with UV detection at the  $\lambda_{\text{max}}$  for each analyte. Analytes were separated on a Waters NovaPak C18 analytical column (150 mm x 3.9 mm (id), 5  $\mu\text{m}$  particle size; Waters Corporation, Milford, MA) using 10mM ammonium acetate (pH 5.7; Mobile Phase A) with a gradient of 10 to 50 % acetonitrile (Mobile Phase B) over 5 minutes.

### 2.2.4 Data Analysis

All experiments were performed in triplicate and the mean analyte concentration was calculated from the integrated peaks in the chromatograms obtained from the HPLC. Total CYP and total UGT hepatic clearance was calculated based on the depletion half-life for incubations performed in the presence of the associated cofactors, using the equation:

$$CL_{int} = \frac{0.693 \times V_{inc}}{t_{1/2} \times P \times f_u}$$

Where  $CL_{int}$  is the *in vitro* intrinsic clearance,  $V_{inc}$  is the incubation volume,  $t_{1/2}$  is the substrate half-life in the incubation,  $P$  is the amount of protein in the incubation and  $f_u$  is the fraction of substrate unbound in the incubation (188). CYP3A4 mediated metabolism was calculated by subtracting the  $CL_{int}$  determined in the presence of CYP3Cide from total CYP  $CL_{int}$ . Microsomal  $CL_{int}$  were used as model inputs defining the metabolic clearance for each drug in the Simcyp® profiles.

### 2.2.5 PBPK Structural Model

Simulations were conducted utilising the Simcyp Simulator® (version 15.1) (189). Absorption was simulated using the advanced dissolution, absorption and metabolism (ADAM) sub-model, which considers various compartments of the gastrointestinal tract and several processes such as dissolution, gastrointestinal fluid transit, gut wall permeation, drug degradation, intestinal metabolism, and active transport (190). The ADAM absorption sub-model was used in conjunction with the whole body PBPK ‘fully-PBPK’ model, comprising individual organ compartments (191-193). The differential equations used by the simulator describing enzyme kinetics and the impact of co-variates have been described previously (181).

### 2.2.6 PBPK Population Profile

EGFR KI profiles were developed and validated utilising the Simcyp Healthy Volunteer population comprising of a 100 healthy individuals divided across 10 trials with 10 subjects each. Virtual subjects were aged between 20 to 50 years with a 50:50 female to male ratio. For simulations performed in cancer patients, the Genentech Cancer Population (194) was used;

this population comprised patients aged 26 to 50 y/o with a 50:50 female to male ratio.

### 2.2.7 PBPK Compound Profiles

PBPK profiles for each compound were created based on individual reported physicochemical and distribution characteristics (177, 195) and *in vitro* microsomal  $CL_{int}$  data assessed by substrate depletion. In the absence of robust *in vitro* data describing intestinal and hepatic transporter kinetics, these parameters were estimated using the Simcyp parameter estimation function. Pharmacokinetic data used to create the compound profile for each EGFR KI are summarised in **Table 2.1**. Once developed, profiles for each compound were validated by comparing pharmacokinetic parameters ( $AUC$ ,  $C_{max}$  and  $t_{max}$ ) describing the simulated concentration-time profiles with those observed in clinical studies that were not used in the development of the profiles. Simulated and observed pharmacokinetic parameters for each EGFR KI are summarised in **Table 2.2**.

**Table 2.1: Substrate and inhibitor parameter values used for KI substrate profile**

	<b>Afatinib</b>	<b>Erlotinib</b>	<b>Gefitinib</b>	<b>Source</b>
<i>Physiochemical properties</i>				
Molecular weight	485.9	393.4	446.9	(195)
log P <sub>o:w</sub>	3.6	3.3	4.1	(177)
Species	Neutral	Neutral	Neutral	(177)
<i>Blood binding properties</i>				
B/P	2.12	1.397	3.206	Simcyp Predicted
f <sub>up</sub>	0.07	0.11	0.15	(177)
<i>Absorption (advanced dissolution, absorption and metabolism model)</i>				
PSA	88.6	74.7	68.7	(177)
HBD	2	1	1	(177)
P <sub>eff,man</sub> (10 <sup>-4</sup> cm/s)	0.838	2.26	2.63	Simcyp Predicted
<i>In vivo pharmacokinetic properties (full PB-PK model)</i>				
V <sub>ss</sub> (L/kg)	18.48	9.26	23.17	Simcyp Predicted
Prediction model	2	2	2	
<i>Metabolism unbound CL<sub>int</sub> (μL/min/mg)</i>				
CYP1A2		0.575		In vitro
CYP2D6			1.91	In vitro
CYP3A4	9.73	13.56	195.8	In vitro
UGT	0.438		0.658	In vitro
<i>Transport CL<sub>int</sub> (μL/min/10<sup>6</sup> cells)</i>				
OATP1B1	1161			Simcyp Predicted
P-gp			105.5	Simcyp Predicted

**Abbreviations:** P<sub>o:w</sub>, neutral species octanol: buffer partition coefficient; B/P, blood-to-plasma partition ratio; f<sub>up</sub>, fraction unbound in plasma; V<sub>ss</sub>, volume of distribution at steady state; CL<sub>po</sub>, oral clearance; PSA, polar surface area; HBD, hydrogen bond donor; P<sub>eff,man</sub>, effective passive permeability in man.

**Table 2.2: Comparison of geometric mean ( $\pm$  95 % CI) simulated pharmacokinetic parameters with those observed in clinical studies.**

Kinase Inhibitor	Dose	Sample Size <sup>a</sup>	Study	Pharmacokinetic Parameter		
				C <sub>max</sub> (ng/mL)	T <sub>max</sub> (hr)	AUC (ng/mL/hr)
Afatinib (196)	40mg	30	Observed	25.2 ( $\pm$ 9.4)	4.0 ( $\pm$ 2.6)	324 ( $\pm$ 114)
			Simulated	26.7 ( $\pm$ 3.5)	3.5 ( $\pm$ 0.4)	352 ( $\pm$ 41)
			Ratio of Means	0.94	1.14	0.92
Erlotinib (197)	150mg	32	Observed	1,003 ( $\pm$ 205)	2.0 ( $\pm$ 1.4)	14,145 ( $\pm$ 6,159)
			Simulated	1,010 ( $\pm$ 112)	2.4 ( $\pm$ 0.3)	14,088 ( $\pm$ 2,236)
			Ratio of Means	0.99	0.83	1.00
Gefitinib (71)	250mg	23	Observed	159 ( $\pm$ 56)	3.0 ( $\pm$ 2.5)	3,381 ( $\pm$ 1,156)
			Simulated	171 ( $\pm$ 22)	2.5 ( $\pm$ 0.3)	3,820 ( $\pm$ 686)
			Ratio of Means	0.93	1.20	0.89

**Abbreviations:** AUC, area under the plasma concentration-time curve; C<sub>max</sub>, maximal plasma concentration; t<sub>max</sub>, time taken to achieve maximal plasma concentration. <sup>a</sup> sample size of observed clinical trial.

**Table 2.3: Comparison of mean simulated AUC and  $C_{max}$  ratios with those observed in clinical studies.**

Kinase Inhibitor	Age Range	Sample Size	Dose	Probe Dosed	Interaction			Study	Interaction Ratios	
					Drug	Dose	Duration		$C_{max}$	AUC
Afatinib (198)	18 to 55	12	40mg	Day 8	Rifampicin	600mg QD	Day 1-7	Observed	0.77	0.67
								Simulated	0.85	0.67
								Ratio	0.91	1.00
Erlotinib (199)	19 to 59	14	150mg	Day 15	Rifampicin	600mg QD	Day 8-14	Observed	0.71	0.34
								Simulated	0.79	0.53
								Ratio	0.90	0.64
Gefitinib (71)	21 to 66	9	500mg	Day 10	Rifampicin	600mg QD	Day 1-16	Observed	0.85	0.65
								Simulated	0.88	0.58
								Ratio	0.97	1.12

## 2.2.8 Assessing the Effect of Various Covariates on Exposure

The effect of gender on EGFR KI exposure assessed by comparing exposure in all male and all female cohorts to an age and ethnicity matched cohort with a 50:50 female to male distribution was performed. The effect of age on EGFR KI exposure was assessed by comparing exposure in a geriatric population aged 65 – 90 years to a healthy 20 to 50 year old population. The effect of ethnicity was also assessed in Japanese, Chinese and South African population comprising males and females (50% female) aged 20 – 50 years. Simulations were also performed in various disease models. The impact of covariates on EGFR KI exposure are summarised in **Table 2.3**.

## 2.3 Results

### 2.3.1 Substrate Depletion by HLM

No depletion of afatinib, erlotinib and gefitinib by HLM was observed in the absence of cofactor. For incubations containing UDP-GlcUA, <10 % substrate depletion was observed over the three hour incubation (**Figure 2.1**). When NADPH was present in the absence of CYP3Cide, substrate depletion of up to 90 % was observed over three hours. The substrate depletion in incubations performed in the presence of both UDP-GlcUA and NADPH was equivalent to the sum of the depletion observed in incubation with each cofactor individually. Minimal (<10 %) substrate depletion was observed in the presence of CYP3Cide with NADPH. Intrinsic clearance values adjusted for non-specific binding to incubation components are summarised in **Table 2.1**. Observed clearances in the presence and absence of CYP3Cide were consistent with a major contribution of CYP3A4 to the metabolism of these drugs (**Figure 2.2**).

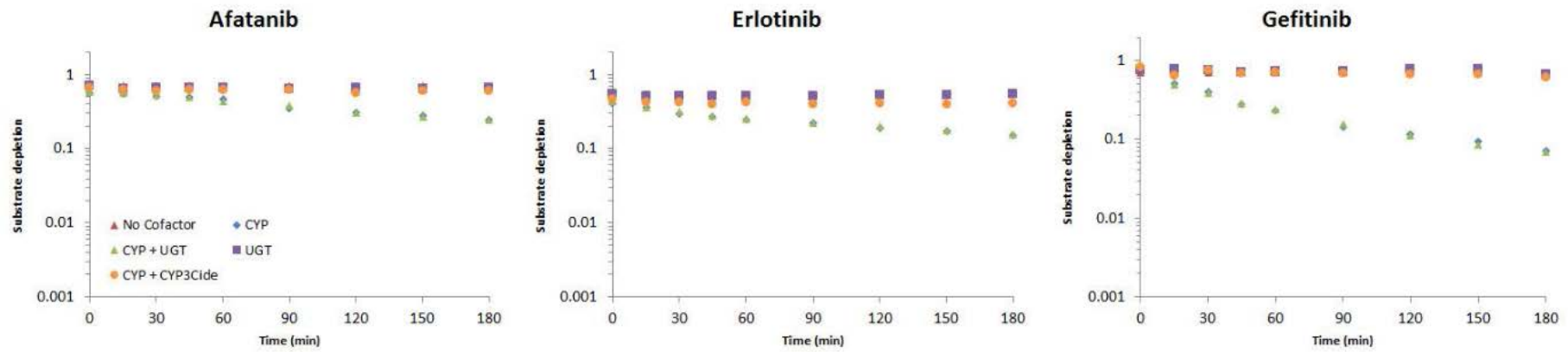


**Figure 2.1: EGFR KI substrate depletion in the absence and presence of appropriate cofactors and CYP3cide.**

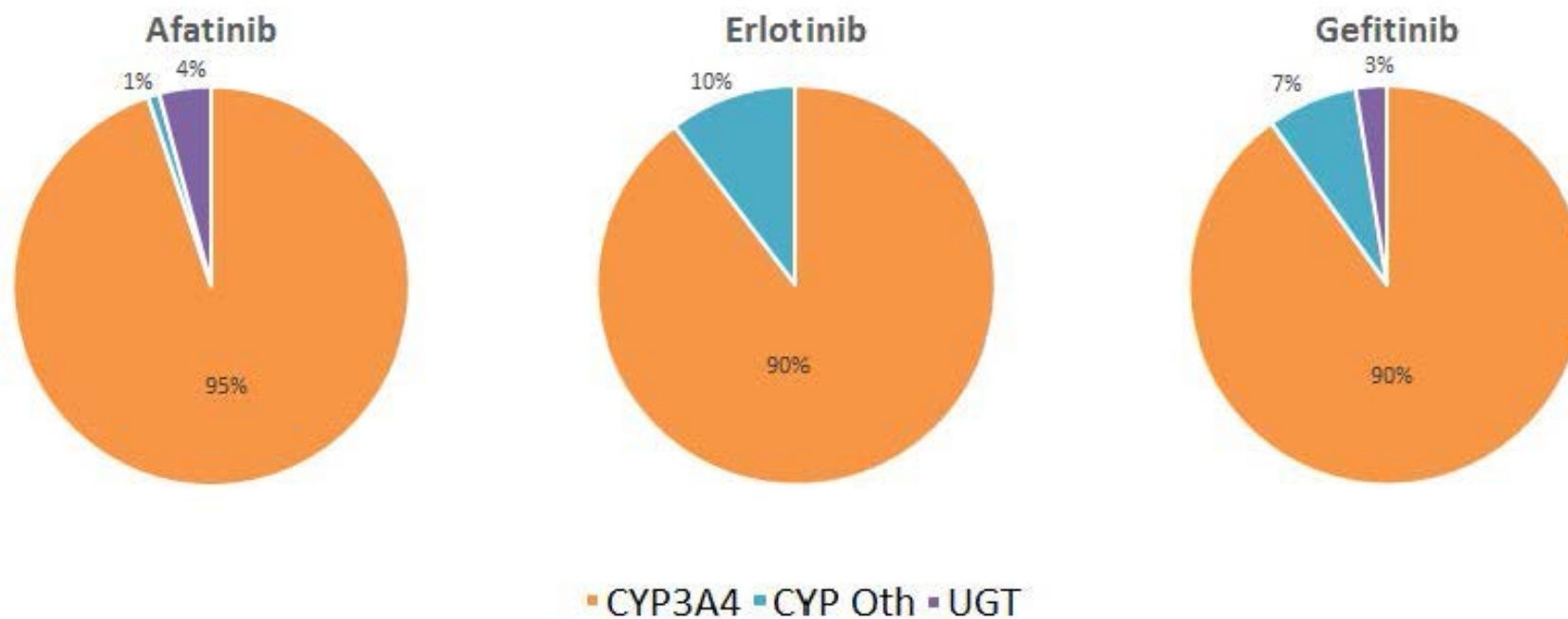


**Figure 2.2:** Pie charts depicting the contribution of CYP3A4, other CYP and UGT to *in vitro* EGFR KI metabolism.

### 2.3.2 Validation of EGFR KI Profiles

A comparison of mean ( $\pm$  95 % confidence interval; CI) model simulated pharmacokinetic parameters describing EGFR KI exposure with those observed in clinical studies are summarised in **Table 2.1**, and visualised in **Figure 2.3**. All ratios of observed to simulated pharmacokinetic parameters were contained within the range 0.8 to 1.2, and in all cases simulated pharmacokinetic parameters describing EGFR KI exposure were contained within the 95% CI for the observed parameter. A comparison of parameter (AUC and  $C_{max}$ ) ratios describing the impact of induction on EGFR KI exposure are summarised in **Table 2.3**. With the exception of the ratio of the AUC ratios for erlotinib (0.64), all observed to simulated parameter ratios describing the change in exposure caused by induction of clearance were contained within the range 0.8 to 1.2. As for parameters describing EGFR KI exposure, all simulated parameter ratios describing the impact of induction on EGFR KI exposure were contained within the 95% CI for the observed ratio.

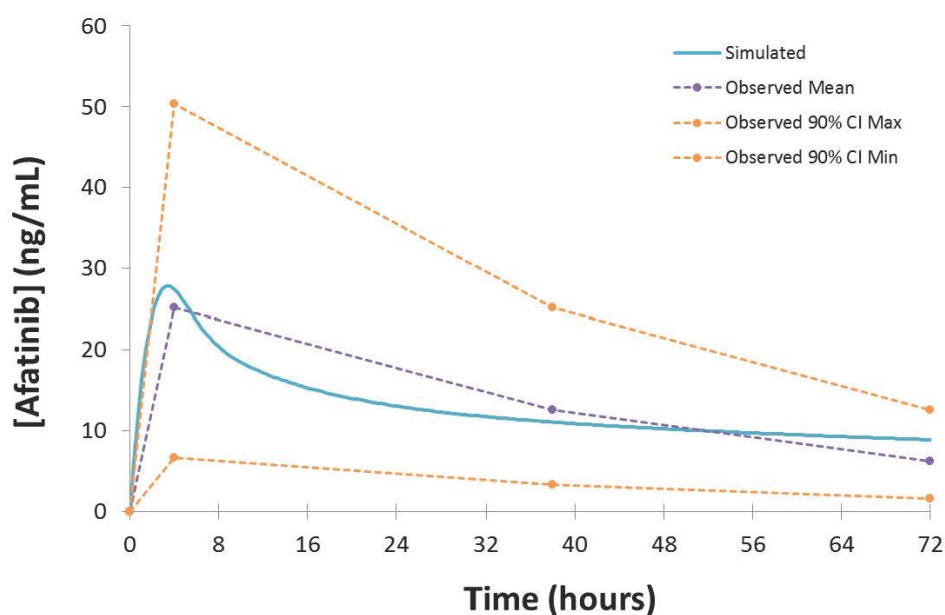


**Figure 2.3: Representative concentration-time profile depicting simulated afatinib exposure (solid line), and observed mean and 95% CI afatinib exposure (dotted lines).**

### 2.3.3 Impact of Covariates on Simulated EGFR KI Exposure

The influence of age, disease, dose, ethnicity and gender on simulated exposure to EGFR KIs was assessed by comparison of the mean AUC in covariate populations to a ‘control’ population (n=50 participants) of healthy 20 to 50 y/o Caucasians (50% female). Simulated populations (n=50 participants) were matched to the control group for all covariates except the one tested.

The mean AUC and % change from the control population for each population are reported in **Table 2.4**. In terms of physiological covariates, gender had no effect on erlotinib or gefitinib exposure, with all population AUCs within 10% of the control population. A modest (19.5%) increase in afatinib AUC was predicted in the all-female cohort. Older age was associated with an increase exposure for all EGFR KIs; mean AUCs were 30 to 35 % higher in the geriatric (65 to 90 y/o) population (**Table 2.3**). Morbid obesity was associated with a modest (~27 %) decrease in AUC for erlotinib and gefitinib, but not afatinib. Asian ethnicity was associated with significant increases in EGFR KI exposure; in the Chinese population AUC was increased by 32.7, 69.3 and 76.7 % for afatinib, erlotinib and gefitinib, respectively, while afatinib, erlotinib and gefitinib AUCs were increased by 17.8, 29.8 and 29.8 %, respectively, in the Japanese population. In contrast, only a modest (20%) increase in afatinib AUC was predicted in the South African (mixed race) population, with essentially no change (<5 %) in AUC for erlotinib or gefitinib. Liver dysfunction (Child Pugh A to C), but not renal dysfunction (reduced GFR) was associated with an increase in EGFR KI exposure. Mild liver dysfunction caused a 20 to 35 % increase in EGFR KI exposure, while more severe liver dysfunction (Child Pugh B and C) caused 60 to 188 % increases in EGFR KI AUCs. No changes in AUC were predicted in the cancer population. When considering the impact of metabolic drug-drug interactions (DDIs), administration of the CYP3A4 inducer rifampicin (600mg QD) for seven days prior to

EGFR KI dosing caused decreases in AUC of 33.7, 69.5 and 46.5 % for afatinib, erlotinib and gefitinib, respectively. Co-administration of the CYP3A4 inhibitor ketoconazole (400mg QD) increased afatinib, erlotinib and gefitinib AUCs by 28.8, 103 and 77.3 %, respectively.

### 2.3.4 Application to Optimised EGFR KI Dosing

The established target threshold trough concentration for gefitinib that are associated with optimal therapeutic outcomes is >200 ng/mL (132). Simulated mean (range) trough gefitinib (250mg QD) concentrations in 1,000 cancer patients following dosing to steady state (14 days) were 259.0 (57.2 to 784.9) ng/mL. In this virtual population, 45 % of patients treated with gefitinib had trough concentrations of <200 ng/mL at day 15 (Figure 2.4).

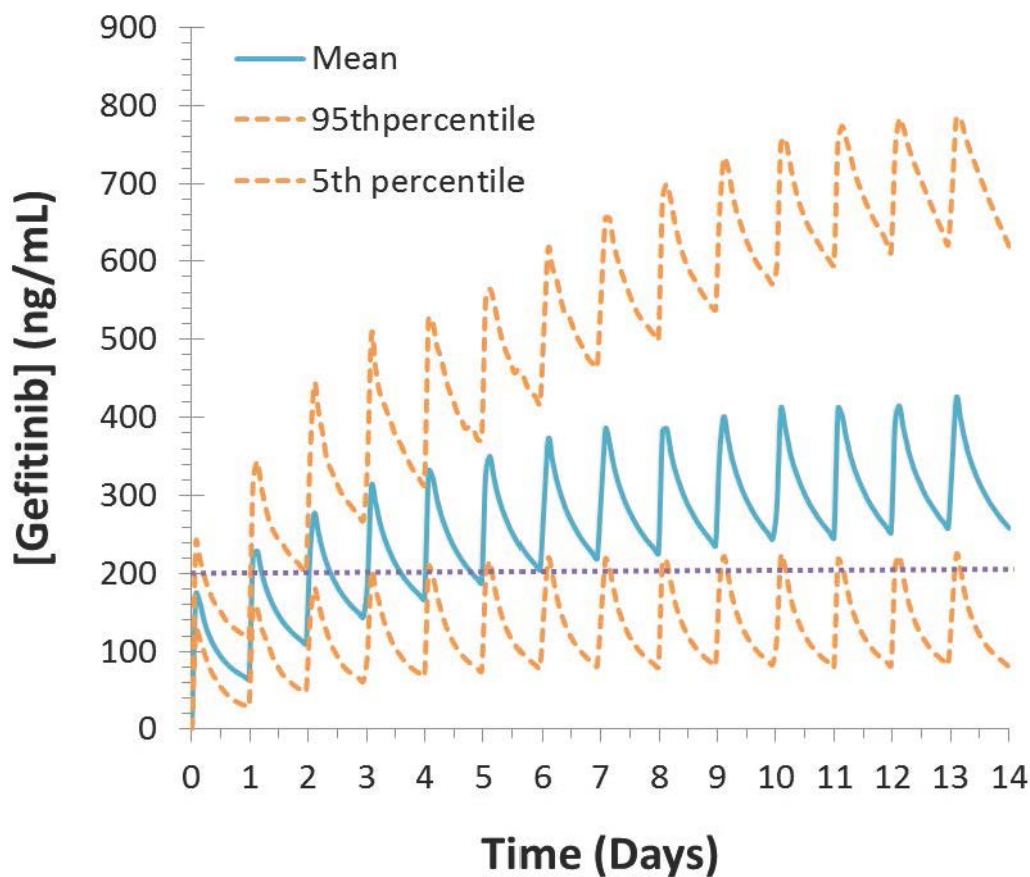


**Figure 2.4: Simulated mean and 95% CI concentration time profiles describing exposure to gefitinib (250 mg QD) when dosed for 14 days in cancer patients (n=1,000).**

**Table 2.4: Impact of covariates on mean simulated EGFR KI exposure**

Covariate	Population	Age Range	Proportion Female	Afatinib		Erlotinib		Gefitinib	
				AUC	% Change	AUC	% Change	AUC	% Change
Physiology	Control	20-50	0.5	341		13,537		4,217	
	Male	20-50	0	321	-6.0	13,046	-3.6	4,037	-4.3
	Female	20-50	1	408	19.5	14,607	7.9	4,577	8.5
	Geriatric	65-90	0.5	450	31.7	17,876	32.1	5,675	34.6
	Morbid obese	20-50	0.5	309	-9.4	9,904	-26.8	3,043	-27.8
Ethnicity	Chinese	20-50	0.5	453	32.7	22,082	63.1	7,133	69.1
	Japanese	20-50	0.5	402	17.8	17,572	29.8	5,443	29.1
	South African	20-50	0.5	411	20.4	12,853	-5.1	4,332	2.7
Disease	Cancer	26-50	0.5	328	-3.9	12,728	-6.0	4,386	4.0
	Child Pugh A	20-50	0.5	412	20.8	17,262	27.5	5,596	32.7
	Child Pugh B	20-50	0.5	562	64.5	29,085	114.9	10,808	156.3
	Child Pugh C	20-50	0.5	553	61.9	30,463	125.0	12,127	187.6
	GFR 30 to 60	20-50	0.5	378	10.6	15,696	15.9	4,575	8.5
	GFR <30	20-50	0.5	324	-5.2	14,584	7.7	4,133	-2.0
DDIs	Induction	20-50	0.5	226	-33.7	4,130	-69.5	2,258	-46.5
	Inhibition	20-50	0.5	439	28.8	27,480	103.0	7,477	77.3

## 2.4 Discussion

This chapter describes for the first time a collection of sophisticated full PBPK models for the first line EGFR KIs used in the treatment of NSCLC. Although outcomes for patients with NSCLC have improved notably since the introduction of EGFR KIs, it is increasingly accepted that outcomes for NSCLC patients may be further enhanced by optimising exposure to these drugs (125, 200, 201). Variability in EGFR KI exposure primarily involves processes that occur in the gastrointestinal tract and liver, but can also be influenced by the tissue distribution of these drugs. In addition, EGFR KIs are known to be BCS class II or IV drugs, where oral absorption can be complicated by permeability and/or solubility. Therefore, in order to simulate exposure to these drugs, profiles based on full PBPK structural models with ADAM absorption sub-models that considered the compartmental distribution and interaction between permeability limited diffusion, transport and metabolism were developed using the Simcyp simulator<sup>®</sup>.

The key difference between the full PBPK profiles developed here and previously reported minimal EGFR KI PBPK profiles (77, 202, 203) is that these full PBPK profiles accurately account for the full range of physiochemical, metabolic and transporter mediated processes that determine exposure to these drugs. By way of example, in the current profiles, by accounting for permeability limited absorption through the use of the ADAM sub-model, these profiles accurately simulated not only the parameters defining EGFR KI absorption, but also the ‘shape’ of the absorption profile. In contrast, previous models have either arbitrarily modified the absorption rate constant to shift or applied a non-physiological ‘lag time’ to artificially model  $t_{max}$ .

In this chapter, substrate depletion was used to assess the contribution of enzyme families to and kinetics of, human liver microsomal EGFR KI metabolism (188). This approach was

chosen as it facilitated the assessment of the enzymatic contribution to microsomal EGFR KI metabolism at physiologically relevant EGFR KI concentrations, and it allowed for the determination of microsomal EGFR KI clearances without the need to individually quantify the substantial number of EGFR KI metabolites. Control experiments performed in the absence of UDP-GlcUA or NADPH demonstrated essentially no (<2 %) depletion of afatinib, erlotinib, and gefitinib by HLM over the three hour incubation period. Similarly, less than 10% depletion was observed when incubations were performed in the presence of UDP-GlcUA alone (**Figure 2.1**), suggesting that UGT enzymes do not play a major role in the hepatic metabolism of these EGFR KIs. This observation is consistent with published literature regarding the contribution of UGT to the metabolism of these drugs (177). When NADPH was present in the absence of CYP3Cide, substrate depletion of up to 95 % was observed over the three hour incubation period; this observation is consistent with the reported major contribution of CYP enzymes to the hepatic clearance of these drugs. The rate of substrate depletion observed in incubations containing UDP-GlcUA and NADPH was equivalent to the sum of the rates observed in incubations performed in the presence of each cofactor separately. This observation demonstrates that CYP and UGT catalyzed pathways have negligible effect on each other. The specific contribution of CYP3A4 to EGFR KI depletion was assessed by subtracting the depletion observed in the presence of NADPH with CYP3Cide (i.e. non-CYP3A4 oxidative metabolism) from the depletion observed in the presence of NADPH only (CYP3A4 and non-CYP3A4 metabolism). Less than 10 % depletion was observed when CYP3Cide was present in incubations, indicating that for these EGFR KIs, CYP3A4 accounts for >90 % of *in vitro* metabolism at substrate concentrations <1  $\mu\text{M}$ . Calculated unbound microsomal  $\text{CL}_{\text{int}}$  values for CYP3A4 catalysed metabolism were 9.7, 13.6 and 195.8  $\mu\text{L}/\text{min}/\text{mg}$  for afatinib, erlotinib, and gefitinib, respectively. Remaining microsomal  $\text{CL}_{\text{int}}$  values are reported in **Table 2.1**. These *in vitro* substrate depletion data were used to develop the compound profiles for each of

the EGFR KI.

The EGFR KI compound profiles were validated by comparing simulated pharmacokinetic parameters (AUC,  $C_{\max}$  and  $t_{\max}$ ) describing exposure with those observed in clinical studies that were not used in the development of the compound profiles. With the exception of the AUC ratio describing the impact of induction on erlotinib exposure (0.64), the ratio of observed to simulated parameters describing exposure, or parameter ratios describing the impact of induction on exposure were contained within the range 0.8 to 1.2. This consistent and high degree of concordance demonstrates the accuracy and validity of the profiles, which is visually depicted in the representative overlay of the simulated and population average concentration-time curves defining afatinib exposure (**Figure 2.3**).

A major challenge for this study related to the validation of the capacity of the compound profiles to account for the impact of induction on EGFR KI exposure. As EGFR KIs exhibit substantial inter- individual variability in exposure and studies used to assess the impact of drug interactions are often undertaken in small ( $n < 10$ ) cohorts, the absolute exposure reported in these studies typically poorly reflects the population average. These studies are however adequately powered to accurately reflect changes in exposure (i.e. intra- individual variability) due to drug-drug interactions. As such, when validating the compound profiles for induction and inhibition, parameter ratios (i.e. the change in exposure) were considered rather than absolute exposures pre- and post- interaction.

Understanding and developing approaches to account for the covariates that impact on EGFR KI exposure is an important aspect of optimising the dosing of these drugs. In terms of physiological covariates, older age (i.e. geriatric population) consistently resulted in higher exposure to EGFR KIs, while morbid obesity resulted in moderately reduced exposure to erlotinib and gefitinib, but not afatinib. In contrast, female gender resulted in a modest increase

in exposure to afatinib, but not to erlotinib or gefitinib. This result is consistent with the known distribution profiles of these drugs; the apparent  $V_d$  for afatinib (2520L) is almost double that of gefitinib (1400L) and ten-fold higher than that of erlotinib (232L) (177). For erlotinib and gefitinib, the increased liver size associated with morbid obesity likely contributes to a higher metabolic clearance of these drugs in morbidly obese patients, however, the substantial distribution of afatinib into the adipose tissue likely offsets any increase in metabolic clearance of this drug in this cohort. Similarly, given the fat distribution profiles of males and females, it is likely that increased distribution into adipose tissue accounts for the increase in afatinib exposure observed in females (204).

Substantial increases in simulated EGFR KI exposure were also observed in age and gender matched Asian (Chinese and Japanese) populations. These simulations indicate that ethnicity may be an important factor in determining exposure to EGFR KIs. The clinical implications in terms of EGFR KI efficacy and tolerability and the physiological differences between Caucasian and Asian individuals that underpin these differences in exposure warrant investigation. Consistent with the mechanism of KI clearance, increasing severity of liver dysfunction, but not renal dysfunction, was associated with a marked increase in EGFR KI exposure. Most notably, erlotinib and gefitinib exposure was increased 2- to 3-fold in virtual patients with moderate or severe (Child Pugh B or C) hepatic dysfunction. While still notable, moderate to severe liver dysfunction had a comparatively smaller effect on afatinib exposure. Consistent with FDA guidance advising against co-administration with strong CYP3A4 inhibitors and inducers, dosing with rifampicin (600mg QD) for seven days prior to the administration of EGFR KIs caused a marked reduction in afatinib, erlotinib and gefitinib exposure. Similarly, co-administration of ketoconazole (400mg QD) caused a moderate increase in afatinib exposure, and marked increases in erlotinib and gefitinib exposures.

The potential applicability of the gefitinib compound profile to optimised KI dosing was demonstrated through simulations performed in 1,000 cancer patients using a dosing regimen based on the recommended fixed dosing protocol for this drug (177). These simulations demonstrated that while the mean trough concentration at day 15 was greater than the established target threshold for this drug (259 versus 200 ng/mL), 448 (45 %) patients were predicted to experience sub-therapeutic exposure (i.e. trough concentrations < 200 ng/mL) at this time (**Figure 2.5**), with some patients experiencing as low as 25% of the established target steady-state threshold exposure. These simulated exposure profiles using a well validated full PBPK gefitinib profile emphasise the need to individualise gefitinib dosing in order to maximise the benefit of this drug. It is worth noting that BSV observed in the verification of these profiles reflected the variability observed within a homogenous (tight trial inclusion criteria) clinical trial population. Substantially greater BSV (Chapter 1) is observed in a heterogenous cancer patient population. Indeed, the limited BSV observed in clinical trials (RCT populations reflect <5% of the actual treatment population) frequently results in an underestimation of the importance of variability in exposure in a treatment population and is a major confounder when evaluating the impact of variability in exposure.

## **2.5 Conclusion**

We have developed and validated robust mechanistic models with the capacity to describe EGFR KI exposure and the impact of covariates on exposure. These models may be applied to inform the impact of different dosing regimens on EGFR KI exposure, the potential impact of poor compliance on EGFR KI efficacy, the need to perform bridging studies when introducing EGFR KIs to new international markets, and the potential impact of DDIs on EGFR KI exposure. With enhancement of the Simcyp population profiles, these profiles may also be applied to assist in optimising dosing in individual patients under the Virtual Twin framework.

---

# CHAPTER III: ASSESSMENT OF INTER-RACIAL VARIABILITY IN CYP3A4 ACTIVITY

---

*The results presented in this chapter have*

*been reported in:*

van Dyk M, Marshall JC, Sorich MJ, Wood LS, Rowland A (2018) Assessment of inter-racial variability in CYP3A4 activity and inducibility among healthy adult males of Caucasian and South Asian ancestries. *European Journal of Clinical Pharmacology*, DOI: 10.1007/s00228-018-2450-4.

### 3.1 Introduction

As outlined in Chapter I, variability in CYP activity is a known source of clinically important differences in drug exposure, response and tolerability (205). This variability may present as inherent differences between individuals (inter-individual variability) due to factors such as genotype, race or gender, or as changes in activity for an individual over time (intra-individual variability) due to factors such as drug-drug interactions (DDIs), diet or disease states. There is also the potential for interplay between these forms of variability. The significance of this interplay being that in addition to differences in baseline exposure between individuals of different genotype, race or gender, there is also the potential for differences in the impact of perturbations of activity by factors such as DDIs. Of particular significance the PBPK analyses performed in Chapter II identified race as a potentially important covariate driving variability in EGFR exposure. Attempts to verify this observation using clinical trial reports specifically related to the KIs of interest or general PK studies identified a gap in the analysis of inter-racial variability in CYP3A4 exposure.

Inter-racial variability in CYP activity is typically attributed to differences in physiology, diet and the frequency of genetic polymorphisms, and has been extensively characterised for some enzymes, such as CYP1A2 (206). For example the major CYP1A2 reduced function (\*1C) allele is observed at higher frequencies in African-American (26 %), Hispanic (26 %) and Asian (21 %) populations compared to Caucasians (1.6 %) (207), while the low inducibility (\*1K) allele is observed at higher frequencies in African (3 %) and Middle Eastern (3.6 %) populations compared to Caucasians (0.5%) (208). As such, these races are considered to be more susceptible to toxicity resulting from impaired clearance of drugs metabolised by CYP1A2. Increased exposure to drugs metabolised by CYP1A2 in South Asians (Thailand, Vietnam, Cambodia, Singapore, Indonesia, Philippines and Malaysia) compared to Caucasians

has been directly shown by comparison of caffeine exposure in these populations (206). It has further been demonstrated that South Asians, but not Caucasians, exhibit diurnal variability in CYP1A2 activity, with reduced activity in the evening compared to the morning (209).

As CYP3A4 is responsible for the metabolism of more than 30 % of clinically used drugs (210), it is the drug metabolising enzyme (DME) of greatest clinical importance. CYP3A4 is a member of the CYP3A sub-family, which also comprises CYP 3A5, 3A7 and 3A43. As these enzymes exhibit substantial overlap in substrate specificity, the clearance of drugs metabolised by CYP3A4 may also be influenced by the activity of CYP 3A5 and 3A7. The *in vivo* clearance of drugs metabolised by CYP3A is known to exhibit substantial (>10-fold) variability (211), while variability in *in vitro* CYP3A activity is even greater (> 30-fold) (212). Despite the clinical importance of CYP3A4, relatively little is known about inter-racial variability in the activity of this enzyme. In the current study, we directly assess the impact of inter-racial variability in CYP3A4 activity and inducibility on midazolam exposure in a cohort of age matched healthy males of Caucasian and South Asian ancestries. This chapter sought to investigate race as a source of variability of CYP3A4 activity.

## **3.2 Methods**

### **3.2.1 Study Protocol**

This study, EPOK-15, is a single centre, open label, single sequence metabolic phenotyping trial. The trial protocol was approved by the Southern Adelaide Clinical Human Research Ethics Committee (SAHREC 11.15), and written informed consent was obtained from each participant. The trial was registered with the Australian New Zealand Clinical Trials Registry (ACTRN 12614001289606).

### 3.2.2 Study Cohort and Medications

Healthy male participants (n = 30) aged 21 to 35 years old were enrolled into the study following screening by physical examination. Participants were required to refrain from use of drugs and herbal products, including tobacco and alcohol, grapefruit juice and consuming large amounts of cruciferous vegetables prior to and for the duration of the study. Participant characteristics are summarised in **Table 3.1**. Midazolam (Pfizer midazolam for injection) was purchased from Pfizer, NSW, Australia; rifampicin (Rifadin) was purchased from Sanofi, NSW, Australia; clarithromycin (Klacid) was purchased from Abbott Laboratories, NSW, Australia.

**Table 3.1: Participant characteristics**

Mean (Range)	Caucasian (n=19)	South Asian (n = 11)	Significance (2-tailed) <sup>a</sup>
Age (years)	25.9 (21 – 34)	26.5 (21 - 34)	0.721
Height (cm)	177 (164 – 193)	174 (165 – 182)	0.264
Weight (kg)	77.6 (62.7 – 108)	71.4 (57.2 – 85.2)	0.115
BMI (kg/m <sup>2</sup> )	24.7 (18.7 – 29.0)	23.6 (19.8 – 30.1)	0.347
CYP3A genotypes <sup>a</sup>			
- CYP3A4 *1/*22 (reduced function)	11 % (2 / 19)	0 % (0 / 11)	0.163
- CYP3A5 *1/*3 (functional)	11 % (2 / 19)	45 % (5 / 11)	0.063

<sup>a</sup> Determined by t-test for equality of means, with equal variance (based by Levene’s test for equality of variance) assumed for age, height, weight, and BMI (variance  $p > 0.3$ ), but not assumed for CYP3A genotypes (variance  $p < 0.02$ ).

<sup>b</sup> CYP3A4 \*1/\*1 (EM phenotype), CYP3A5 \*3/\*3 (PM phenotype) unless specified.

### 3.2.3 Study Design

CYP3A4 activity was assessed at baseline (Day 1) following a 7 day course of rifampicin and following a 3 day course of clarithromycin. As per the protocol shown in **Figure 3.1**, on days 1, 8 and 15 participants (n=30) were orally administered 1 mg of midazolam (1 mL of 5 mg/mL midazolam for injection diluted in 4 mL saline) and timed blood samples were collected prior to and at 0.25, 0.5, 0.75, 1, 2, 3, 4 and 6 hrs post dosing. Within 1 hr of sample collection, plasma was isolated from whole blood by centrifugation at 4,000 g for 5 min and stored at -80°C until analysis. Between day 1 and 8 participants self-administered 300 mg rifampicin (300mg QD PO) each evening, then between day 12 and day 14 participants self-administered clarithromycin (250 mg BD) each morning and evening. Rifampicin and clarithromycin plasma concentrations were determined pre-midazolam dosing on day 8 and 15, respectively.

### 3.2.4 Sample Preparation

One hundred microliters of plasma sample was diluted in 300 µL of methanol containing 0.1 % formic acid and 7.5 ng/mL d<sub>6</sub>-midazolam (assay internal standard) then vortexed for 3 min using a MixMate® Vortex Mixer (Eppendorf, Sydney, Australia) to precipitate proteins. Samples were then centrifuged at 16,000 g for 5 min, and a 2.5 µL aliquot of the resultant supernatant fraction was analysed by ultra-performance liquid chromatography mass spectrometry (UPLC-MS). Quality control (QC) and calibration standards (n=6) were prepared by spiking known concentrations of midazolam into drug free plasma over a concentration range of 2.5 to 25 ng/mL.

### 3.2.5 Sample Analysis

Samples were analysed using a validated assay (172). Briefly, analytes were separated from the sample matrix by UPLC performed on a Waters ACQUITY™ BEH C18 column (100 mm

× 2.1 mm, 1.7 µm; Waters Corp., Milford, USA) using a Waters ACQUITY™ UPLC system. The column temperature was maintained at 40 °C, while the sample compartment was maintained at 15 °C. Analytes were separated by linear gradient elution at a flow rate of 0.25 mL/min. Initial conditions were 70 % water containing 0.1 % formic acid (mobile phase A) and 30 % acetonitrile containing 0.1 % formic acid (mobile phase B). The proportion of mobile phase B was increased to 60 % over 4 min, then returned to initial conditions.

Column elutant was monitored by MS, performed on a Waters Q-ToF Premier™ quadrupole, orthogonal acceleration time-of-flight tandem mass spectrometer (Q-ToF-MS) operating in positive electron spray ionisation (ESI+) mode. The desolvation gas was set at a flow rate of 400 L/h at a temperature of 250 °C, while the cone gas was set at a flow rate of 50 L/h. The source temperature was 90 °C. Source capillary and cone voltages were 2.8 kV and 50 V, respectively. ToF data were collected in wide pass MS mode, with the resolving quadrupole acquiring data between m/z 150 and 600 to yield a total ion count (TIC) chromatogram. Data were collected as centroid spectra using the extended dynamic range function at an acquisition rate of 0.1 sec, with a 0.05 sec inter-scan delay. The collision cell energy was 2 eV. Selected ion data was extracted at the analyte [M+H]<sup>+</sup> precursor m/z. Resulting pseudo-MRM spectra were analysed using Waters TargetLynx™ software. Plasma analyte concentrations were determined by comparison of normalised peak areas in participant samples to those of calibrators.

The lower limit of quantification (LLOQ) for midazolam by this approach was 0.2 ng/mL, while the intra- and inter- day precision at the LLOQ were 1.9 and 2.3 %, respectively, and the accuracy (measured as % deviation at the LLOQ) was 5.1 %. The calibration range was 0.5 to 50 ng/mL (213).

### 3.2.6 CYP3A Genotype

CYP3A genotyping was performed in kind by collaborators at the Early Clinical Development Group at Pfizer Worldwide Research and Development. For technical reference genomic DNA was isolated from whole blood using a QIA Symphony (QIAGEN) automated platform running a DSP DNA Mini Kit, quantified by NanoDrop and normalized to 20ng/μL. DNA was genotyped for CYP3A4 and CYP3A5 using a custom designed TaqMan™ OpenArray™ that was analysed on a QuantStudio™ 12K Flex Real-Time PCR System (Applied Biosystems). The specific assays used on the array were C\_\_59013445\_10 for CYP3A4\*22, C\_\_26201809\_30 for CYP3A5\*3, C\_\_30633867\_20 for CYP3A5\*5, C\_\_30203950\_10 for CYP3A5\*6, and C\_\_32287188\_10 for CYP3A5\*7.

### 3.2.7 Data Analysis

Non-compartmental methods (PK Functions for Microsoft Excel, Department of Pharmacokinetics and Drug Metabolism, Irvine, CA, USA) were used to estimate the area under the plasma-concentration time curve from the time of dosing to the last measured sample (AUC) and maximal concentration ( $C_{max}$ ) for midazolam at baseline (Day 1), following a 7-day course of rifampicin (Induction (IND) phase; Day 8) and following a 3-day course of clarithromycin (Mechanism based inhibition (MBI) phase; Day 15). Midazolam AUC was defined as the primary outcome. The midazolam AUC of each group was reported as the exponentiation of the mean of the log transformed AUC. Univariate and multivariable linear regression were undertaken to evaluate the crude and independent effect, respectively, of race (Caucasian vs South Asian), CYP3A4 genotype (\*1/\*1 vs \*1/\*22) and CYP3A5 genotype (\*3/\*3 vs \*1/\*3) on logarithmically transformed midazolam AUC. Back transformation was utilised to provide crude and covariate adjusted point estimates and 95% confidence intervals (95% CI). Differences in midazolam AUC ratio in the absence and presence of rifampicin

(induction ratio;  $IND_{ratio}$ ) and clarithromycin (MBI ratio;  $MBI_{ratio}$ ) and  $C_{max}$  were assessed as secondary outcomes using the same approach. Exploratory univariate analyses were also performed to evaluate whether age, weight, height and BMI were associated with midazolam AUC and  $C_{max}$ .

## 3.3 Results

### 3.3.1 Trial Conduct

Thirty male subjects completed the study (19 Caucasian and 11 South Asian). Three subjects experienced minor adverse events that were attributed to study interventions, but that did not affect their completion of the study (one participant experienced discomfort at cannulation site on Day 8, one experienced dry mouth during the rifampicin dosing phase, and one experienced stomach discomfort during the clarithromycin dosing phase). Based on clinically relevant allelic variants in CYP3A4 and CYP3A5, two subjects (both Caucasian) were classified as CYP3A4 intermediate metabolisers (CYP3A4 \*1/\*22), and seven subjects (5 South Asian and 2 Caucasian) were CYP3A5 intermediate metabolisers (CYP3A5\*1/\*3). All remaining participants were CYP3A4 extensive metabolisers (CYP3A4 \*1/\*1) and poor (non-functional) CYP3A5 metabolisers (CYP3A5 \*3/\*3 or \*3/\*5).

Adherence to rifampicin and clarithromycin dosing was determined by assessment of analyte concentrations in pre-midazolam dosing blood samples on Day 8 and Day 15, respectively. Mean ( $\pm$  standard deviation; S.D.) plasma rifampicin and clarithromycin concentrations were  $513 \pm 146$   $\mu\text{g/L}$  and  $334 \pm 81$   $\mu\text{g/L}$ , respectively. These observed concentrations were consistent with anticipated exposure profiles for these drugs with the respective dosing regimens, and are indicative of good adherence in all participants. Rifampicin and

clarithromycin exposure was not observed to differ between Caucasian and South Asian participants.

### 3.3.2 Covariate Assessment

No statistically significant difference in midazolam AUC was detected between participants with CYP3A4 \*1/\*22 (n=2, 1032  $\mu\text{g/L}/\text{min}$ ) and \*1/\*1 (n=28, 934  $\mu\text{g/L}/\text{min}$ ) genotype ( $p=0.75$ ), or between participants with CYP3A5 \*1/\*3 (n=7, 883  $\mu\text{g/L}/\text{min}$ ) and \*3/\*3 (n=23, 958  $\mu\text{g/L}/\text{min}$ ) genotype ( $p=0.66$ ). Weight ( $p = 0.037$ ), but not age or height were not found to be associated with midazolam AUC and  $C_{\text{max}}$  ( $p > 0.2$ ) in exploratory analysis.

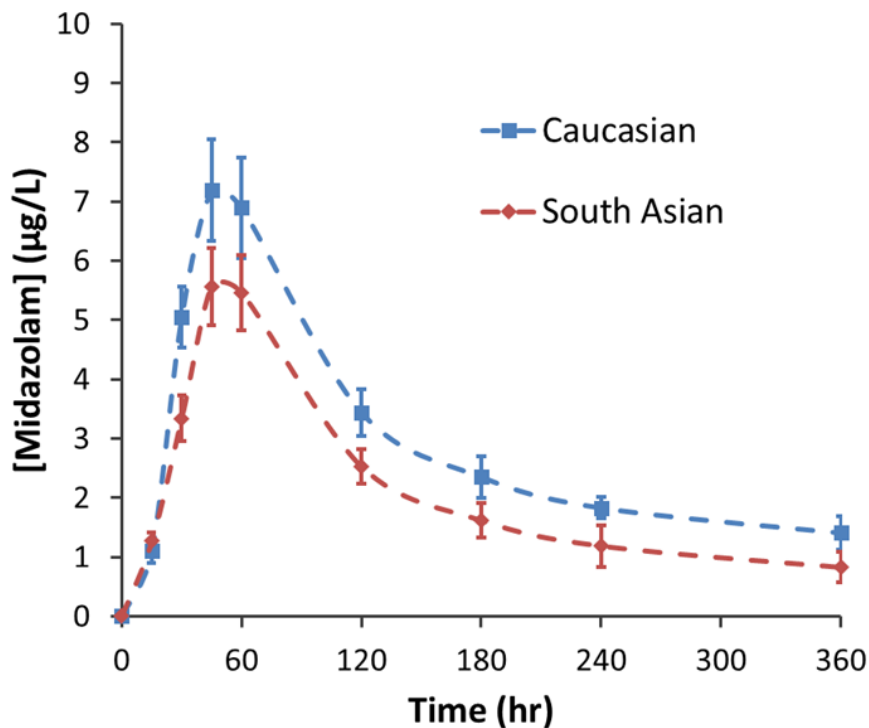


**Figure 3.1: Mean midazolam concentration-time curves for Caucasian (n=19) and South Asian (n=11) cohorts.**

### 3.3.3 Baseline CYP3A4 activity in Caucasians and South Asians

A summary of the geometric mean (95% CI) baseline AUC and  $C_{\max}$  defining midazolam exposure in Caucasian and South Asian cohorts is reported in **Table 3.2**, while the coefficients defining differences in baseline midazolam exposure between Caucasian and South Asian participants are reported in **Table 3.3**. The geometric mean baseline midazolam AUC in the Caucasian cohort (1057  $\mu\text{g/L}/\text{min}$ ) was 27 % greater than that observed in South Asian cohort (768  $\mu\text{g/L}/\text{min}$ ). Similarly, the mean baseline midazolam  $C_{\max}$  in the Caucasian cohort (7.2  $\mu\text{g/L}$ ) was 24 % greater than that observed in South Asian cohort (5.5  $\mu\text{g/L}$ ) (**Figure 3.1**). Linear regression demonstrated that the difference in AUC, but not  $C_{\max}$ , between the Caucasian and South Asian cohorts was statistically significant ( $p \leq 0.05$ ) in both the crude (unadjusted) and genotype adjusted regression analyses.

### 3.3.4 CYP3A4 Inducibility and Inhibition Potential in Caucasians and South Asians

A summary of the geometric mean (95% CI) AUC and  $C_{\max}$  defining midazolam exposure in Caucasian and South Asian cohorts post- rifampicin induction and clarithromycin inhibition is reported in **Table 3.2**, while the coefficients defining differences in the change in midazolam exposure post induction (IND AUC Ratio) and mechanism based inhibition (MBI AUC Ratio) between Caucasian and South Asian participants are reported in **Table 3.3**. The geometric mean post-induction midazolam AUC in the Caucasian cohort (308  $\mu\text{g/L}/\text{min}$ ) was 50% greater than that observed in South Asian cohort (154  $\mu\text{g/L}/\text{min}$ ), while the geometric mean post-inhibition midazolam AUC in the Caucasian cohort (1834  $\mu\text{g/L}/\text{min}$ ) was 41% greater than that observed in South Asian cohort (1079  $\mu\text{g/L}/\text{min}$ ) (**Figure 3.2**). Linear regression demonstrated a trend towards a difference in the post-induction AUC Ratio ( $p = 0.067$ ) between the Caucasian and South Asian cohorts in the crude (unadjusted) regression model. The

significance of this trend was reduced ( $p = 0.131$ ) in the model was adjusted for CYP 3A4 and 3A5 genotypes. No difference in post-inhibition (MBI) ratio was observed between the Caucasian and South Asian cohorts.

**Table 3.2: Pharmacokinetic parameters describing midazolam exposure**

Parameter	Study Phase	Caucasian			South Asian		
		Geometric Mean	95% Confidence Interval		Geometric Mean	95% Confidence Interval	
			Lower	Upper		Lower	Upper
AUC	Baseline	1057	880	1270	768	648	1037
	Induced	308	150	464	154	74	234
	Inhibited	1834	1209	2460	1079	632	1526
C <sub>max</sub>	Baseline	7.2	5.5	8.9	5.5	4.3	6.8
	Induced	2.7	1.7	3.6	1.2	0.7	1.7
	Inhibited	12.6	7.6	17.7	8.3	4.6	11.9

**Units:** AUC (µg/L/min); C<sub>max</sub> (µg/L)

**Table 3.3: Coefficients defining differences in midazolam exposure between Caucasian and South Asian healthy males**

Parameter	Model	Caucasian			South Asian			Difference			Sig ( <i>p</i> )
		Point Estimate	95% Confidence Interval		Point Estimate	95% Confidence Interval		Point Estimate	95% Confidence Interval		
			Lower	Upper		Lower	Upper		Lower	Upper	
AUC	Crude	1057	880	1270	767	649	1037	-289	-408	-20	0.04 **
	Adjusted <sup>a</sup>	1052	855	1292	743	623	1052	-309	-428	0	0.05 **
C <sub>max</sub>	Crude	7.2	5.7	8.7	5.5	3.1	8.0	-1.7	-4.2	0.8	0.169
	Adjusted <sup>a</sup>	7.5	5.8	9.1	5.3	2.6	8.0	-2.2	-4.9	0.6	0.118
IND AUC Ratio <sup>b</sup>	Crude	3.9	3.0	4.8	5.3	3.8	6.4	1.4	-0.1	2.5	0.067
	Adjusted <sup>a</sup>	4.2	3.2	5.2	5.4	3.8	7.0	1.2	-0.4	2.9	0.131
MBI AUC Ratio <sup>c</sup>	Crude	1.9	1.5	2.3	1.5	0.8	2.2	-0.4	-1.1	0.3	0.257
	Adjusted <sup>a</sup>	2.0	1.5	2.4	1.7	1.0	2.5	-0.3	-1.0	0.8	0.456

**Units:** AUC (µg/L/min); C<sub>max</sub> (µg/L)

<sup>a</sup> Adjusted for independent variables; CYP3A4 \*1/\*22 and CYP3A5 \*1/\*3 genotype, <sup>b</sup> Ratio of Day 1 midazolam AUC (baseline) / Day 8 midazolam AUC (post rifampicin), <sup>c</sup> Ratio of Day 15 midazolam AUC (post clarithromycin) / Day 1 midazolam AUC (baseline), \*\* Statistically significant ( $p \leq 0.05$ ).

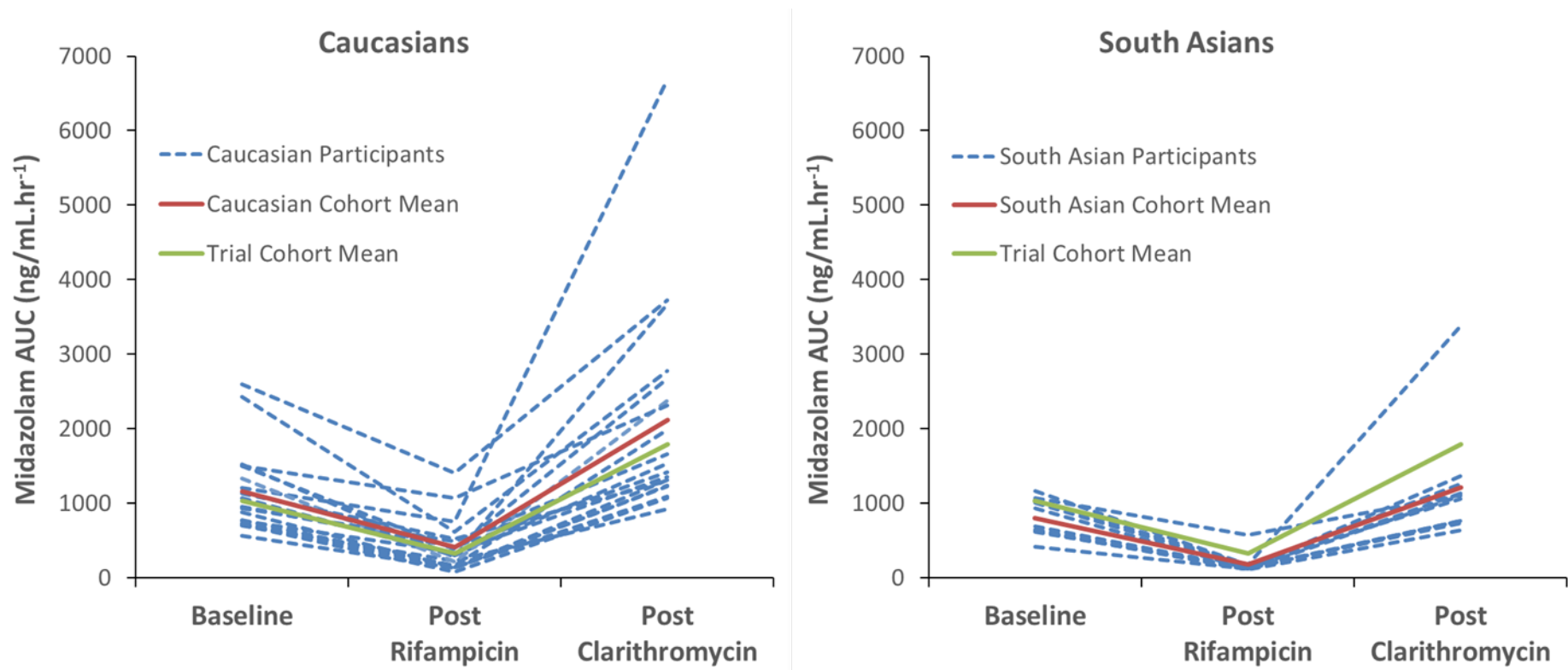


**Figure 3.2: Spaghetti plot showing changes in AUC from baseline, following rifampicin and clarithromycin dosing. Panel A; Caucasians, Panel B; South Asians. Dotted lines represent individual participant data, while the solid line represent the cohort means.**

### 3.4 Discussion

This chapter demonstrate significantly higher midazolam clearance in healthy age matched males of South Asian compared to Caucasian ancestry. These data are consistent with, and provide evidence for the clinical importance of, a prior study of Yamaori et al. (214), which described 2- to 3- times higher expression of CYP3A mRNAs in Japanese compared to Caucasian livers. Furthermore, the trend ( $p = 0.067$ ) toward greater inducibility of CYP3A activity in the South Asian cohort observed in the current study supports the conclusion of Yamaori et al. that the mechanisms regulating hepatic CYP3A expression may be different between racial groups.

The higher midazolam clearance among South Asians reported here is inconsistent with a prior analysis of midazolam clearance reported by He et al. (215), where no difference in midazolam oral clearance related to Asian race was observed. Notably however, while the prior analysis was similar in terms of total cohort size (i.e.  $n = 26$  vs  $30$ ), this prior cohort had greater heterogeneity in terms of gender, age and race, and limited power to assess the impact of Asian race, with only 2 of 26 participants of Asian ancestry.

To date, the broader assessment of inter-racial differences in CYP3A has primarily focused on characterizing differences in genotype frequencies between Caucasian, Asian and African-American populations (216-218). In this regard, the major reduced function variant (CYP3A4\*22) is observed at a higher frequency in Caucasians compared to other racial groups, while functional CYP3A5 (CYP3A5\*1) is comparatively uncommon in Caucasians compared to other races, with 95% of the population exhibiting the homozygous non-functional (CYP3A5\*3/\*3) genotype (218). In contrast, functional CYP3A5 (\*1/\*1 or \*1/\*3) genotypes are observed at a frequency of 25 to 40 % in Asian populations (219, 220). Consistent with these reported CYP3A allelic frequencies, in the current study the frequency of CYP3A4 (\*1/\*22)

genotype was lower in the South Asian cohort, while the frequency of functional CYP3A5 (\*1/\*3) genotype was higher. Notably, however, while these genotypes are biologically consistent with the observed higher midazolam clearance in the South Asian cohort, analysis of the difference in midazolam exposure and CYP3A inducibility adjusted for CYP3A genotypes demonstrated that the higher midazolam clearance in the South Asian cohort was independent of genotype, thus indicating that other factors are responsible for the higher CYP3A activity in this population. This observation is consistent with prior analyses that have demonstrated that the frequency of genetic variants in CYP3A4 and CYP3A5 correlate poorly with *in vivo* CYP3A-mediated drug metabolism (207, 215, 216, 221, 222).

The inability of genotyping (an established DME diagnostic) to define inter-racial differences in CYP3A activity highlights a major challenge to individualized (or precision) dosing more generally; that is the lack of a reliable marker of activity for an enzyme that is responsible for the metabolism of approximately one third of clinically used drugs (210). Intriguingly, the findings of Yamaori et al. suggest that assessment of hepatic CYP3A4 mRNA expression may be a robust marker to account for variability in CYP3A activity. The limitation being that Yamaori et al. utilized surgically resected liver tissue (in many cases from individuals post-mortem) to assess expression of hepatic CYP3A mRNAs, an approach is preclusively invasive for routine clinical application.

In this regard, it has been demonstrated that factors known to impact drug metabolising enzyme (DME) activity such as aging and pregnane X receptor (PXR) expression significantly affect expression of CYP3A mRNAs in more diagnostically amenable tissues such as peripheral blood mononuclear cells (PBMCs) (223). However, attempts to correlate CYP3A4 mRNA expression in peripheral blood mononuclear cells (PBMCs) with activity or induction have demonstrated that PBMC mRNA expression does not reflect systemic CYP3A mediated drug

clearance (224, 225), and current evidence does not support the quantification of mRNA expression in PBMCs as a robust surrogate for CYP3A activity or inducibility. Given the importance of understanding variability in CYP3A activity there is a considerable need for novel strategies to define robust surrogates for hepatic CYP3A activity or expression in diagnostically amenable tissue. This enhanced understanding of the impact of factors, that contribute to variability in CYP3A activity is likely to be of greatest importance for classes of narrow therapeutic index drugs where CYP3A4 activity is a major determinant of exposure, such as small molecule kinase inhibitors (177) and HIV protease inhibitors (226). While such insights may, at least partially, be derived from approaches such as PBPK modelling (227, 228), robust verification of such approaches still requires high quality biological and clinical evidence.

### **3.5 Conclusion**

In conclusion, the data presented here demonstrate significantly higher midazolam clearance in healthy age matched males of South Asian compared to Caucasian ancestry that was not explained by differences in the frequencies of CYP3A genotype. These data suggest that race is possible a systematic source of variability in KI exposure, the implication being that higher CYP3A4 activity may result in lower KI exposure in South Asian patients. Unfortunately, the current lack of direct comparison of KI exposure between Caucasian and South Asian patient cohorts precludes the immediate verification of this finding, however, these results do suggest that future studies are warranted.

---

# CHAPTER IV: ASSESSMENT OF A DIETARY MARKER OF VARIABILITY IN CYTOCHROME P450 3A4 ACTIVITY

---

*The results presented in this chapter have  
been submitted for publication in:*

van Dyk M, Miners JO, Marshall JC, Wood LS, Sorich MJ, Rowland A (2018) Assessment of the caffeine to trimethyluric acid ratio as a dietary marker of variability in cytochrome P450 3A4 activity, *Drug Metabolism and Disposition*.

## 4.1 Introduction

As discussed in Chapter I and II, CYP activity can be affected by genetic, physiological (e.g. age, body weight and gender), disease (e.g. impaired hepatic function), and environmental (e.g. drug interactions, alcohol consumption, smoking and diet) factors (229). Although CYP3A4 between subject variability (BSV) (referred to as inter-individual variability in chapters I, II, III and V, but BSV in the publications associated with this chapter and chapter VI) is thought to be primarily due to non-genetic differences in protein expression, which are currently difficult to quantify in humans (210, 230). By contrast, CYP3A5 is expressed polymorphically, with only approximately 15% of Caucasians expressing the active wild-type enzyme (230). Despite significant BSV in CYP3A activity, it is not routine practice to define an individual's CYP3A activity (229) and often fixed dosing protocols are implemented (125). The limited consideration of BSV in CYP3A activity is primarily due to the challenges associated with developing a robust evidence base for the value of dose individualisation using traditional approaches such as pharmacogenetic testing (231) and therapeutic drug monitoring, particularly in populations such as cancer patients and patients with mental illness (232). The need for a diagnostically amenable strategy to define CYP3A activity is clear (230, 233), however, a robust, efficient and cost-effective approach has not yet been established and the inability to account for variability in CYP3A4 activity in patients continues to be a clinical challenge (234-237). Currently, assessment of the area under the midazolam plasma concentration curve (AUC) is the gold standard to phenotype CYP3A4 activity. This strategy is commonly used to assess inhibition or induction of this enzyme in a research setting. However despite the well-established value of this approach in research, midazolam phenotyping has not, and likely will never, be translated into clinical practice due to logistical and safety issues associated with dosing patients (230, 235, 238).

In addition to drugs, CYP3A4 is also responsible for the metabolism of endogenous chemicals (237). For example, CYP3A4 converts testosterone to 6 $\beta$ -hydroxytestosterone, cortisol to 6 $\beta$ -hydroxycortisol, cortisone to 6 $\beta$ -hydroxycortisone and cholesterol to 4 $\beta$ -hydroxycholesterol (237). Indeed, each of these compounds have been studied extensively as endogenous markers of CYP3A4 activity, but are only able to explain a small proportion ( $r^2$  0.1 to 0.4) of CYP3A4 BSV (237, 239-241). Not only are the correlations relatively weak but results are inconsistent (239), and consequently quantification of these compounds has not provided a robust strategy to assess differences in CYP3A activity (237). Caffeine is metabolised extensively in humans, primarily via N-demethylation but to a lesser extent by 8-hydroxylation (to form 1,3,7-trimethyluric acid, TMU) (242). Measurement of caffeine N3-demethylation activity (to form paraxanthine) is a well-established marker of CYP1A2 activity in vivo. In contrast to N-demethylation, enzyme activity inhibition, activation and correlation studies with human liver microsomes as the enzyme source indicate that CYP3A is mainly responsible for TMU formation (243). The study reported in this chapter sought to assess the conversion of caffeine to TMU as a potential novel dietary biomarker for CYP3A4 activity.

## **4.2 Materials and Methods**

### **4.2.1 Study Protocol**

The EPOK-15 study protocol was reported in Chapter III. Briefly, healthy male genotyped participants ( $n = 30$ ) aged 21 to 35 years were enrolled into the study following screening by physical examination. Exposure to a 1 mg oral dose of midazolam and dietary caffeine (~35 mg in 375 mL of 'Coke Zero') was assessed at baseline (Day 1) and following a 7 day course of rifampin (Day 8). Timed blood samples were collected prior to and for up to 6 hr post

midazolam and caffeine dosing. Between Day 1 and Day 8 participants self-administered rifampin (300mg QD PO).

#### **4.2.2 Midazolam Concentrations**

The sample preparation and analysis of midazolam plasma concentrations was reported in Chapter III. Briefly, 100  $\mu$ L of plasma sample was diluted in 300  $\mu$ L of methanol containing 0.1 % formic acid and 7.5 ng/mL d<sub>6</sub>-midazolam (assay internal standard) vortexed for 3 min, then centrifuged at 16,000 g for 5 min. Analytes in a 2.5  $\mu$ L aliquot of the resulting supernatant were separated from the sample matrix by ultra-performance liquid chromatography (UPLC) performed on a Waters ACQUITY™ BEH C18 column (100 mm  $\times$  2.1 mm, 1.7  $\mu$ m; Waters Corp., Milford, USA) using a Waters ACQUITY™ UPLC system. Column elutant was monitored by mass spectrometry (MS), performed on a Waters Q-ToF Premier™ quadrupole, orthogonal acceleration time-of-flight tandem mass spectrometer (Q-ToF-MS) operating in positive electron spray ionisation (ESI+) mode. Selected ion data was extracted at the analyte [M+H]<sup>+</sup> precursor m/z. Resulting pseudo-MRM spectra were analysed using Waters TargetLynx™ software. Plasma analyte concentrations were determined by comparison of normalised peak areas in participant samples to those of calibrators.

#### **4.2.3 Caffeine Metabolomics**

Prior to analysis of EPOK-15 participant samples, a metabolomics approach was employed to predict the most appropriate caffeine metabolites to evaluate as markers of CYP3A4 activity using archived samples from a cohort of healthy 21 to 40 year olds administered a fixed dose of caffeine (100mg) as a component of a cocktail drug interaction study (172). Plasma samples were prepared and analysed using the approach described below for caffeine and TMU, and mass spectral data were interrogated using the Waters MetaboLynx™ platform.

#### 4.2.4 Caffeine and 1,3,7-trimethyluric Acid Concentrations

The sample preparation and analysis of Caffeine and TMU plasma concentrations were performed as described previously (213), with minor modification to optimise sensitivity for quantification of TMU. Briefly, 100  $\mu$ L of plasma sample was diluted in 300  $\mu$ L of methanol containing 0.1 % formic acid and internal standard then vortexed for 1 min, then centrifuged at 16,000 g for 5 min. Analytes in a 5  $\mu$ L aliquot of the resulting supernatant were separated from the sample matrix on a Waters ACQUITY™ BEH C18 column (100 mm  $\times$  2.1 mm, 1.7  $\mu$ m; Waters Corp., Milford, USA) using a Waters ACQUITY™ UPLC system. Column elutant was monitored using a Waters Q-ToF Premier™ Q-ToF-MS operating in positive (caffeine) and negative (TMU) ESI modes. Selected ion data was extracted at the analyte  $[M+H]^+$  (caffeine) or  $[M-H]^+$  (TMU) precursor  $m/z$ . Resulting pseudo-MRM spectra were analysed using Waters TargetLynx™ software. Plasma analyte concentrations were determined by comparison of normalised peak areas in participant samples to those of calibrators.

#### 4.2.5 Data and Statistical Analysis

Non-compartmental methods were used to estimate midazolam AUC and maximal  $C_{max}$  at baseline (Day 1) and following a 7-day course of rifampin (Day 8). Plasma caffeine and TMU concentrations were quantified at 3hr, 4hr and 6hr post caffeine dosing on Day 1 and Day 8. Caffeine/TMU ratios were calculated as the plasma caffeine concentration divided by the plasma TMU concentration at each time point. The geometric mean, SD and 95% confidence interval (95 % CI) for midazolam AUC and caffeine/TMU ratios were determined using IBM SPSS Statistics for Windows, Version 22.0. (IBM Corp, Armonk, NY).

Pearson's correlations were performed to assess the concordance between midazolam AUC and caffeine/TMU ratios at 3, 4 and 6 hr at baseline and following the seven day course of

rifampin. Each of these experimental data sets were then randomised (2:1) into training and verification data sets and linear regression was performed using the training data set to derive an equation relating the caffeine/TMU ratio to the midazolam AUC. The validity of each equation was assessed by Bland Altman analysis with post-hoc linear regression modelling using IBM SPSS Statistics for Windows, Version 22.0. (IBM Corp, Armonk, NY). Pearson's correlations were also performed to assess the relationship between change in midazolam AUC ( $\Delta$ AUC) and the change in caffeine/TMU ratios ( $\Delta$ caffeine/TMU ratio), post-/pre- rifampin dosing, as a secondary outcome. One-way ANOVAs were performed to assess differences in caffeine/TMU ratios (1) pre- and post- rifampin dosing, and (2) between Caucasian and South Asian study participants, as exploratory outcomes. *p*-values <0.05 were considered statistical significant.

## **4.3 Results**

### **4.3.1 Caffeine Metabolomics**

Metabolomic screening of archived human plasma samples (n=12) was performed to characterise the caffeine metabolite profile in human plasma, and to predict the best caffeine metabolite for the assessment of CYP3A4 activity. Of the 8 metabolites identified in human plasma, the only metabolite that demonstrated a correlation between caffeine/metabolite ratio and midazolam AUC was TMU. The  $r^2$  for the correlation between midazolam AUC and caffeine/TMU ratio at 6 hr following a fixed dose of caffeine (100 mg) was 0.88. On this basis, caffeine/TMU ratio was selected as the investigational dietary caffeine test to predict CYP3A4 activity.

### 4.3.2 Study Conduct

Thirty male subjects completed the study. Two subjects experienced minor adverse events that were attributed to study interventions, but that did not affect their completion of the study (one participant experienced discomfort at cannulation site on Day 8 and one experienced dry mouth during the rifampin dosing phase). Based on clinically relevant allelic variants in CYP3A4 and CYP3A5, two subjects were classified as CYP3A4 intermediate metabolisers (CYP3A4 \*1/\*22), and seven subjects were CYP3A5 intermediate metabolisers (CYP3A5\*1/\*3). All remaining participants were CYP3A4 extensive metabolisers (CYP3A4 \*1/\*1) and poor (non-functional) CYP3A5 metabolisers (CYP3A5 \*3/\*3 or \*3/\*5). Both CYP3A4 \*1/\*22 participants were CYP3A5 \*3/\*3.

Adherence to rifampin dosing was determined by assessment of rifampin concentrations in pre-midazolam dosing blood samples on Day 8. Mean ( $\pm$  S.D.) plasma rifampin concentrations were  $513 \pm 146$   $\mu\text{g/L}$ . Observed concentrations were consistent with predicted exposure profiles with the respective dosing regimens, and are indicative of good adherence in all participants.

### 4.3.3 Midazolam Exposure

A summary of the geometric mean (95% CI) baseline and post induction AUC and  $C_{\text{max}}$  values defining midazolam exposure and the changes in midazolam exposure caused by induction of CYP3A4 are reported in **Table 4.1**. The geometric mean baseline midazolam AUC was 1029  $\mu\text{g/L/hr}$ , while the mean baseline midazolam  $C_{\text{max}}$  was 6.6  $\mu\text{g/L}$ . The mean (95% CI) change in midazolam AUC post rifampin dosing was 4.4- (3.8-5.1-) fold.

**Table 4.1: Midazolam AUC and  $C_{max}$  values at baseline and following rifampin induction**

	Study Phase	Mean	95% Confidence Interval	
			Lower	Upper
AUC	Baseline	1029	996	1061
	Induced	326	306	346
$C_{max}$	Baseline	6.58	6.37	6.79
	Induced	2.11	1.99	2.24

Units: AUC ( $\mu\text{g/L/hr}$ );  $C_{max}$  ( $\mu\text{g/L}$ )

#### 4.3.4 Caffeine and TMU Exposure

A summary of the geometric mean (95% CI) plasma caffeine/TMU ratios are reported in **Table 4.2**. Caffeine/TMU ratios were 2.1- to 2.6- fold higher post rifampin dosing compared to baseline. One-way ANOVA demonstrated that in all cases the increase in caffeine/TMU ratio post- rifampin dosing was statistically significant ( $p < 0.005$ ).

**Table 4.2: Caffeine/TMU ratios at baseline and following rifampin induction**

Time	Study Phase	Ratio (Mean)	95% Confidence Interval	
			Lower	Upper
3hr	Baseline	461.3	313.5	609.1
	Induced	228.3	159.2	297.4
4hr	Baseline	396.6	314.7	478.4
	Induced	196.9	140.1	253.6
6hr	Baseline	360.6	265.3	455.8
	Induced	157.9	112.5	203.3

**Table 4.3: Bias in CYP3A activity measured by the caffeine/TMU ratio and midazolam AUC.**

Time	Study Phase	Equation	Mean Absolute Error (%)	Constant Bias		Proportional Bias	
				Mean Difference	sig ( <i>p</i> )	t value	sig ( <i>p</i> )
3hr	Baseline	$0.55^*y + 3.5948$	0.51	-0.04201	0.443	1.512	.151
	Induced	$1.31^*y - 1.4356$	1.84	-0.06983	0.561	-0.982	0.341
4hr	Baseline	$0.815^*y + 1.9693$	0.60	0.09369	0.142	-.044	0.966
	Induced	$1.38^*y - 1.669$	1.83	-0.06169	0.561	-0.359	0.725
6hr	Baseline	$0.688^*y + 3.0001$	0.45	-0.11318	0.126	0.329	0.746
	Induced	$1.29^*y - 0.8034$	1.77	0.09649	0.382	-0.158	0.876

### 4.3.5 Prediction of CYP3A4 Activity Using Caffeine/TMU Ratios

The correlation of caffeine/TMU ratios at 3, 4 and 6 hr post-dose with midazolam AUC pre- (Day 1) and post- (Day 8) rifampin dosing are shown in **Figure 4.1**. The relationship between caffeine/TMU ratio and midazolam AUC at baseline and post induction was best described by a linear model. At baseline,  $r^2$  values for the correlation were 0.82, 0.79 and 0.65 at 3, 4, and 6 hr, respectively. The strength of correlations were retained post-induction with  $r^2$  values of 0.72, 0.87 and 0.82 at 3, 4, and 6 hr, respectively. Bland Altman plots for CYP3A4 activity measured by each approach in the verification data sets are shown in **Figure 4.2** and the statistics defining the concordance between the two measures of CYP3A4 activity are presented in **Table 4.3**. In all cases the mean percent absolute error for the derived equation relating the caffeine/TMU ratio to midazolam AUC was  $< 2.5\%$ . Bland Altman analysis demonstrated strong concordance between the two measures of CYP3A4 activity in the verification data sets with  $p > 0.1$  for all experimental conditions. Similarly, linear regression modelling adjusted for mean CYP3A activity demonstrated a lack of proportional bias between the two measures of CYP3A activity. Overall, the strongest correlation between caffeine/TMU ratio and midazolam AUC was observed for the 4 hr post dosing data set. Notably however, appreciably weaker correlations were observed between the  $\Delta$ midazolam CL/F and  $\Delta$  caffeine/TMU ratio, with  $r^2$  values ranging from 0.30 to 0.41. These data support a robust capacity to define BSV in CYP3A4 activity using the 4hr caffeine/TMU ratio, but a poor capacity to track within subject variability (WSV) in CYP3A4 activity due to induction using any caffeine/TMU ratio.

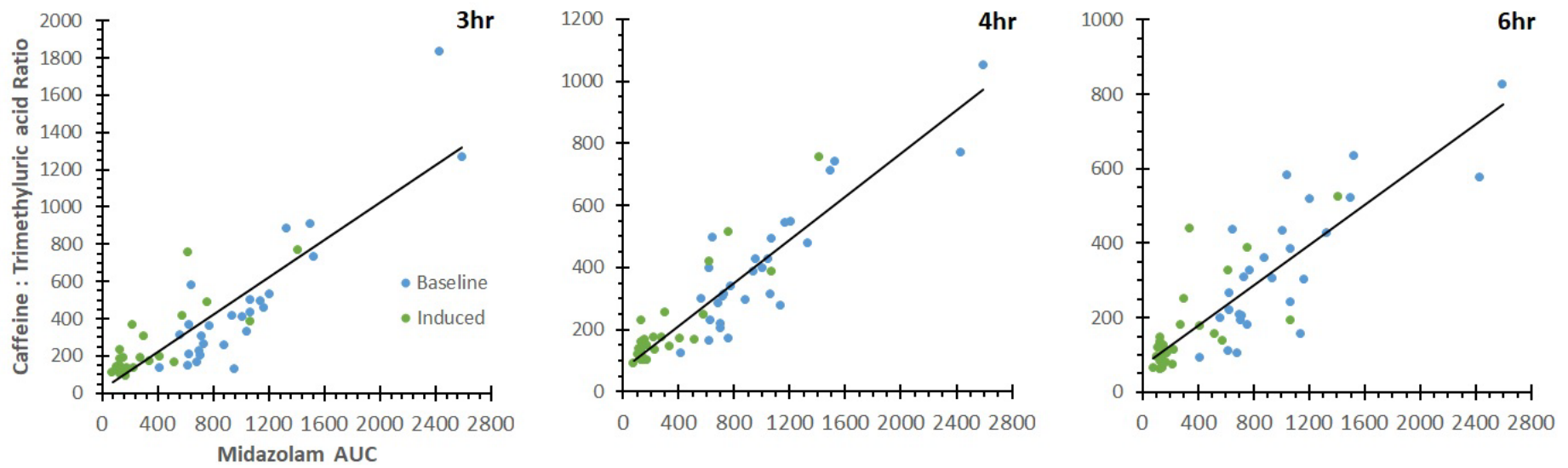


**Figure 4.1: Correlation between baseline (blue) and post induction (green) midazolam AUC and caffeine/TMU ratio.**

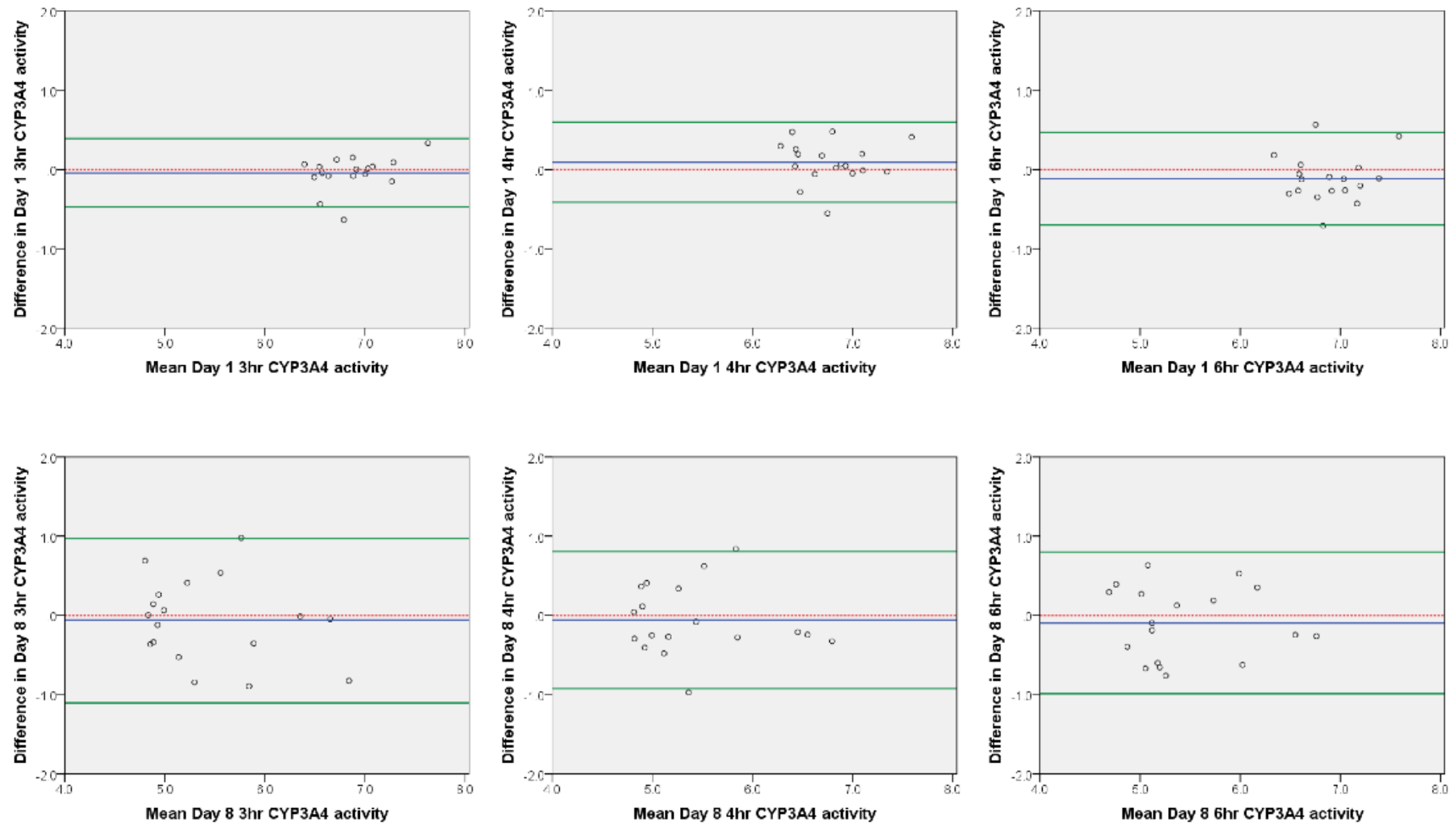


**Figure 4.2: Bland Altman plots for the measurement of CYP3A4 activity by midazolam AUC and caffeine/TMU ratio at 3, 4, and 6 hr post dosing on Day 1 and Day 8.**

### 4.3.6 Impact of Race on Caffeine/TMU Ratio

Based on the observed impact of ethnicity on midazolam oral clearance (Chapter III), the capacity of the caffeine/TMU ratio to describe inter-racial variability in CYP3A4 activity was evaluated as an exploratory outcome. Statistics describing caffeine/TMU ratios and midazolam AUC in Caucasian and South Asian cohorts, and the difference between cohorts for each study phase are reported in **Table 4.4**. While there were multiple trends supporting a difference in caffeine/TMU ratio between Caucasian and South Asian cohorts ( $p < 0.1$ ), with the exception of the Day 8 6hr caffeine/TMU ratio ( $p = 0.038$ ), this study did not demonstrate statistically significant inter-racial variability in CYP3A4 activity using caffeine/TMU ratios. Consistent with prior reports, there was a significant difference in midazolam AUC between Caucasian and South Asian study participants pre- ( $p = 0.026$ ) and post- ( $p=0.027$ ) rifampicin dosing.

**Table 4.4: Impact of race on the caffeine/TMU ratio and midazolam AUC.**

Test	Phase	Cohort	Mean	95% Confidence Interval		Sig ( $p$ )
				Lower	Upper	
3 hr Caffeine / TMU ratio	D1	Caucasian	502	333	671	0.092
		South Asian	332	245	418	
		Difference	171	-30	371	
	D8	Caucasian	269	171	367	0.068
		South Asian	161	109	214	
		Difference	108	-9	225	
	D1/D8 ratio	Caucasian	1.96	1.58	2.33	0.390
		South Asian	2.32	1.61	3.02	
		Difference	-0.36	-1.22	0.50	
4 hr Caffeine /	D1	Caucasian	430	314	546	
		South Asian	342	264	420	

TMU ratio		Difference	88	-59	234	0.230
	D8	Caucasian	230	147	314	
		South Asian	142	117	167	
		Difference	88	-4	181	0.060
	D1/D8 ratio	Caucasian	2.17	1.79	2.55	
		South Asian	2.51	1.86	3.16	
Difference		-0.34	-1.15	0.48	0.392	
6 hr Caffeine / TMU ratio	D1	Caucasian	359	263	455	
		South Asian	282	190	373	
		Difference	78	-62	217	0.262
	D8	Caucasian	174	115	233	
		South Asian	105	88	121	
		Difference	69	4	135	0.038 *
D1/D8 ratio	Caucasian	2.55	1.89	3.22		
	South Asian	2.81	1.74	3.87		
	Difference	-0.26	-1.60	1.09	0.693	
Midazolam AUC	D1	Caucasian	1172	905	1438	
		South Asian	804	659	949	
		Difference	368	49	687	0.026 *
	D8	Caucasian	380	231	528	
		South Asian	177	97	257	
		Difference	203	25	380	0.027 *
D1/D8 ratio	Caucasian	4.10	3.19	5.01		
	South Asian	5.29	4.34	6.23		
	Difference	-1.19	-2.57	0.19	0.089	

## 4.4 Discussion

This chapter describes the evaluation of a dietary marker to describe variability in CYP3A activity. The importance of this potential novel marker for variability in CYP3A activity being that as both genetic and non-genetic factors contribute to BSV in the activity of this enzyme, it is difficult to predict exposure to drugs metabolised by CYP3A. Despite extensive study no genetic test currently accounts for a meaningful proportion of BSV in CYP3A4 activity. As such, alternate approaches have been extensively studied but currently have major limitations. Midazolam has proven to be a robust drug probe to describe CYP3A activity but the use of this probe is limited by the logistical complexity and safety issues associated with administering a highly restricted drug and measuring exposure over a prolonged intense sampling period. This limitation has been partially alleviated with the validation of midazolam micro-dosing and the limited sampling strategies, each of which are used in research settings. Indeed, potentially, the greatest advance in the evaluation of CYP3A4 activity in the past decade has been the validation of the midazolam micro-dose test. While this approach addresses many of the safety concerns, it still requires the administration of a highly restricted drug and subsequent intense period of blood sampling (244).

Previous studies have assessed potential endogenous biomarkers, however correlations with midazolam clearance have been poor with  $r^2$  values typically below 0.50 (245, 246). The most extensively studied of these endogenous biomarkers is cortisol. It has been demonstrated that the change in the ratio of urinary cortisol to its metabolite 6 $\beta$ -hydroxycortisol correlates strongly ( $r^2=0.83$ ) with induction of CYP3A expression (247). However, in contrast, multiple studies have demonstrated weak concordance of this metabolic ratio with absolute CYP3A4 activity (240, 244, 247). It has been suggested that diurnal and nocturnal fluctuation in cortisol levels together with variability in urinary clearance of cortisol can affect the formation

clearance of the metabolite. Another proposed reason for the observed inconsistent results with cortisol is the capacity for cortisol and 6 $\beta$ -hydroxycortisol to interconvert to cortisone and 6 $\beta$ -hydroxycortisone. In order to attempt to address this confounding factor, it has been proposed that these metabolites are quantified in combination. While assessment of cortisol metabolic ratios is a safe and efficient approach, high BSV and WSV and the inability to define absolute CYP3A4 activity limit the value of this metabolic ratio as a reliable biomarker for CYP3A4 activity. Another potential endogenous biomarker that has been extensively studied is the ratio of urinary 6 $\beta$ -hydroxycholesterol and cholesterol. Superior concordance has been demonstrated between the ratio of urinary 6 $\beta$ -hydroxycholesterol to cholesterol and midazolam clearance compared to the cortisol metabolic ratio (246). However, circulating cholesterol levels also significantly fluctuate between days limiting the value of this endogenous biomarker for the prediction of CYP3A4 activity. Steroid hormones, in particular testosterone, have also been evaluated as biomarkers for CYP3A4 activity (237). While plausible biomarkers for CYP3A4 activity, due to the complexity of steroid synthesis and degradation, the interconversion between analytes and the temporal variability in steroid levels, these chemicals have largely been discounted as viable biomarkers of CYP3A4 activity.

In the absence of robust endogenous biomarker, dietary chemicals provide an alternative approach. Caffeine is a relatively ubiquitous dietary chemical and hence represents a logistically feasible dietary biomarker. Caffeine is already used as a marker of CYP1A2 activity (as the ratio of caffeine to its primary N-demethylated metabolite paraxanthine). Caffeine exhibits complex metabolism involving multiple pathways, including the conversion to TMU, which is primarily catalysed by CYP3A4 (248). Therefore, dietary caffeine was considered a potential probe for the prediction of CYP3A4 activity. Consistent with the reported contribution of CYP to caffeine metabolism, while a metabolomic screen using archived samples (n=12) from healthy individuals administered a fixed dose of caffeine

(100mg) identified 8 caffeine metabolites in human plasma, the only metabolite ratio that demonstrated any concordance with midazolam AUC was the caffeine/TMU ratio.

The emphasis of the current study was to extend this finding, and determine whether dietary caffeine could be used to predict CYP3A activity. This was achieved by correlating the caffeine/TMU ratio at three time points (3, 4 and 6 hr) post-dose with midazolam AUC. Moderate to strong concordance was demonstrated between each caffeine/TMU ratio and midazolam AUC both at baseline and post induction, with  $r^2$  values ranging from 0.65 to 0.87. Bland Altman analysis with post-hoc logistical regression demonstrated a lack of bias in CYP3A4 activity described by each approach both at baseline and post induction. These data support the capacity of the caffeine/TMU ratio to explain BSV in CYP3A4 activity. Notably, however comparatively weak correlations were observed between the change in midazolam AUC and the change in caffeine/TMU ratio (Day 8 / Day 1), with  $r^2$  values ranging from 0.3 to 0.41. It is plausible that this inability of the caffeine/TMU ratio to describe the change in CYP3A4 activity caused by induction with rifampin is due to the differential effects of rifampin on alternate caffeine metabolic pathways. Specifically, BSV in the effects of rifampin on the dominant CYP1A2 mediated pathways may perturb the caffeine concentration thus confounding the observed change in the minor CYP3A catalyzed pathway.

Although significant correlations with midazolam AUC and caffeine/TMU ratios were observed, it is important to note that the cohort was small and homogenous. As such, these findings need to be replicated in a larger and more diverse cohort in terms of age and gender in order to verify this outcome. Specifically, as this study consisted of all male participants, gender could not be assessed as a covariate affecting the capacity of the caffeine/TMU ratio to describe CYP3A4 activity and would need to be included in any follow-up study as it is known that CYP3A4 activity is higher in females. Notably, consistent trends ( $p < 0.1$ ) were observed

supporting the capacity of the caffeine/TMU ratio to define inter-racial variability in CYP3A4 activity between Caucasians and Southeast Asians.

## **4.5 Conclusion**

In conclusion, it is unlikely that caffeine/TMU ratio alone is sufficient to explain all forms of variability in CYP3A4 activity, however, these results indicate that the caffeine/TMU ratio may be an important tool to define BSV in CYP3A4 activity, and may be a useful marker in a panel based metric to assess variability in CYP3A4 activity.

---

# CHAPTER V: A NOVEL APPROACH TO ASSIST IN OPTIMISED KI DOSING

---

*The results presented in this chapter have  
been reported in:*

van Dyk M, Miners JO, Kichenadasse G, McKinnon RA, Rowland A (2016) A novel approach for the simultaneous quantification of 18 small molecule kinase inhibitors in human plasma: a novel platform for optimised KI dosing. *Journal of Chromatography B*, 1033, 17-

25.

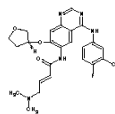
## 5.1 Introduction

As explained in Chapter I, variable KI exposure frequently manifests as therapeutic failure due to reduced tumour exposure resulting from enhanced clearance or impaired uptake, or toxicity due to increased systemic exposure resulting from impaired clearance or enhanced uptake (249). As discussed in previous chapters, variability in KI exposure is inadequately addressed by the routinely used fixed-dose schedule of administration (44, 45) resulting in the sub-optimal use of these drugs (250). One of the identified strategies to achieve optimal KI dosing is with TDM (section 1.6.1). The benefit of TDM-guided KI dosing has been reported for a limited number of KIs including axitinib, imatinib, pazopanib and sunitinib (125, 133, 251, 252). However, due to the rapid expansion of this novel drug class and relative slow development of TDM platforms (both in terms of the analytical platforms to quantify plasma-KI concentrations and validated target plasma-KI concentration ranges), the capacity to achieve optimised KI dosing through TDM in a timely manner remains limited, particularly for newer KIs.

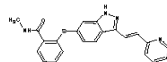
TDM platforms routinely use LC with detection of analytes by UV absorbance, fluorescence or MS. Indeed, a number of LC based approaches, utilising UV or MS detection have been reported for the quantification of plasma-KI concentrations. Typically approaches utilising UV detection facilitate the measurement of only a single analyte, and as such are of limited clinical utility in terms of TDM platforms. More recently, a number of studies have reported LC-MS panel-based approaches for the quantification of 3 (253, 254), 4 (255), 6 (251, 256, 257); 8 (258) or 9 KIs (259, 260). However, these approaches focus on a common panel of 11 KIs (axitinib, dasatinib, erlotinib, gefitinib, imatinib, lapatinib, nilotinib, pazopanib, regorafenib, sorafenib and sunitinib), and as such do not facilitate pharmacokinetic (PK) analysis for newer KIs, which are required to universally establish optimised plasma-KI concentration ranges.

Recognising a need to address the limited scope of existing analytical approaches for the quantification of plasma-KI concentrations, this chapter sought to develop and validate a substantially more extensive platform.

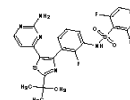
**Afatinib**  
 Molecular Formula =  $C_{22}H_{25}ClFN_5O_3$   
 Formula Weight = 485.9384032  
 Monoisotopic Mass = 485.162996 Da  
 [M+H]<sup>+</sup> = 486.170272 Da



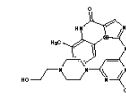
**Axitinib**  
 Molecular Formula =  $C_{22}H_{18}N_4OS$   
 Formula Weight = 386.46952  
 Monoisotopic Mass = 386.120131 Da  
 [M+H]<sup>+</sup> = 387.127408 Da



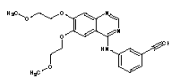
**Dabrafenib**  
 Molecular Formula =  $C_{25}H_{30}F_3N_4O_5S_2$   
 Formula Weight = 519.5624096  
 Monoisotopic Mass = 519.10105 Da  
 [M+H]<sup>+</sup> = 520.108326 Da



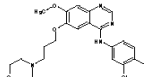
**Dasatinib**  
 Molecular Formula =  $C_{23}H_{26}ClN_7O_3S$   
 Formula Weight = 488.00554  
 Monoisotopic Mass = 487.155721 Da  
 [M+H]<sup>+</sup> = 488.162997 Da



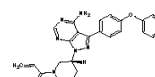
**Erlotinib**  
 Molecular Formula =  $C_{22}H_{23}N_3O_4$   
 Formula Weight = 393.43672  
 Monoisotopic Mass = 393.168856 Da  
 [M+H]<sup>+</sup> = 394.176133 Da



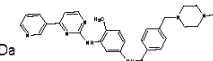
**Gefitinib**  
 Molecular Formula =  $C_{22}H_{24}ClFN_4O_3$   
 Formula Weight = 446.9023632  
 Monoisotopic Mass = 446.152097 Da  
 [M+H]<sup>+</sup> = 447.159373 Da



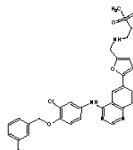
**Ibrutinib**  
 Molecular Formula =  $C_{25}H_{24}N_6O_2$   
 Formula Weight = 440.49706  
 Monoisotopic Mass = 440.196074 Da  
 [M+H]<sup>+</sup> = 441.20335 Da



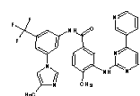
**Imatinib**  
 Molecular Formula =  $C_{29}H_{31}N_7O$   
 Formula Weight = 493.60274  
 Monoisotopic Mass = 493.259009 Da  
 [M+H]<sup>+</sup> = 494.266285 Da



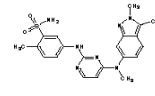
**Lapatinib**  
 Molecular Formula =  $C_{29}H_{26}ClFN_4O_6S$   
 Formula Weight = 581.0575432  
 Monoisotopic Mass = 580.134731 Da  
 [M+H]<sup>+</sup> = 581.142008 Da



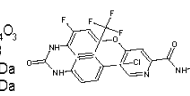
**Nilotinib**  
 Molecular Formula =  $C_{28}H_{22}F_3N_7O$   
 Formula Weight = 529.5157896  
 Monoisotopic Mass = 529.183783 Da  
 [M+H]<sup>+</sup> = 530.191069 Da



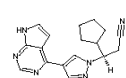
**Pazopanib**  
 Molecular Formula =  $C_{21}H_{23}N_7O_3S$   
 Formula Weight = 437.51802  
 Monoisotopic Mass = 437.163393 Da  
 [M+H]<sup>+</sup> = 438.170669 Da



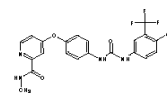
**Regorafenib**  
 Molecular Formula =  $C_{21}H_{16}ClF_4N_4O_3$   
 Formula Weight = 482.8154128  
 Monoisotopic Mass = 482.076881 Da  
 [M+H]<sup>+</sup> = 483.084157 Da



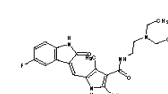
**Ruxolitinib**  
 Molecular Formula =  $C_{17}H_{18}N_6$   
 Formula Weight = 306.36502  
 Monoisotopic Mass = 306.159295 Da  
 [M+H]<sup>+</sup> = 307.166571 Da



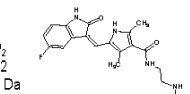
**Sorafenib**  
 Molecular Formula =  $C_{21}H_{16}ClF_3N_4O_3$   
 Formula Weight = 464.8249496  
 Monoisotopic Mass = 464.086303 Da  
 [M+H]<sup>+</sup> = 465.093579 Da



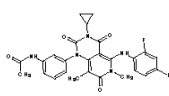
**Sunitinib**  
 Molecular Formula =  $C_{22}H_{21}FN_4O_2$   
 Formula Weight = 398.4737832  
 Monoisotopic Mass = 398.211804 Da  
 [M+H]<sup>+</sup> = 399.219081 Da



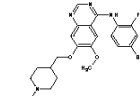
**N-desethyl Sunitinib**  
 Molecular Formula =  $C_{20}H_{23}FN_4O_2$   
 Formula Weight = 370.4206232  
 Monoisotopic Mass = 370.180504 Da  
 [M+H]<sup>+</sup> = 371.187781 Da



**Trametinib**  
 Molecular Formula =  $C_{26}H_{23}FIN_5O_4$   
 Formula Weight = 615.3947932  
 Monoisotopic Mass = 615.077867 Da  
 [M+H]<sup>+</sup> = 616.086144 Da



**Vandetanib**  
 Molecular Formula =  $C_{22}H_{26}BrFN_4O_2$   
 Formula Weight = 475.3539632  
 Monoisotopic Mass = 474.106659 Da  
 [M+H]<sup>+</sup> = 475.113936 Da



**Vemurafenib**  
 Molecular Formula =  $C_{27}H_{19}ClF_3N_3O_3S$   
 Formula Weight = 489.9221264  
 Monoisotopic Mass = 489.072546 Da  
 [M+H]<sup>+</sup> = 490.079822 Da

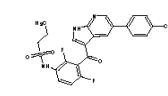


**Figure 5.1: Chemical characteristics for KIs relevant to their detection by mass spectrometry**

## **5.2 Methods and Materials**

### **5.2.1 Chemicals and Reagents**

Afatinib, axitinib, dabrafenib, dasatinib, erlotinib, gefitinib, ibrutinib, imatinib, lapatinib, nilotinib, pazopanib, ruxolitinib, sorafenib, sunitinib, vandetanib and vemurafenib were obtained from LC Laboratories, Woburn, USA. Regorafenib, N-desethyl sunitinib, trametinib, d6-erlotinib hydrochloride, d3-O-methyl-gefitinib, d7-lapatinib di-hydrochloride and d3-sorafenib were obtained from Toronto Research Chemicals, Ontario, Canada. High purity water was obtained using a MilliQ Synergy UV Ultrapure water system (Merck Millipore, Sydney, Australia). All chemicals and reagents were of LC-MS grade. Z Serum Sep Clot Activator (ref no: 455078, lot no: A1310018), Lithium Heparin (ref no: 455084, lot no: A1310031), Lithium Heparin Sep (LH-S) (ref no: 455083, lot no: A141237C) and K<sub>3</sub>EDTA (refno: 455036, lot no: A111106P) specimen collection vacuettes were purchased from Greiner Bio-One.

### **5.2.2 Sample Collection and Preparation**

#### **5.2.2.1 Plasma Samples**

Venous blood from healthy volunteers and oncology patients (approved by Southern Adelaide Clinical Human Research Ethics Committee; 515.13 - HREC/13/SAC/ 347) was collected into an 9 mL LH-S vacuettes, centrifuged (4000 g for 5 min at room temperature), and the plasma separated and stored at -80 °C until analysis. A pool of human plasma obtained from the Flinders Medical Centre Blood Transfusion Service was used for method development, quality control samples and calibrator matrix.

#### **5.2.2.2 Internal Standard Selection**

Given the analytical complexity and substantial cost, and hence reduced feasibility, of

including separate deuterated internal standards (IS) for each of the 18 analytes, an optimised panel of four deuterated IS was employed on the basis of chromatographic retention and recovery characteristics.

### **5.2.2.3 Sample Preparation**

For QC and calibration standards, human plasma was spiked with KIs individually and as a panel. Plasma samples were subjected to solvent precipitation in order to isolate analytes of interest. One hundred  $\mu\text{L}$  of sample or standard was mixed with 50  $\mu\text{L}$  of IS (500 ng/mL d6-erlotinib, d3-O-methyl-gefitinib, d7-lapatinib and d3-sorafenib in methanol) and 300  $\mu\text{L}$  of 1 % formic acid in methanol then vortexed for 30 sec using a MixMate<sup>®</sup> Vortex Mixer (Eppendorf, Sydney, Australia). This mixture was centrifuged for 5 min at 18000 g, and a 250  $\mu\text{L}$  aliquot of the supernatant fraction was transferred to Waters Acquity auto-sampler vial containing an LC-MS grade glass insert (Waters, Sydney, Australia); a 5  $\mu\text{L}$  aliquot was injected directly onto the analytical column. In order to accommodate the substantially higher plasma concentration range for pazopanib (up to 3 orders of magnitude higher than other KIs), patient samples were diluted 1 in 20 by mixing 5  $\mu\text{L}$  of patient plasma with 95  $\mu\text{L}$  of blank calibrator matrix. Diluted samples were treated as per the standard protocol described above.

### **5.2.3 Chromatography**

Chromatographic separations were achieved on a Waters ACQUITY<sup>™</sup> T3 HSS C18 analytical column (150 mm x 2.1 mm, 1.8  $\mu\text{m}$ ) using a Waters ACQUITY<sup>™</sup> UPLC system. The column temperature was maintained at 40 °C, while the sample compartment was maintained at 15 °C. Analytes were separated by gradient elution at a flow rate of 0.25 mL/min. Initial conditions were 80% ammonium formate (10 mM) with 10 % acetonitrile (mobile phase A) and 20 % ammonium formate (10 mM) in 90 % acetonitrile (mobile phase B). The proportion of mobile phase B was increased to 70% over 11 min, then reconditioned to initial conditions over 0.5

min. The total run time for the separation of 18 analytes, including reconditioning, was 15 min.

## 5.2.4 Mass Spectrometry

Column elutant was monitored by mass spectrometry, performed on a Waters Q-ToF Premier™ quadrupole, orthogonal acceleration time-of-flight tandem mass spectrometer (Q-ToF-MS). Electron spray ionisation (ESI) was performed in positive ion mode; ion path within the time-of-flight (ToF) chamber was set in ‘V’ mode for maximum analyte sensitivity. Instrument acquisition settings are described in **Table 5.1**. ToF data were collected in wide pass MS mode, with the resolving quadrupole acquiring data between  $m/z$  250 and 750 to yield a TIC chromatogram. Data was collected using the extended dynamic range function in MassLynx™, and as such was collected as centroid spectra. The collision cell energy was 2 eV. Selected ion data was extracted at the precursor  $m/z$  of analytes  $[M+H]^+$  as described in **Table 5.2**. Resulting pseudo-MRM spectra were analysed using Waters TargetLynx™ software.

**Table 5.1: Mass spectrometer instrument settings**

Parameter	Setting
Capillary voltage (keV)	2.4
Sampling cone voltage (eV)	25
Extraction cone voltage (eV)	5.0
Source temperature (°c)	90
Desolvation temperature (°c)	270
Cone gas flow (L/Hr)	50
Desolvation gas flow (L/Hr)	400
Collision energy (eV)	2
Detector voltage (eV)	1950

### 5.2.5 Calibration

Master stock solutions were prepared for all analytes (1 mg/mL) in MS-grade methanol and stored at -20 °C for no longer than 60 days. Aliquot working stocks were stored at 4 °C for no longer than two weeks. Analyte stability in stock solutions stored under these conditions was confirmed for the respective usage periods. Calibration standards (n = 6 non-zero plus blank) were prepared by dilution of KIs in drug free plasma from healthy individuals, such that the final concentration spanned three orders of magnitude, in all cases incorporating from 0.2 to 5 times the range reported in patient cohorts (**Table 5.2**). A single batch of plasma was used to prepare all calibration standards. Calibration standards were extracted in the same manner as plasma samples. Standard curves prepared in plasma were created by plotting the peak area ratio of the analyte to the associated deuterated IS. Analyte identification within samples was determined based on retention time and m/z value. Post-preparative analyte stability for samples stored at 15°C (autosampler set-temperature) was assessed in the lowest and highest calibration standards over 96 hours (analysis time for 480 samples).

**Table 5.2: Analyte quantification characteristics**

Analyte	Calibration Range (ng/mL)	Calibration Curve Linear Regression Equation	Coefficient of determination (r <sup>2</sup> )	Analyte m/z	Retention Time (min)	Limit of Detection (ng/mL)	Accuracy at LLOQ <sup>a</sup> (% True)
Afatinib	5 – 500	$y = 0.9780x - 0.1006$	0.9998	486.143	3.50	1.28	103
Axitinib	5 – 500	$y = 0.7815x - 0.0261$	0.9997	387.127	5.05	0.90	105
Dabrafenib	10 – 1000	$y = 0.4746x - 0.0372$	0.9998	520.108	9.20	1.27	99
Dasatinib	10 – 1000	$y = 0.2348x + 0.0112$	0.9966	488.162	10.18	1.43	102
Erlotinib	50 – 5000	$y = 0.2293x + 0.0168$	0.9981	394.176	5.18	0.60	106
Gefitinib	50 – 5000	$y = 0.1840x + 0.0022$	0.9998	447.159	3.21	1.22	110
Ibrutinib	5 – 500	$y = 0.8205x + 0.0631$	0.9993	441.175	8.02	1.37	98
Imatinib	25 – 2500	$y = 0.4248x - 0.0049$	0.9951	494.246	3.76	0.15	95
Lapatinib	10 – 1000	$y = 0.2364x - 0.0209$	0.9987	581.142	6.60	0.55	97
Nilotinib	25 – 2500	$y = 0.1935x + 0.0065$	0.9994	530.191	6.84	0.43	112
Pazopanib	1000 – 100000 <sup>b</sup>	$y = 0.0199x + 0.0054$	1.0000	438.170	3.82	13.0	101
Regorafenib	50 – 5000	$y = 0.2302x + 0.0015$	0.9995	483.084	10.18	0.25	107
Ruxolitinib	50 – 5000	$y = 0.1930x + 0.0053$	0.9975	307.166	5.18	0.43	97
Sorafenib	50 – 5000	$y = 0.3720x + 0.0112$	0.9999	465.093	9.81	0.52	108

Sunitinib	2.5 – 250	$y = 0.6367x + 0.0095$	0.9936	399.219	4.68	0.15	103
<i>N</i> -desethyl Sunitinib	2.5 – 250	$y = 0.6392x - 0.0107$	0.9943	371.187	4.11	0.55	98
Trametinib	2.5 – 250	$y = 0.6012x + 0.0246$	0.9984	616.085	8.99	0.07	104
Vandetinib	5 – 500	$y = 0.6820x + 0.0354$	0.9992	475.098	3.69	0.65	98
Vemurafenib	25 – 2500	$y = 0.1939x + 0.0064$	0.9980	490.079	9.68	0.07	107

<sup>a</sup> Lower limit of quantification (LLOQ) defined as the lowest calibration standard.

<sup>b</sup> Effective calibration range based on 1 in 20 dilution of patient samples but not calibrators; actual calibrator concentration range 50 to 5000 ng/mL.

## 5.2.6 Method Validation

### 5.2.6.1 Specimen Tube Comparison

Variability in analyte recovery between specimen collection tubes was assessed in triplicate for a panel of specimen tubes with control samples prepared in glass culture and plastic Eppendorf tubes. One hundred millilitres of blank whole blood was spiked with the panel of 18 analytes (100 µg/L) and mixed thoroughly. Five millilitres of spiked whole blood was then aliquoted into Z Serum Sep Clot Activator, Lithium Heparin (LH-S), and K<sub>3</sub>EDTA specimen collection vacuettes (Greiner Bio-One), glass culture and plastic Eppendorf tubes. Samples were mixed according to the appropriate protocol for each specimen tube type and left to stand at room temperature for 1 hr. Serum or plasma was then isolated using the protocol described in section 5.2.2.1. ANOVA Tukey Post Hoc HSD analysis was performed to assess differences in recovery across the tubes using IBM SPSS Statistics (with an assigned significance at the 0.05 level).

### 5.2.6.2 Analytical Precision and Recovery

Assay precision was assessed on the basis of intra- and inter-day variability for each analyte spiked at three concentrations; the lowest, middle and highest concentrations in corresponding calibration curves (**Table 5.3**). Inter-day variability was assessed in triplicate on 5 occasions, while intra-day variability was assessed in 8 individually prepared samples analysed on a single day.

Analyte recovery was determined both in terms of absolute and relative recovery for each analyte. In order to ensure the accuracy of pazopanib quantification in diluted samples, a comparative analysis was performed with patient samples (n = 4) ranging in concentration from 250 µg/L (tapering of therapy) to 90,000 µg/L (maximal concentration) against undiluted samples analysed using a validated HPLC method with UV detection (111). Relative recovery

was assessed by comparison of calibration slopes attained from extracted standards (n = 6) prepared in matrices of plasma and mobile phase (control), while absolute recovery was assessed by comparison of the calibration slope attained from extracted standards (n = 6) prepared in plasma and volume adjusted un-extracted (pure authentic) standards prepared in mobile phase (control) (**Table 5.3**).

**Table 5.3: Assay precision and recovery.**

Analyte	Precision: Variability (% RSD)						Recovery (%)	
	Lowest		Mid		Highest			
	Intra-day	Inter-day	Intra-day	Inter-day	Intra-day	Inter-day	Absolute	Relative
Afatinib	6.8	2.0	5.1	10.9	2.9	1.2	95	96
Axitinib	2.7	12.9	1.8	7.6	2.1	11.7	92	106
Dabrafenib	7.9	16.7	6.6	11.2	2.3	9.7	101	113
Dasatinib	5.0	4.1	2.1	5.4	3.1	4.3	92	108
Erlotinib	3.6	9.9	4.6	10.1	2.5	12.8	98	105
Gefitinib	4.5	12.9	3.3	9.7	1.5	5.6	103	105
Ibrutinib	6.6	13.1	7.1	3.3	2.6	1.8	92	107
Imatinib	1.2	10.6	3.6	9.7	2.9	14.9	108	99
Lapatinib	2.6	6.8	1.8	8.8	2.9	14.6	113	104
Nilotinib	5.1	15.4	3.5	7.7	3.6	3.1	100	101
Pazopanib	4.1	7.5	2.2	8.0	1.4	8.6	101	102
Regorafenib	5.3	7.6	4.8	8.7	3.1	12.1	107	97
Ruxolitinib	2.9	7.4	4.1	9.1	1.9	5.1	104	111

Analyte	Precision: Variability (% RSD)						Recovery (%)	
	Lowest		Mid		Highest			
	Intra-day	Inter-day	Intra-day	Inter-day	Intra-day	Inter-day	Absolute	Relative
Sorafenib	3.8	12.2	6.4	10.3	1.2	2.8	110	112
Sunitinib	4.8	8.9	2.7	11.8	5.3	9.0	104	110
N-desethyl Sunitinib	5.3	8.1	9.4	7.4	3.8	7.8	95	105
Trametinib	4.7	1.7	3.6	4.0	6.9	10.7	103	107
Vandatinib	6.5	7.5	7.2	9.1	1.4	3.7	101	111
Vemurafenib	6.9	15.7	6.7	11.2	3.6	12.8	105	108

**Table 5.4: Assay accuracy.**

Analyte	QC Concentrations (µg/L)								
	Low			Mid			High		
	Nominal	Measured	% True	Nominal	Measured	% True	Nominal	Measured	% True
Afatinib	12.5	14.3	114	125	133	105	375	370	99
Axitinib	12.5	13.1	104	125	141	113	375	375	100
Dabrafenib	25	25.3	101	250	267	107	750	756	101
Dasatinib	25	23.8	95	250	230	92	750	746	99
Erlotinib	125	122	98	1250	1310	105	3750	3864	103
Gefitinib	125	142	113	1250	1112	89	3750	3582	96
Ibrutinib	12.5	12.7	101	125	133	106	375	368	98
Imatinib	75	74.4	99	750	705	94	1875	1910	102
Lapatinib	25	26.2	105	250	272	109	750	757	101
Nilotinib	75	81.3	108	750	718	96	1875	1910	102
Pazopanib	2500	2576	103	25000	25924	104	75000	76452	102
Regorafenib	125	130	104	1250	1227	98	3750	3552	95
Ruxolitinib	125	115	92	1250	1364	109	3750	3986	106

Analyte	QC Concentrations (µg/L)								
	Low			Mid			High		
	Nominal	Measured	% True	Nominal	Measured	% True	Nominal	Measured	% True
Sorafenib	125	141	113	1250	1368	110	3750	3913	104
Sunitinib	6.25	6.31	101	62.5	68.6	110	187.5	185	99
N-desethyl Sunitinib	6.25	5.60	90	62.5	64.1	102	187.5	178	96
Trametinib	6.25	6.05	97	62.5	71.4	114	187.5	191	102
Vandatinib	12.5	12.7	101	125	128	102	375	371	99
Vemurafenib	62.5	63.5	102	625	609	97	1875	1872	100

### **5.2.6.3 Analytical Accuracy and Matrix effects**

Assay accuracy was assessed on the basis of accuracy of QC sample determination, and matrix effects. The accuracy of QC samples prepared at 3 concentrations within the calibration range was assessed in five replicates on three separate days (**Table 5.4**).

Matrix effects were assessed by quantifying the concentration of analytes in spiked plasma from 6 separate individuals (3 healthy volunteers and 3 oncology patients). The potential for variability in analyte response due to suppression or enrichment of ionization by matrix components (primarily phospholipids) was characterised by determining the chromatographic retention of the most abundant phospholipids and fragments reported to affect sample ionization with an ESI+ source (261-263). In-source suppression and enrichment of ionization was also assessed by post column infusion. Post-column infusion experiments were conducted in which a 250 µg/L analyte solution in mobile phase B was constantly infused (10 µL/min) post-column into the MS. A 200 µL aliquot of drug free plasma was prepared as described in Section 5.2.2.3, and injected pre-column (264).

### **5.2.6.4 Linearity, Lower Limit of Detection and Quantification Range**

Assay sensitivity and linear detection range were determined for each analyte. The lower limit of detection (LLOD) was defined on the basis of a 5:1 signal to noise ratio. The LLOQ was defined as the lowest calibration standard for each analyte. This criteria for the LLOQ is acceptable on the basis that for all analytes the lowest calibrator was greater than the LLOD (analyte response at least 5 times the response compared to blank response), and analyte peaks were identifiable, discrete, and reproducible with a precision defined by a % relative standard deviation (RSD) less than 20% and accuracy within 80 and 120% of the true value. Linear response, assessed by least squares regression of 6 non-zero calibrators and expressed as a coefficient of determination ( $r^2$ ) > 0.99, was confirmed across the respective calibration ranges

for each analyte. The linear regression equation and  $r^2$  for each analyte are specified in **Table 5.2**.

#### **5.2.6.5. Selectivity**

Assay selectivity was assessed by evaluating the endogenous response from healthy individuals and oncology patients ( $n = 6$ ) not currently undergoing therapy with a KI.

### **5.3. Results**

#### **5.3.1 Sample Collection and Preparation**

Statistical analysis (Appendix Table 1) demonstrated comparable analyte recovery across all KIs from LH-S vacuettes (Greiner bio-one - ref no: 455083, lot no: A141237C) compared to controls (glass and Eppendorf plastic tubes). For all other collection tubes tested, a significant difference in recovery was observed for one or more analytes compared to the control tubes.

#### **5.3.2 Analyte Separation, Detection and Quantification**

Analytes were detected at  $m/z$  values corresponding to the  $[M+H]^+$  for the parent compound (**Table 5.2** and **Figure 5.1**). To optimise the sensitivity and selectivity of the assay,  $m/z$  spectra were used to determine ionization maxima for each analyte. A range of capillary voltages, sample cone voltages and collision energies were assessed and it was determined that optimal detection and quantification of analytes was achieved at capillary, sample cone and collision energies 2.4 keV, 25 eV and 2 eV, respectively (**Table 5.1**). Blank plasma and mobile phase samples were also subjected to the same sample preparation and then analysed to ensure there were no co-eluting peaks originating from the matrix or sample preparation protocol. Employing the optimised chromatographic and mass spectrometer conditions outlined in

Sections 5.2.3 and 5.2.4 clear, sharp peaks were obtained for all analytes, with individual analytes eluting at retention times between 3.2 and 10.2 min (**Table 5.2**). Individual selected ion extraction (pseudo-MRM) data from a representative plasma sample containing all analytes is shown in **Figure 5.2** (panels 1 to 19).

Based on the chromatographic resolution and recovery characteristics of the individual KIs, d6-erlotinib, d3-O-methyl-gefitinib, d7-lapatinib and d3-sorafenib were selected as the IS panel (**Figure 5.2**; panels 21-24). Individual deuterated IS were used to normalise the response of co-eluting analytes; d6-erlotinib (RT 5.11 min) the for analytes eluting between 4.6 and 5.2 min, d3-O-methyl-gefitinib (RT 3.16 min) for analytes eluting between 3.2 and 4.2 min, d7-lapatinib (6.62 min) for analytes eluting between 6.6 and 8.1 min, and d3-sorafenib (RT 9.75 min) for analytes eluting between 9.0 and 10.2 min.

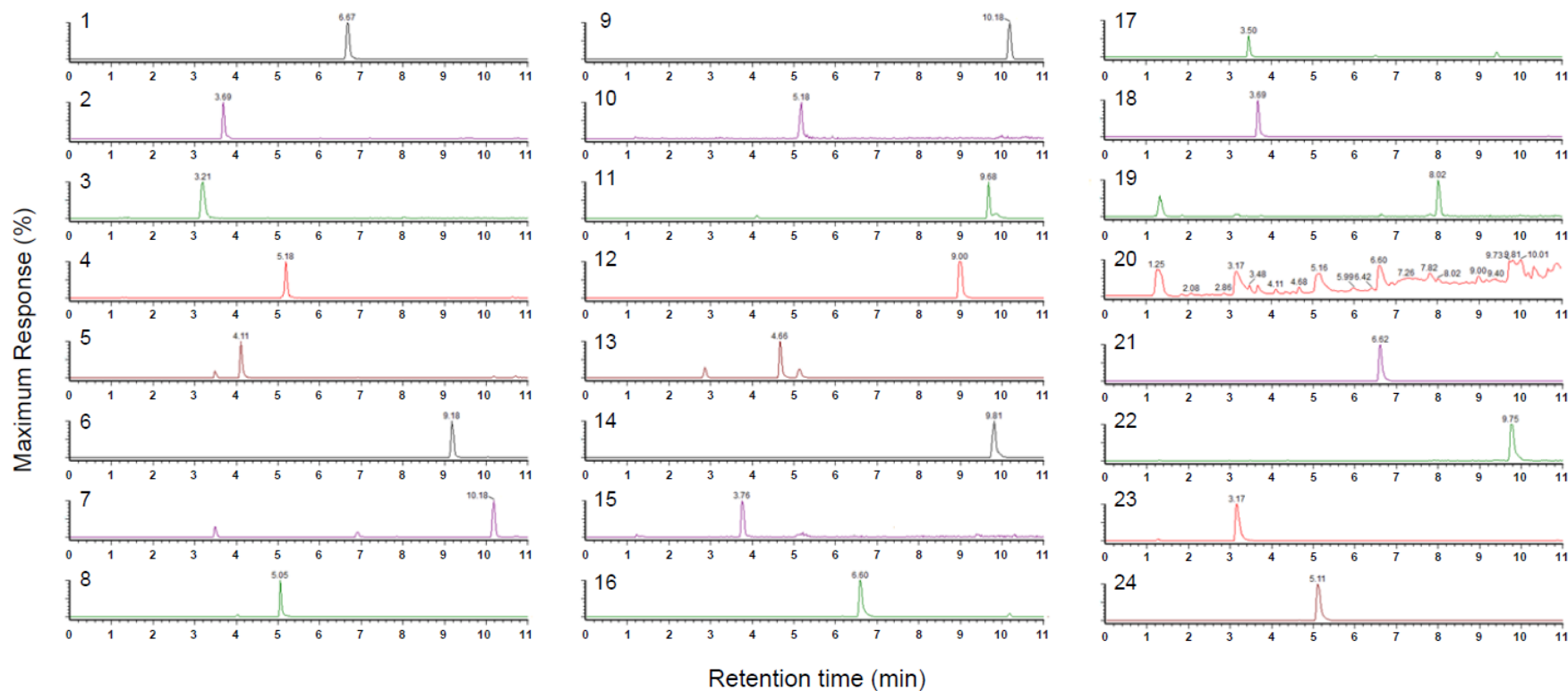


**Figure 5.2: Representative pooled spiked plasma (100 µg/L) chromatogram (quadrupole acquiring data between m/z 250 and 750).**

*Panels 1 to 19: extracted ion chromatograms at resolution of  $\pm 0.05$  AMU for each of the analytes of interest; panel 1: nilotinib (m/z 530.191), panel 2: vandetanib (m/z 475.098), panel 3: gefitinib (m/z 447.159), panel 4: ruxolitinib (m/z 307.166), panel 5: N-desethyl sunitinib (m/z 371.187), panel 6: dabrafenib (m/z 520.108), panel 7: regorafenib (m/z 483.084), panel 8: axitinib (m/z 387.127), panel 9: dasatinib (m/z*

488.162), panel 10: erlotinib ( $m/z$  394.176), panel 11: vemurafenib ( $m/z$  490.079), panel 12: trametinib ( $m/z$  616.085), panel 13: sunitinib ( $m/z$  399.219), panel 14: sorafenib ( $m/z$  465.093), panel 15: imatinib ( $m/z$  494.246), panel 16: lapatinib ( $m/z$  581.142), panel 17: afatinib ( $m/z$  486.143), panel 18: pazopanib ( $m/z$  438.170), panel 19: ibrutinib ( $m/z$  441.175). Panel 20: total ion count chromatogram. Panels 21 to 24: extracted ion chromatograms at resolution of  $\pm 0.05$  AMU for each of the deuterated internal standards: panel 21:  $d_7$ -lapatinib ( $m/z$  588.175), panel 22:  $d_3$ -sorafenib ( $m/z$  468.0945), panel 23:  $d_3$ -*O*-methyl-gefitinib ( $m/z$  450.186), panel 24:  $d_6$ -erlotinib ( $m/z$  400.207). Y-axis (% Maximal Response) scale is -5 to 95%

### 5.3.3 Calibration and Validation

Calibration curves generated for each analyte were linear over the concentration ranges described in **Table 5.2**. Coefficients of determination ( $r^2$ ) were invariably greater than 0.99. Assay precision was assessed on the basis of inter- and intra-day variability at three concentrations as described in section 5.2.6.2. Results are shown in **Table 5.3**. The percent relative standard deviation (%RSD; also known as the coefficient of variation) for intra-day and inter-day variability was less than 10 and 17 %, respectively, for all analytes. With the exception of the inter-day precision determination at the LLOQ for dabrafenib, nilotinib and vemurafenib the % RSD did not exceed 15 %, in these cases the % RSD did not exceed 20%. Precision determination are within the specified acceptable criteria of “<15 % in all cases except for the LLOQ (< 20 %)” for all analytes.

Assessment of absolute analyte recovery by quantification of detector response obtained for extracted plasma samples compared to that for a true concentration of pure authentic standard (non-extracted) demonstrated mean recovery of between 92 and 113 % for all analytes (**Table 5.3**). Assessment of relative recovery (plasma versus mobile phase extracted calibration curves) demonstrated >95 % mean recovery for all analytes. Assay sensitivity was determined on the basis of the LLOD and assay precision and accuracy at the LLOQ (defined as the lowest calibrator) for all analytes. Following the criteria described in section 5.2.6.4, the LLOD ranged from 0.07 to 1.43 µg/L for undiluted samples (**Table 5.2**; 13 µg/L post-dilution for pazopanib). Assay precision and accuracy (defined as the mean % deviation from the nominal value in five replicates) at the LLOQ was invariably < 20 %, and within 80 to 120 %, respectively, for all analytes (**Table 5.2**).

Matrix effects were assessed by comparison of the recovery of each analyte spiked into human plasma from 6 individuals (3 healthy volunteers and 3 oncology patients), characterisation of

the chromatographic retention of common matrix components implicated in suppression and enrichment of ionization, and post-column infusion of analytes into a drug free plasma matrix. In all cases variability across the 6 samples (assessed as %RSD) was less than 10 %. Quantification of diluted pazopanib patient samples using the UPLC-MS approach described here when compared to undiluted samples analysed by a validated HPLC-UV approach resulted in measured analyte concentrations within 8%. Assay selectivity was assessed in blank plasma from 6 individuals (3 healthy volunteers and 3 oncology patients); no peaks resulting from endogenous analytes were observed at the RT and m/z values for any of the analytes (KIs) measured. A lack of endogenous response in plasma from oncology patients demonstrated is consisted with a lack of effect from concomitant medications. Furthermore, the chromatographic retention of matrix components (phospholipids) and their fragments known to affect (through enrichment or suppression) ionization within an ESI+ source was assessed. These analyses demonstrated a lack of co-elution of the most common plasma phospholipids 1-Stearoyl-2-arachidonoyl-sn-glycero-3-phosphocholine (m/z 810.5), 1-(9Z,12Z-Octadecadienoyl)-2-(5Z,8Z,11Z,14Z-eicosatetraenoyl)-sn-glycero-3-phosphocholine (m/z 806.5), Glycerophosphocholine 36:2 (m/z 786.5), 1-Hexadecanoyl-2-(9Z,12Z-octadecadienoyl)-sn-glycero-3-phosphocholine (m/z 785.5), 1-Stearoyl-2-hydroxy-sn-glycero-3-phosphocholine (m/z 524.3), 1-Palmitoyl-2-hydroxy-sn-glycero-3-phosphocholine (m/z 496.3), and their fragments (m/z 184.3 and 104.0) implicated in the suppression or enrichment of ionization within an ESI+ source (261, 264). Post-column infusion of analytes demonstrated an absence of matrix effect for all analytes between 1.5 and 10.5 min; representative extracted response change chromatograms associated with post-column infusion of analytes with a pre-column injection of drug free plasma are shown in the supplemental **Figure 5.1**. Taken together, these analyses demonstrate clear chromatographic resolution between all analytes of interest and the major matrix components implicated in suppression or

enrichment of source ionization, and a lack of matrix effect for all analytes.

Post-preparative analyte stability was assessed at the lowest and highest calibrator concentrations at 15 °C over 96 hours. Over this time course, detector response diminished by less than 6 % for all analytes. This time course for analyte stability would facilitate analysis of 480 samples.

#### **5.3.4 Application to Clinical Trial Samples**

The primary application of this approach will be the quantification of KI concentrations in pharmacokinetic studies and subsequently in clinical practice. Indeed, the approach described here is currently being used to support clinical studies (HREC/13/SAC/347). Increasingly treatment regimens including multiple KIs are being trialled (e.g. combination dabrafenib / trametinib for metastatic melanoma). The capacity to simultaneously quantify multiple KIs in a single patient sample is an important and novel feature of the current approach. The capacity of this approach to quantify multiple KIs (dabrafenib / trametinib) and the parent KI plus metabolite (sunitinib / *N*-desethyl sunitinib) in oncology patient samples is demonstrated in **Figures 5.3 and 5.4 and 5.6**

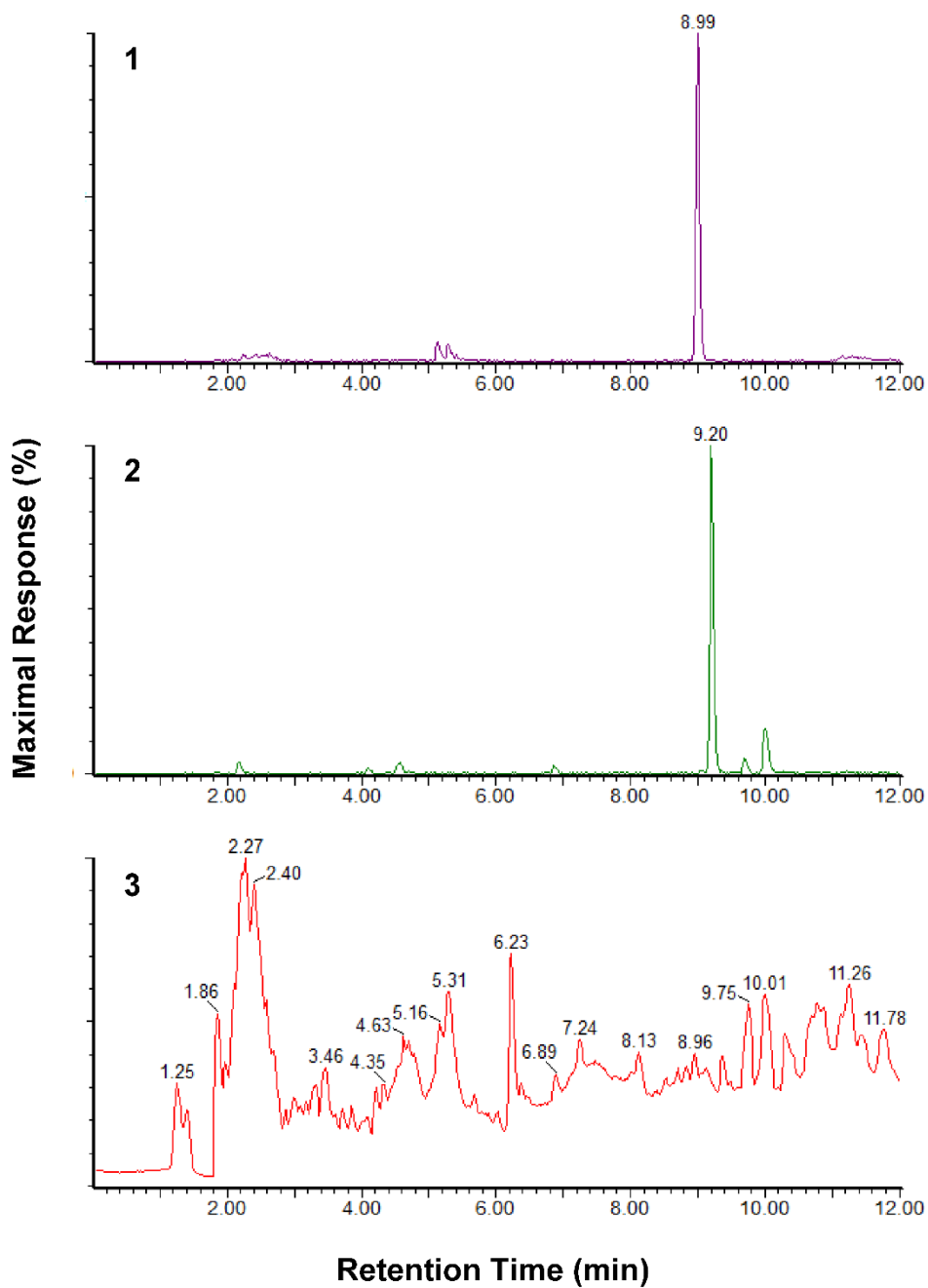


**Figure 5.3: Representative chromatogram for a patient taking a standard combination dose of dabrafenib (150mg BD) and trametinib (2mg OD).**

*Panel 1 and 2: extracted ion chromatogram at resolution of  $\pm 0.05$  AMU for trametinib ( $m/z$  616.085) and dabrafenib ( $m/z$  520.108), respectively. Panel 3: total ion count chromatogram. Y-axis (% Maximal Response) scale is 0 to 100%*

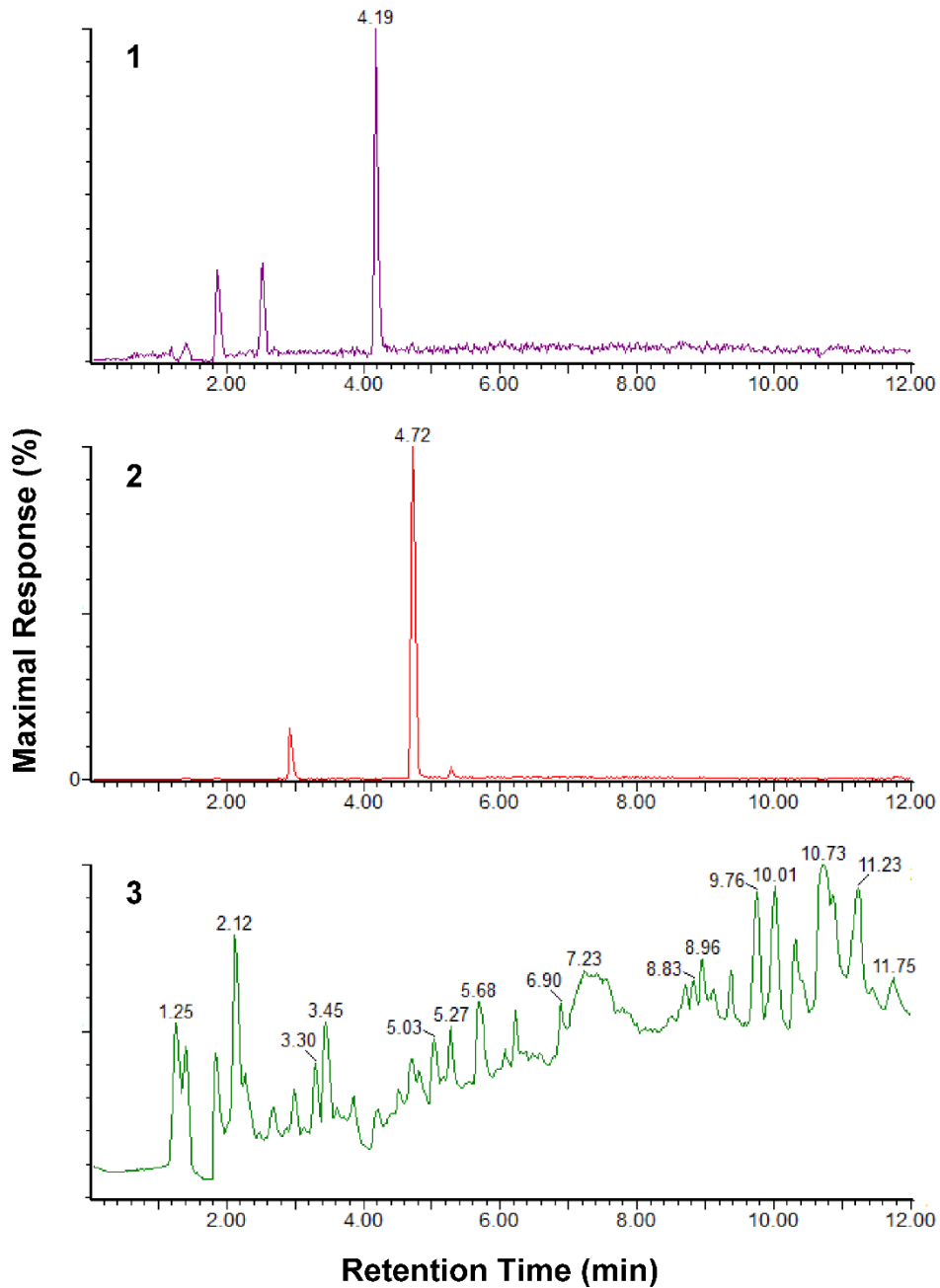


**Figure 5.4: Representative chromatogram for a patient taking a standard dose of sunitinib on a 4 week on and 2 weeks off cycle.**

*Panel 1 and 2: extracted ion chromatogram at resolution of  $\pm 0.05$  AMU for N-desethyl sunitinib ( $m/z$  371.187) and sunitinib ( $m/z$  399.219), respectively. Panel 3: total ion count chromatogram. Y-axis (% Maximal Response) scale is 0 to 100%*

## 5.4. Discussion

The rapid development of KIs as a class of antineoplastic drugs has substantially improved the outcomes for patients with a range of malignancies. However, potential for additional benefit from the use of KI through optimised dosing remains to be universally addressed. This chapter describes a simple and robust UPLC-QToF-MS approach that facilitates the quantification of the plasma-KI concentration for a panel of 18 KIs. In order to facilitate direct application as a clinical trials platform, this approach has been developed, validated and reported in accordance with the 2015 version of the FDA guidance for industry on analytical procedures and methods validation for drugs and biologics.

While the importance of standardised specimen collection and storage protocols are widely accepted (265, 266) for clinical trials, specific conditions (e.g. the chemistry of specimen tubes) routinely vary between studies, potentially confounding comparison of results. As KIs are lipophilic ( $\log P$  values  $> 2.5$ ) weak organic bases that are generally non-ionized at physiological pH (111), variable recovery from specimen tubes is a potential major confounder. Thus, a comparison of analyte recoveries from a panel of collection tube of differing chemistries was performed. This analysis demonstrated that for all analytes analysed, LH-S (Greiner Bio-One) specimen collection vacuettes provided consistent and high recoveries comparable to control tubes.

In addition to this approach providing the most extensive platform for the quantification of plasma-KI concentrations, another key feature is the extended dynamic range providing linear response across up to three orders of magnitude for an individual analyte and across five orders of magnitude between analytes. As the doses, distribution and elimination characteristics of KIs vary substantially between individual agents, plasma-KI concentrations vary across several orders of magnitude. As identified by van Erp et al. 2013 (257), limitations in terms of dynamic

range have previously precluded the incorporation of KIs such as pazopanib in multi-analyte platforms due to the comparatively high plasma concentrations resulting in non-linear response. The approach described here facilitates calibrated linear response for analytes as low as 2.5 µg/L (sunitinib, trametinib) and up to 5,000 µg/L (erlotinib, gefitinib, regorafenib, ruxolitinib and sorafenib) using a common sample preparation protocol, in all cases facilitating the quantification of plasma-KI concentrations across a clinically relevant plasma concentration range for the analyte. In the case of pazopanib patient plasma samples were diluted 1 in 20 using blank calibrator matrix to facilitate linear detection across a substantially higher concentration range (1,000 – 100,000 µg/L). Validation studies demonstrated that dilution in matched blank matrix (i.e. calibration blank plasma) did not alter relative analyte response, assay precision or accuracy. For individual analytes, the extended linear dynamic range for achieved using this approach (typically three orders of magnitude) is critical to facilitate PK (particularly dose escalation) studies, which may be performed across a spectrum of doses. Evidence has recently shown improved efficacy against resistance in patients with metastatic melanoma undergoing combination KI therapy with dabrafenib and trametinib compared to dabrafenib alone (267). Given that combination KI therapy is quite novel with increasing prevalence, a panel based UPLC-MS-MS approach for the quantification of plasma concentrations of these small molecule kinase inhibitors are of great importance to make inter-individual variability with KI exposure available to aid in TDM to ensure optimal use of these powerful drug class. The assay described is particularly advantageous for the establishment of target trough concentrations through retrospective studies for the newer KIs. The assay described is one of the first approaches to facilitate the simultaneous quantification of plasma concentrations for such a broad range of KIs that includes the recently approved combination of dabrafenib and trametinib.

## 5.5. Conclusion

This chapter describes the development and validation of a novel ultra-performance liquid chromatography, quadrupole time-of-flight mass spectrometry (UPLC-QToF-MS) based approach for the quantification of plasma concentrations for 18 KIs (**Figure 5.1**). The approach provides a robust analytical platform to facilitate PK studies to establish optimised concentration ranges for newer KIs and a TDM platform to assist in guiding KI dosing for agents where an optimised KI-concentration range exists.

The novel UPLC-QToF-MS approach described in this chapter represents a substantial advance in the quantification of plasma-KI concentrations, with a capacity to quantify twice the number of analytes of any existing approach, including the recently approved KI combination of dabrafenib and trametinib. This approach provides immediate clinical utility as a TDM platform for monitoring of plasma-KI concentrations where an established or accepted 'target concentration range' exists (i.e. axitinib, erlotinib, gefitinib, imatinib, pazopanib, sorafenib and sunitinib) (125). The approach also provides a platform to support PK studies involving a diverse range of KIs where such concentration ranges remain to be established (i.e. afatinib, dabrafenib, dasatinib, ibrutinib, lapatinib, nilotinib, regorafenib, ruxolitinib, vandetanib and vemurafenib). Accordingly, this approach will facilitate a significant expansion in the number of KIs with established target concentration ranges. Furthermore, as this occurs, this approach will facilitate the most comprehensive TDM platform for KI dose optimisation.

---

# CHAPTER VI: APPLICATION OF PRECISION DOSING STRATEGIES IDENTIFIED IN THIS THESIS

---

*The results presented in this chapter  
contributed substantially to the manuscript:*

Rowland A, van Dyk, M, Hopkins AM, Mounzer R, Polasek TM, Rostami A, Sorich MJ  
(2018) Physiologically-based pharmacokinetic modelling to identify physiological and  
molecular characteristics driving variability in drug exposure. *Clinical Pharmacology and  
Therapeutics*, in press (Accepted 20<sup>th</sup> March 2018).

## 6.1 Introduction

Chapter I of this thesis introduced the potential for inconsistent patient outcomes due to variability in KI exposure. Subsequent chapters described the development and verification of strategies that may be used to help characterise variability in such KI exposure ranging from PBPK modelling (Chapter II), to reaction phenotyping (Chapter IV) and TDM (Chapter V). The results presented in this chapter demonstrate the potential application of two of these approaches.

The first approach involves the use of a case study to demonstrate the application of model informed precision dosing (MIPD) for dabrafenib. Like many KIs, dabrafenib is generally well tolerated but exhibits substantial BSV in exposure (268). A recent study of 27 patients with metastatic BRAF<sup>V600mut</sup> melanoma reported that a dabrafenib  $C_{ss\_trough}$  of  $> 48\text{ng/mL}$  was associated with an increased risk of Grade  $\geq 2$  adverse events requiring dose reduction (269). While intriguing, the clinical utility of this finding to guide dosing would traditionally require a costly prospective clinical trial sufficiently powered to demonstrate any advantages of using this upper-limit of concentration to inform prescribing (232). Novel and efficient strategies to predict which patients may be at risk of steady-state plasma concentrations  $> 48\text{ ng/mL}$  could decrease the costs involved in translating such evidence into clinical practice.

Chapter II introduced the mechanistic basis of PBPK models, which combine physiological and molecular characteristics ('population variables') with drug physiochemical and *in vitro* kinetic data ('drug variables') to predict PK (270, 271). Currently, PBPK models are used throughout drug development to support decisions about when and how to conduct clinical PK studies in specific populations and to support dose recommendations (272, 273). Given the mechanistic basis of PBPK models, it is likely that this strategy may also be valuable for MIPD; a proof-of-concept study for this approach was recently been published by this

laboratory using olanzapine (228, 274). Interrogation of simulation outputs at a physiological and molecular level represents a novel and efficient approach to predict baseline markers that drive BSV in drug exposure. Importantly, the ‘population variables’ contained within PBPK platforms such as Simcyp® are based on reported demographic characteristics from broad but defined populations, and are more likely to reflect the ‘real world’ treatment population compared with a clinical trial cohort. Additionally, PBPK modelling is now recommended by the major regulatory agencies (275, 276), meaning that the parameters that underpin the population files must already, by extension, be accepted as at least partially validated.

The aim of the first study described in this chapter was to apply a PBPK model for dabrafenib to identify baseline physiological and molecular characteristics that drive BSV in exposure to this drug. The capacity to discriminate a dabrafenib  $C_{ss\_trough}$  above and below 48 ng/mL was evaluated as an exploratory extension.

It was also introduced in Chapter I that TDM can be utilised to optimise KI dosing to maximise efficacy while minimising toxicity. Target concentrations for a subset of KIs have been established to guide such optimised dosing (section 1.6.1). The aim of the second study described in this chapter was to conduct a pilot study to measure KI trough concentrations in a ‘real world’ oncology cohort to assess BSV and to compare the results to established target concentrations. A case study from this cohort is described as an example of how KI TDM can be applied.

## 6.2 Methods

### 6.2.1 Application 1: Identification of physiological and molecular characteristics driving between subject variability in dabrafenib exposure

#### 6.2.1.1 Dabrafenib PBPK Model

The physicochemical, blood binding, absorption, distribution, elimination, interaction and transport parameters used to construct the dabrafenib compound file are summarised in **Table 6.1**. Physicochemical properties were taken from published literature (177). Unless specified, blood binding, permeability and distribution parameters were predicted in Simcyp® based on physicochemical properties using previously validated in-built prediction tools.

Metabolism and interaction parameters were based on reported *in vitro* data (97). Robust determination of *in vitro* dabrafenib transporter kinetics is precluded by limited aqueous solubility, which confounds assessment of compartmentalised drug concentrations in systems such as trans-well based transporter assays (111). In the absence of robust *in vitro* data, intestinal and hepatic transporter (transporter-mediated intrinsic clearance;  $CL_{intT}$ ) and diffusion (passive diffusion clearance;  $CL_{PD}$ ) kinetics were determined using the parameter estimation (PE) function in Simcyp® (277). Parameter estimations were based on *in vivo* data from a phase I single dose escalation trial [GSK trial ID: 112680] involving 94 melanoma patients over 6 dose levels (37.5 to 300 mg). Data from this trial were not used in the subsequent verification of the dabrafenib model and no adjustment to the model was required during the verification phase (**Figures 6.1** and **6.2**). Simulations performed to assess markers of dabrafenib  $C_{ss\_trough}$  in oncology patients used the ‘Genentech Cancer’ population (194).

**Table 6.1: Input parameters for the dabrafenib compound file.**

Parameter	Value	Source
<i>Physiochemical properties</i>		
Molecular weight	519.56	(177)
log P <sub>o:w</sub>	4.8	(177)
Species	Neutral	(177)
<i>Protein Binding</i>		
B/P	0.708	Predicted
f <sub>up</sub>	0.0038	(177)
<i>Absorption (advanced dissolution, absorption and metabolism model)</i>		
f <sub>a</sub>	0.2246	Predicted
k <sub>a</sub> (1/hr)	0.0776	Predicted
PSA	147.5	(177)
HBD	2	(177)
P <sub>eff,man</sub> (10 <sup>-4</sup> cm/s)	0.189	Predicted
Dosage form	Immediate release	
Reabsorption after biliary excretion	100	Parameter estimation
<i>In vivo pharmacokinetic properties (full PBPK model)</i>		
V <sub>ss</sub> (L/kg)	0.31	Predicted (Model 2)
<i>Metabolism: HLM enzyme kinetics (CL<sub>int</sub>; μL/min/mg)</i>		
CYP2C8	46.20	(97)
CYP3A4	4.79	(97)
<i>Intestinal Transport (CL<sub>int,T</sub>; μL/min)</i>		
Apical Uptake (Apical Influx)	0.05	Parameter estimation
Apical Efflux (P-gp)	341.8	Parameter estimation
<i>Hepatic Transport (CL<sub>int,T</sub>; μL/min/10<sup>6</sup> cells)</i>		

Passive diffusion ( $CL_{PD}$ )	7.165	Parameter estimation
P-gp (Cannicular Efflux)	341.8	Parameter estimation
<i>Competitive inhibition (<math>K_i</math>; <math>\mu M</math>)</i>		
CYP2C8	4.1	(97)
CYP3A4	8.0	(97)
<i>CYP3A4 Induction</i>		
Calibrated $IND_{max}$	30.0	(97)
$IndC_{50}$ (nM)	1.0	(97)

**Abbreviations:**  $P_{o:w}$ , neutral species octanol:buffer partition coefficient; B/P, blood-to-plasma partition ratio;  $f_{up}$ , fraction unbound in plasma;  $f_a$ , fraction available from dosage form;  $k_a$ , absorption rate, PSA; polar surface area, HBD; hydrogen bond donor;  $P_{eff,man}$ , human jejunum effective permeability;  $V_{ss}$ ; volume of distribution at steady state;  $CL_{int}$ , *in vitro* intrinsic clearance;  $CL_{int,T}$ , *in vitro* transporter mediated intrinsic clearance;  $CL_{PD}$ , passive diffusion clearance;  $K_i$ , concentration that supports half maximal inhibition;  $Ind_{max}$ ; maximum fold induction;  $IndC_{50}$  concentration that supports half maximal induction.

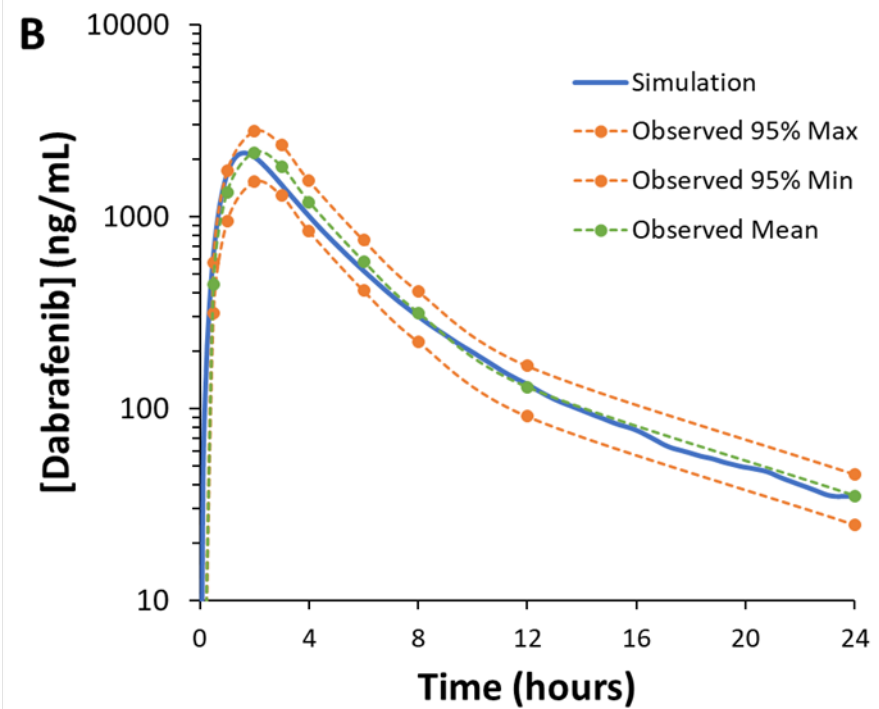
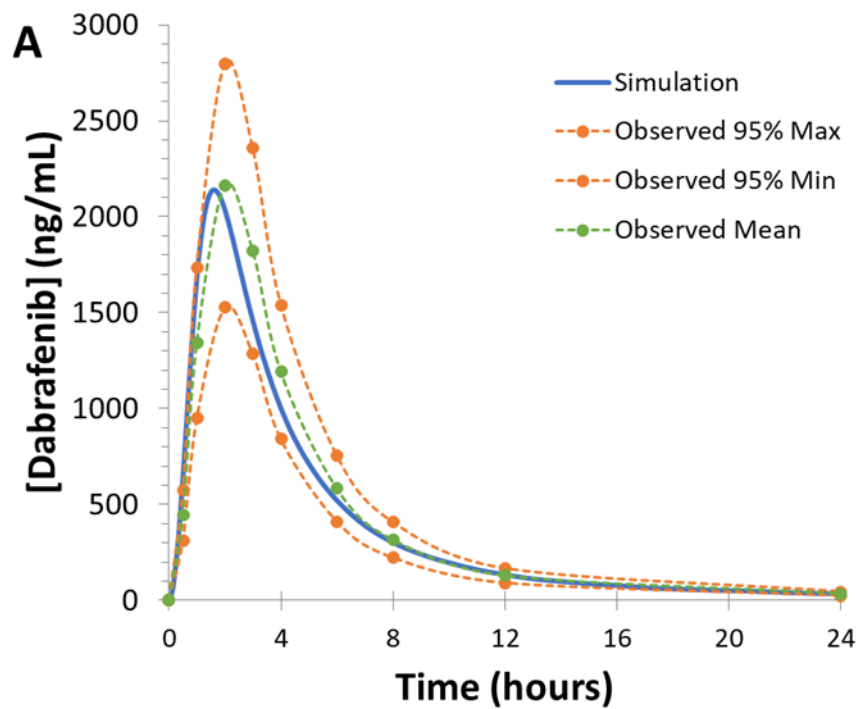


**Figure 6.1: Representative [GSK trial ID: 11346] overlay showing the simulated and observed (95% observed range) plasma concentration time curves (0 to 24 hours) for dabrafenib following a single 150 mg oral dose.**

*Solid line is the mean model predicted exposure, dark (green) dotted line is the mean observed exposure and light (orange) dotted lines are 95% minimal and maximal observed range of exposures. Panel A: linear plasma concentration scale, Panel B: logarithmic plasma concentration scale.*

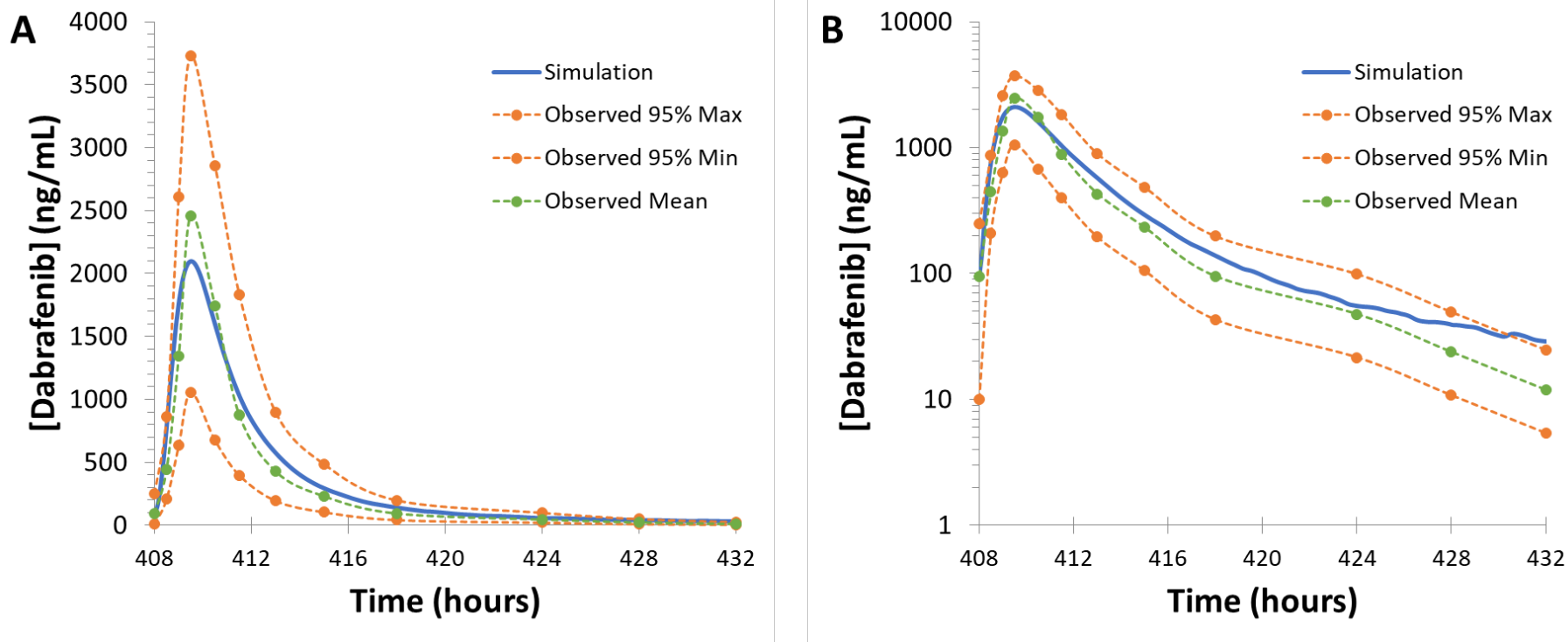


**Figure 6.2: Representative [GSK trial ID: 113771 Part D] overlay showing the simulated and observed (95% observed range) plasma concentration time curves (408 to 432 hours) for dabrafenib when dosed for 14 days (150 mg BD).**

*Solid line is the mean model predicted exposure, dark (green) dotted line is the mean observed exposure and light (orange) dotted lines are 95% minimal and maximal observed range of exposures. Panel A: linear plasma concentration scale, Panel B: logarithmic plasma concentration scale.*

### 6.2.1.2 Trial Design

A verified dabrafenib model was used to evaluate potential associations between physiological and molecular characteristics and dabrafenib exposure, taken as  $C_{ss\_trough}$ . Ten virtual trials each comprising 100 subjects (total = 1000) from the Genentech Cancer population (**Table 6.2**) were simulated over 336 hours, with 150mg of dabrafenib dosed orally in a fasted state every 12 hours for 14 days. The  $C_{ss\_trough}$  was determined 12 hours after the final dose of dabrafenib on day 14. Univariate logistic regression analysis was used to screen the associations between the characteristics and  $C_{ss\_trough} > 48\text{ng/mL}$ . Continuous variables were evaluated for normality and non-linearity of association. A baseline multivariate logistic regression model was developed via backwards deletion (AIC) of the baseline characteristics significant in the univariate analysis. The predictive performance of the developed multivariable models was assessed via the area under the receiver operating characteristic curve (ROC AUC) and model prediction accuracy (% of model predictions that match the observed data). The predictive performance was externally validated in two separate verification cohorts of 250 cancer patients.

**Table 6.2: Characteristics describing the core simulated cancer patient cohort (n = 1,000).**

	Mean	Range
<i>Physiological characteristics</i>		
Female (% of cohort)	48.7	
Age (Years)	58.9	29.2 – 87.8
Weight (kg)	71.5	39.0 – 123
Height (cm)	168	143 – 194
BSA (m <sup>2</sup> )	1.80	1.28 – 2.44
BMI (kg/m <sup>2</sup> )	25.4	16.1 – 45.7
Combine kidney weight (g)	304	110 – 621
Liver weight (g)	1531	875 – 2612

Cardiac output (L/h)	282	191 – 413
Haematocrit (%)	37.1	23.5 – 56.3
Albumin (g/L)	38.3	28.3 – 53.0
GFR (mL/min/1.73m <sup>2</sup> )	90.4	29.8 – 232.1
<i>Intestinal CYP abundance (nmol P450)</i>		
CYP3A4	64.7	6.6 – 421
CYP3A5	4.0	0 – 91.2
<i>Liver CYP abundance (nmol P450)</i>		
CYP2C8	1132	78 – 9927
CYP3A4	6231	288 – 54309
CYP3A5	944	0 – 18574
CYP3A7	174	0 – 5577
<i>Active CYP 3A5 / 3A7 (% of cohort)</i>		
CYP3A5	17.6	
CYP3A7	10.7	
<i>CYP3A4 induction (% baseline expression)</i>		
Liver	180.6	106 – 459
Intestine	519.7	161 - 1504
<i>Liver transporter abundance (nmol protein)</i>		
P-gp	28.6	3.8 – 234
OATP1B1	595	58.2 – 4525
OATP1B3	589	108 - 2881

**Abbreviations:** BSA, body surface area; BMI, body mass index; GFR, glomerular filtration rate.

## **6.2.2 Application 2: Use of KI TDM in a ‘real world’ Cohort**

### **6.2.2.1 Study Protocol**

TKI-Opt was an observational study evaluating the cohort of oncology patients treated at Flinders Centre for Innovation in Cancer with KIs for various cancer indications. The trial protocol was approved by the Southern Adelaide Clinical Human Research Ethics Committee (SAHREC EC00188), and written informed consent was obtained from each participant. The study was conducted according to the principles stated in the Declaration of Helsinki and is compliant with CPMP/ICH/135/95 GCP standards.

### **6.2.2.2 Study Cohort**

Adult male and female (18+ years old) patients from all demographic, ethnic and cultural backgrounds were included to facilitate analysis of a diverse patient cohort. Patients with documented impaired cognitive function, who were deemed incapable of providing legitimate informed consent, were excluded from this study.

### **6.2.2.3 Study Design**

Two blood samples were collected at steady-state two weeks apart to confirm KI trough concentrations. Patient results were used for research purposes and results were made available only upon requests from the patient’s treating oncologist. If dose-adjustments were made and TDM was requested, further blood samples were collected.

### **6.2.2.4 Sample Preparation and Analysis**

The method that was used to perform sample preparation and analysis has previously been described in Chapter V, section 5.2.2.1-5.2.2.3.

## 6.3 Results

### 6.3.1 Application 1: Identification of physiological and molecular characteristics driving between subject variability in dabrafenib exposure

The results of the univariate logistic regression analysis assessing the association between various molecular and physiological characteristics and a  $C_{ss\_trough} > 48 \text{ ng/mL}$  are presented in **Table 6.3**.

*Table 6.3: Univariate logistic regression analysis of physiological and molecular characteristic associated with a dabrafenib  $C_{ss\_trough} > 48 \text{ mg/mL}$*

Variable	Level	OR	(95% CI)	P -value	AUC
<i>Physiological characteristics</i>					
Gender	Female			0.732	0.51
	Male	0.96	(0.74-1.24)		
Age		1.02	(1.01-1.03)	0.003	0.56
Weight		1.02	(1.01-1.03)	< 0.001	0.58
BSA		2.95	(1.5-5.87)	0.002	0.56
BMI		1.09	(1.05-1.12)	< 0.001	0.59
Cardiac output		1.00	(1-1.01)	0.057	0.54
Haematocrit		1.00	(0.97-1.03)	0.914	0.51
Albumin		1.03	(0.99-1.06)	0.137	0.53
GFR		1.00	(1-1.01)	0.407	0.52
<i>CYP phenotypes</i>					
CYP2C19	PM			0.073	0.54

	IM	1.08	(0.48-2.32)		
	ExM	1.11	(0.49-2.37)		
	U.ExM	0.76	(0.34-1.62)		
CYP2D6	PM			< 0.001	0.59
	IM	1.71	(1.04-2.82)		
	ExM	1.77	(1.07-2.91)		
	U.ExM	0.82	(0.5-1.34)		
CYP3A5	PM			0.493	0.51
	ExM	0.89	(0.64-1.25)		
CYP3A7	PM			0.215	0.51
	ExM	0.77	(0.52-1.17)		
<i>Absolute CYP and transporter abundances</i>					
CYP1A2	log	0.69	(0.57-0.83)	< 0.001	0.57
CYP2B6	log	0.93	(0.83-1.04)	0.180	0.53
CYP2C8	log	0.20	(0.16-0.25)	< 0.001	0.77
CYP2C9	log	0.65	(0.53-0.79)	< 0.001	0.59
CYP2J2	log	0.95	(0.86-1.06)	0.382	0.52
CYP3A4	log	0.20	(0.16-0.25)	< 0.001	0.79
P-gp	log	1.89	(1.52-2.36)	< 0.001	0.61
OATP1B1	log	1.11	(0.93-1.33)	0.251	0.53
OATP1B3	log	0.87	(0.68-1.1)	0.235	0.52

**Abbreviations:** BSA; body surface area, BMI; body mass index, ExM; extensive metaboliser, GFR; glomerular filtration rate, IM; intermediate metaboliser, OR; odds ratio, PM; poor metaboliser, U.ExM; ultra-extensive metaboliser

A multivariable logistic regression model that considered baseline weight (Odds ratio (OR) 1.05; 95% CI 1.02-1.08), BMI (OR 1.09; 95% CI 0.99 – 1.19), and ln CYP2C8 (OR 0.05; 95% CI 0.03-0.08), CYP3A4 (OR 0.07; 95% CI 0.05-0.1) and P-gp (OR 6.68; 95% CI 4.47-10.25) liver abundance provides a strong predictive performance of  $C_{ss\_trough} > 48\text{ng/mL}$  (ROC AUC = 0.94; Accuracy = 86%). The predictive performance of the multivariable model was maintained, as represent by a ROC AUC of 0.94 and 0.93, and an accuracy of 88% and 85% for verification cohort's 1 and 2, respectively (**Figure 6.3**).

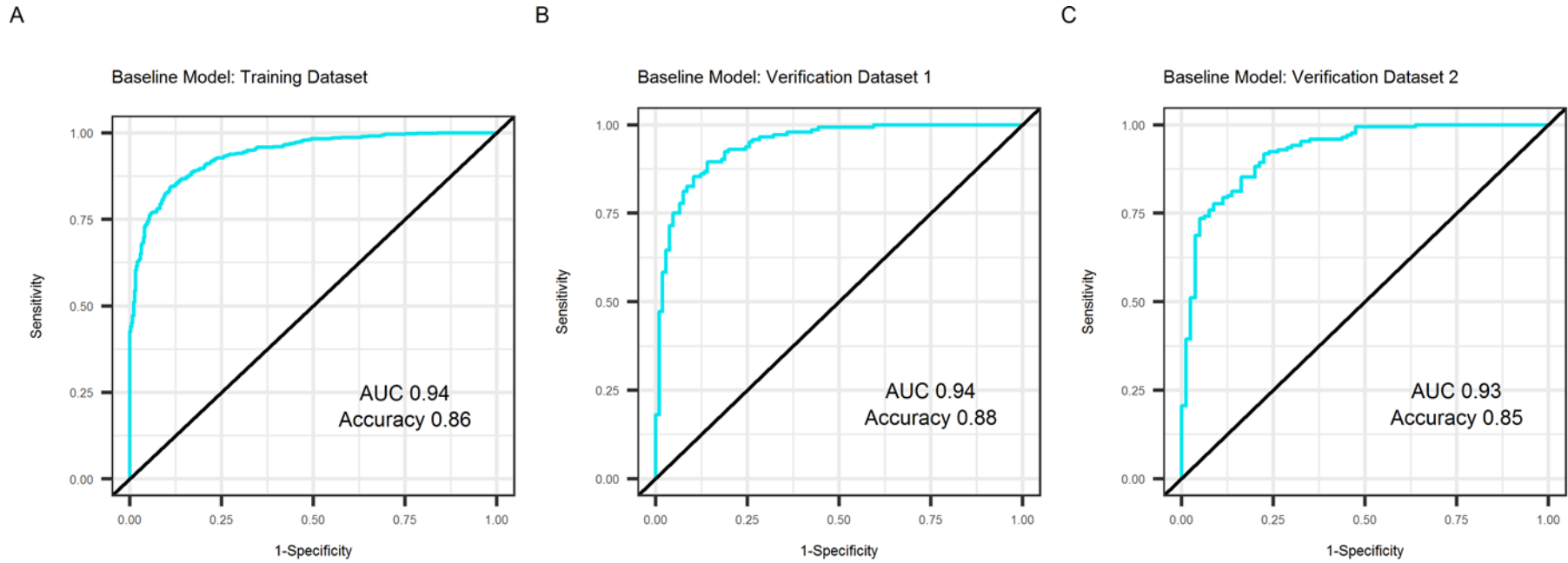


**Figure 6.3: Receiver operating characteristic curves demonstrating multivariate model performance in the training set (Panel A) and verification sets (Panel B and C)**

### 6.3.2 Application 2: TDM Patient Population

Between March 2014 and November 2017, 40 patients taking a KI for various cancers were enrolled. Of these 30 patients completed both PK blood samples and were evaluable for assessment. Four of these patients were evaluated for both dabrafenib and trametinib (administered as a combination therapy). Ten patients did not complete the study due to either disease progression or death. **Table 6.4** describes the demographic data for included patients.

**Table 6.4: Participant demographics by drug**

	<b>Dabrafenib</b>	<b>Erlotinib</b>	<b>Gefitinib</b>	<b>Imatinib</b>	<b>Osimertinib</b>	<b>Sunitinib</b>	<b>Pazopanib</b>	<b>Trametinib</b>
N	6	5	3	4	2	6	4	4
Age	58-78	32-73	77	43-78	35-73	58-73	54	58-78
% female	50	60	0	25	50	0	25	75
<i>Height (cm)</i>								
Mean	168	161	162	173	162	172	170	163
Range	162-180	155-167	158-166	162-193	NA	NA	159-182	162-163
<i>Weight (kg)</i>								
Mean	84	65	73	87	70	75	76	72
Range	54-109	50-76	66-80	63-105	NA	NA	52-124	54-90
<i>BMI (kg/m<sup>2</sup>)</i>								
Mean	29	25	28	29	27	25	26	27
Range	20-34	21-27	26-29	24-35	NA	NA	18-37	20-34
<i>Ethnicity (%)</i>								
Caucasian	100	60	100	100	100	83	100	100
Other		40				17		

### 6.3.3 Plasma Concentrations

**Table 6.5** presents a summary of the trough concentrations obtained from this cohort. The performance of standard fixed dosing of KIs was assessed using the following criteria (i) BSV as % of mean and absolute (fold) (ii) the proportion of patients who failed to achieve the desired exposure (% of patients below threshold) and (iii) the lowest exposure for an individual relative to the desired exposure (i.e. worst case scenario; maximum deviation as % of target).

Wide variability was observed in this small cohort with BSV showing a 335, 147, 87, 65, 62, 159, 149, and 28 % of the mean concentrations for dabrafenib, erlotinib, gefitinib, imatinib, osimertinib, pazopanib, sunitinib and trametinib, respectively. The absolute BSV was between 1.3- and 6- fold for the majority of the KIs with dabrafenib and sunitinib showing substantially greater variability of 16- and 32- fold, respectively. Sixty percent of patients tested were below the established minimum target concentrations. The maximum individual patient variability relative to the target concentration differed considerably between KIs ranging from 6 to 850 % of the established target concentration.

The poorest exposure was observed for sunitinib with one patient achieving a  $C_{ss\_trough}$  that was only 6 % of the established target concentration (i.e. 3 vs 50ng/mL). Poor compliance was excluded as the cause of this low exposure. To provide context to the potential implications of sub-therapeutic dosing an interesting observation will be described. One patient treated with adjuvant imatinib following the surgical removal of a primary gastrointestinal stromal tumour (GIST) had an observed imatinib  $C_{ss\_trough}$  of 913ng/mL. Imatinib was continued for 19 months before disease recurrence was observed in 2017. At this time imatinib  $C_{ss\_trough}$  were analysed and the concentration was measured to be 360ng/mL, nearly 3- fold less than the starting concentration. This observation is consistent with auto-induction of CYP3A4 by imatinib, resulting in greater clearance and lower exposure to this drug. At this time dose adjustments of

up to double the standard dose were made and although the patient tolerated this dose well, scans showed that the patient had already progressed with lesions in multiple organs therefore imatinib was discontinued. Poor compliance was excluded and a case of increased imatinib clearance was suspected. A more extensive patient case study is described below as a strong exemplar of the potential benefit of the application of TDM guided KI dosing.

**Table 6.5: Variability in KI exposure relative to target concentration**

KI	Concentration (trough ng/mL)			Between Subject Variability		Maximum deviation as % of target	% of patients below threshold
	Mean	Range	Established target	% of mean	Absolute (fold)		
Dabrafenib	118	13-408	<48 <sup>a</sup>	335	32	850	33 <sup>b</sup>
Erlotinib	533	164-948	>500	147	6	33	60
Gefitinib	261	134-360	>200	NE	NE	67	33
Imatinib	1,164	637-1,397	>1100	65	2	58	50
Osimertinib	176	121-230	NA	NE	NE	NA	NA
Pazopanib	11,993	4,713-23,716	>20,000	159	5	24	75
Sunitinib	39	3-61	50-100	149	20	6	67
Trametinib	18	16-21	NA	28	1.3	NA	NA

<sup>a</sup> threshold for toxicity, all other targets associated with efficacy. <sup>b</sup> above threshold.

Abbreviations: NA; not applicable, NE; not evaluated.

### 6.3.4 Therapeutic Drug Monitoring Case Study

A 32 year old, non-smoker, physically active (ECOG 0-1) Caucasian male was diagnosed with stage 4 NSCLC with a primary lesion in his left lung measuring 43 x 34mm and bilateral metastatic lymph node involvement (**Figure 6.4 A**). The primary lesion was positive for an EGFR active mutation (E746\_A750del; see section 1.4.2). The tumour was inoperable and the patient was treated with 150mg erlotinib daily. No concomitant medications or morbidities were reported. Initially the treatment was effective with a partial response observed five months after commencing erlotinib (**Figure 6.4 B**). The patient developed recurrent Grade 2 skin rashes that impacted on the patient's medication adherence.

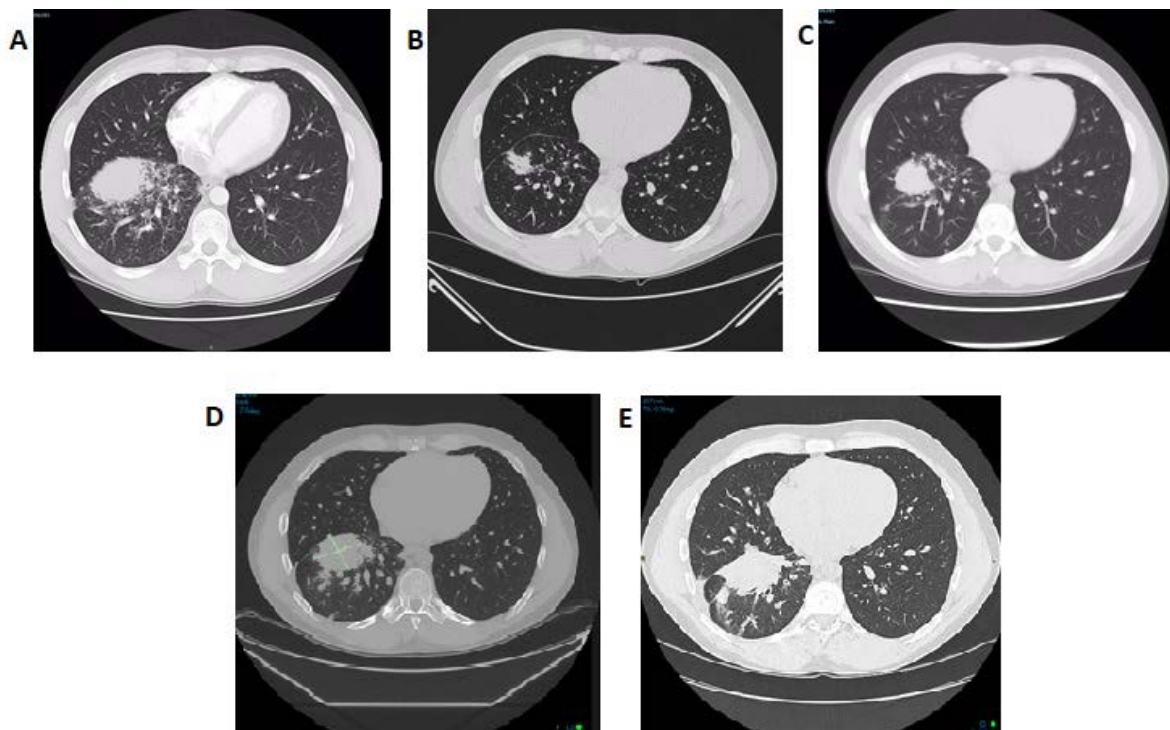


**Figure 6.4: Computed tomography (CT) scan showing primary tumour**

*Panel A: 4cm taken November 2014, Panel B: 1cm taken April 2015. Panel C: 2.5cm taken May 2016, Panel D: 3.5cm taken November 2016. Panel E: 4cm taken February 2017.*

Monitoring of disease between April 2015 and May 2016 demonstrated slow disease progression and between December 2015 and January 2016 two rounds of concurrent IV chemotherapy were administered. This was not tolerated well by the patient and it was preferred by the patient to cease chemotherapy. The CT scan in May 2016 (**Figure 6.4 C**) demonstrated marked disease progression that was not associated with the development of the T790M EGFR mutation which causes resistance to erlotinib. It is standard practice at this time to commence the second-line treatment. Instead, TDM was performed and revealed trough concentrations of 164 and 248 ng/mL on two different days which were more than 2-fold lower than the established target trough concentration (target >500ng/mL) for erlotinib. Erlotinib was therefore increased to 175mg daily. Erlotinib trough concentrations were measured and observed to be >400ng/mL with good tolerance and compliance. A CT scan performed in November 2016 demonstrated a slowing of disease progression attributed to the increased erlotinib dose.

A CT scan taken in February 2017 demonstrated continued disease progression and the patient progressed to a second line KI (osimertinib). Through the application of erlotinib TDM this patient achieved a total time to progression (TTP) of 27 months. The median TTP for first-line EGFR MT+ NSCLC is 9.7 months as reported in Lancet Oncology (52). Notably, this case demonstrated an increase in TTP of 9 months directly resulting from adjustment of dosing based on the capacity to evaluate erlotinib exposure.

## 6.4 Discussion

This is the first report describing the use of a PBPK modelling strategy to identify baseline physiological and molecular characteristics driving BSV in drug exposure. Novel strategies, such as the one described here, play an increasingly important role in guiding the efficient generation of evidence defining relationships between patient characteristics and BSV in drug exposure. Specifically, this strategy will be useful during drug development to prospectively guide collection of pertinent patient information during clinical trials. The strategy is also useful for existing drugs, as it can be applied to inform analysis of archived samples from pivotal RCTs to help define such associations. In this regard, Pfizer recently retrospectively genotyped patients in pivotal axitinib RCTs for CYP3A genotype using archived blood samples (231). The analysis was unsuccessful due to the poor ability of genotype to predict CYP3A activity but did demonstrate the ability to retrospectively and efficiently generate high-quality evidence and the interest of industry and trialists in identifying baseline predictors of exposure.

The requirement for more sophisticated modelling to robustly define physiological and molecular characteristics defining BSV in exposure is highlighted with dabrafenib. As a BCS Class II drug that exhibits pH dependent solubility, dabrafenib absorption is influenced by intestinal pH and food, in particular high fat meals [GSK trial ID: 113468]. As such, there is potential for BSV in intestinal permeability, metabolism and transporter to influence exposure. The ADAM absorption sub-model in Simcyp® considers each of these factors and provided a robust description of the dabrafenib absorption phase as demonstrated by the concordance of simulated and observed  $C_{max}$  and  $T_{max}$  values. Indeed, following dosing recommendations to administer dabrafenib in a fasted state, i.e. 1 hour before or 2+ hour after a meal, the mean (90% confidence interval; CI) simulated and observed oral bioavailabilities were 91.6% (78.4 to 104.8%) and 94.5% (81.3 to 109.7%), respectively [GSK trial ID: 113479]. Similarly, mean

simulated and observed times to peak plasma concentration ( $T_{max}$ ) were concordant in the range 1.0 to 4.0 hours. Furthermore, in order to robustly evaluate potential physiological and molecular characteristics driving BSV in clearance, a sound mechanistic description of all pathways involved in the clearance of the drug is crucial. Dabrafenib is primarily cleared by CYP2C8 and CYP3A4 mediated metabolism to form hydroxy-dabrafenib, which is further oxidized via CYP3A4 to form carboxy-dabrafenib which is excreted in bile and urine. Carboxy-dabrafenib can be decarboxylated in the gastrointestinal tract via a non-enzymatic processes to form desmethyl-dabrafenib, which is reabsorbed (entero-hepatic recirculation) (278), a process that is accounted for in the dabrafenib PBPK model. Dabrafenib is also a substrate for intestinal uptake and P-gp mediated hepatic and intestinal efflux. Approximately 75% of the dose is recovered, primarily as metabolites, in the faeces and approximately 25% is recovered as metabolites in the urine. Further adding to the complexity of PK analyses, but still readily defined within the PBPK model, the mean (90% CI) elimination half-life for dabrafenib in Caucasians following a single oral dose of 4.2 (3.1 – 9.6) hours, is reduced to 2.1 (1.1 to 3.6) hours with steady state dosing, indicating that with repeated dosing dabrafenib has the capacity to induce its own clearance. Indeed, in addition to being a substrate for CYP2C8 and CYP3A4, dabrafenib is also a known competitive inhibitor of these enzymes, with  $K_i$  values of 4.1 and 8.0  $\mu\text{M}$ , respectively, and strong inducer of CYP3A4 (rifampin normalized  $\text{IND}_{max} = 30\text{-fold}$ ). Importantly, as displayed by the multiple dose simulations, by defining dabrafenib's induction and inhibition capacity (**Table 6.1**), this auto-induction is described by the PBPK model. While accounting for these PK complexities, using dabrafenib as a test-case, we propose that assessment of baseline weight, BMI, and CYP2C8, CYP3A4 and P-gp protein abundances is likely to predict the increased risk of steady state exposure associated with dose limiting toxicity (assessed as a trough concentration  $>48\text{ng/mL}$ ) (269).

Understanding and accounting for factors that contribute to BSV in drug exposure has important benefits throughout a drug's life-span. During drug development failure to account for sources of variability in exposure has the potential to contribute to an unexplained lack of effect or increased incidence of toxicity within certain populations, and is overrepresented as a factor contributing to the post-marketing failure of a drug. Similarly, in clinical practice, failure to account for sources of variability in drug exposure can result in sub-optimal patient outcomes). Standard population PK analyses are often used as a component of regulatory submissions. However, as these models are built by fitting observed parameters to reported exposure in trial populations, these models are implicitly limited to describing the influence of observed parameters and cannot readily predict or define the influence of unknown factors that underpin the observed effect. Understanding these core covariates that drive BSV in drug exposure will facilitate the optimal implementation of clinical precision dosing platforms such as Virtual Twin™ (279, 280). In practice PBPK model informed biomarker discovery is the first step in a process of precision dosing. The identified markers will guide individual assessment of characteristics beyond genotype that lead to more insightful individualisation. The identified markers inform a second round of simulation (Virtual Twin) where individual patient exposure is simulated based on individual assessment of the characteristics known to most substantially influence exposure.

In the second study KI trough concentrations were measured in a 'real world' oncology cohort to assess BSV and to compare the results to established target concentrations. The study cohort comprised of 70% males and 30% females. The older age (32-78 years old), weight and height range observed in this cohort were consistent with typical cancer patient demographics (194). Ninety-three percent of the cohort were Caucasian with two patients identified as Indigenous and Torres Strait Islander.

When BSV was assessed, wide variability was observed in this cohort with concentrations showing a 335, 147, 65, 159, 149, and 28 % variability of the mean concentrations for dabrafenib, erlotinib, imatinib, pazopanib, sunitinib and trametinib, respectively. BSV was not evaluated for gefitinib (n=3) or osimetinib (n=2) due to low sample size. With the exception of dabrafenib and sunitinib, which exhibited variability of 16- and 32- fold, respectively, the absolute BSV of 1.3 to 6- fold were observed for the majority of the KIs. It is worth noting however that a limitation of this study was that it comprised only 30 patients with four to six patients per KI; the large BSV observed in this cohort is consistent with larger studies (125).

When KI trough concentrations were compared to the established target concentrations it was found that 60 % of patients were under the established target concentrations, which is also consistent with several studies from the literature as summarised in recent publications resulting from this thesis (268) and other groups (125). When dabrafenib concentrations were compared to the target  $C_{ss\_trough}$  of <48ng/mL, it was observed that two of the six patients were significantly above the target concentration with 208 and 404 ng/mL. These observed higher concentrations are not entirely explainable, however, the patient with the highest observed concentration of 404 ng/mL died shortly after commencing dabrafenib. It was unclear if this patient's death was directly related to severe toxicity. The maximum individual patient variability relative to the target concentration differed considerably between KIs ranging from 6-67 % of the established target concentration with dabrafenib showing a much higher variability of 850 %. In scenarios where extremely low (< 20% minimum threshold) is observed, increasing dose alone may not be the most suitable strategy.

Given that CYP3A4 is the major enzyme responsible for KI clearance in most instances, it is possible that the co-administration of a pharmacokinetic enhancer such as cobicistat or ritonavir, which inhibit CYP3A4, may be a more appropriate and cost effective strategy. Indeed

there are existing examples such as HIV protease inhibitor cocktails where these drugs are used to improve exposure to high cost CYP3A4 substrates (281).

With the majority of patients under the target concentrations with some patients only achieving 6 % of the established target concentration (i.e. 3 vs 50 ng/mL) and some patients experiencing over exposure of up to 850 %, it is clear that this demonstrates some of the potential complications arising from standard fixed KI dosing regimens. Another interesting finding further underlined complications with such dosing protocols for patients taking KIs long-term. One of the patients experienced a decrease in imatinib trough concentration of more than 3-fold over the course of 19 months. As compliance was excluded, this may have been a case of increased clearance as described by Eechoute et al (2012), where a study of 50 patients demonstrated a 30% decrease in imatinib plasma trough concentrations after as soon as three months (282). This patient was taking imatinib for 19 months when the decreased concentration was observed. Given that imatinib is used for long-term treatment in many patients for up to several years, it further demonstrates the potential benefit that TDM can provide in such patients.

When a patient case study was analysed as an example of the potential benefit of the application of TDM guided KI dosing it was observed that a TTP of 27 months was achieved when 9.7 months have been reported previously. This study demonstrated that an additional 9 months were observed as a direct attribution of TDM. Although, this study has shown where the approach of TDM can be effective, this approach is not currently able to be translated into clinical practice.

---

# GENERAL CONCLUSIONS

---

As discussed throughout this thesis KIs are an important novel and rapidly expanding class of anti-cancer medicines used to target the identified hallmark characteristics of cancer. KIs exhibit many complex and unconventional pharmacokinetic characteristics with both CYP mediated metabolism and P-gp mediated transport involved in determining exposure. As such KIs exhibit marked BSV in exposure which can have clinically important consequences that may manifest as sub-optimal outcomes or toxicity. As narrow therapeutic index drugs the general principle of optimising KI dosing on the basis of exposure is intuitively supported.

Indeed, prior to this thesis studies had demonstrated the benefit of using TDM to individualise KI dosing on the basis of plasma-KI concentration. Despite this evidence precision KI dosing has not been broadly translated into clinical practice. The broader clinical uptake of precision KI dosing is hindered by: (i) the requirement to establish and validate separate analytical methods for each KI as they enter clinical practice in order to perform TDM, and (ii) the preclusive cost and complexity of generating sufficiently powered evidence to support the clinical validity of the benefit of concentration guided dosing. Given these limitations, novel and practical strategies are required to: (i) optimise the efficiency of TDM based precision KI dosing, and (ii) provide complementary avenues to support prospective dose optimisation and assist in identifying patients for whom TDM is most critical. By addressing these challenges it will be possible to more readily facilitate the clinical application of KI dose optimisation.

The first major challenge to addressing prospective KI dose optimisation is the currently incomplete understanding of the molecular and physiological characteristics driving variability in KI exposure. Results presented in Chapter II confirm that CYP3A4 is the major enzyme involved in KI clearance and that variability in CYP3A4 activity is likely a major cause of

variability in KI exposure. Given that EGFR KIs have shown promising results in the treatment of NSCLC but indeed exhibit substantial BSV in exposure which may result in either a lack of efficacy or toxicity due to fixed dosing regimens, PBPK profiles for afatinib, erlotinib and gefitinib were developed and validated. A more comprehensive demonstration of the application is later described using dabrafenib as an example in Chapter VI.

The capacity of the profiles to account for the impact of covariates on *in vivo* clearance was assessed by quantifying the rate of microsomal KI metabolism in the presence and absence of CYP and UGT cofactors as well as a selective CYP3A4 inhibitor (CYP3Cide). Microsomal clearance was assessed on the basis of the substrate depletion. Robust mechanistic models with the capacity to describe EGFR KI exposure and the impact of covariates such as age, gender, and ethnicity, and the impact of co-administration with strong CYP3A4 inhibitors and inducers on exposure were developed and validated. Such PBPK modelling may be used to account for sources of variability in KI exposure and may be applied to inform the impact of different dosing regimens on EGFR KI exposure, the potential impact of poor compliance on EGFR KI efficacy, the need to perform bridging studies when introducing EGFR KIs to new international markets, and the potential impact of DDIs on EGFR KI exposure.

In particular for EGFR inhibitors PBPK modelling demonstrated that race was a likely source of variability in exposure that was currently poorly accounted in clinical trials. Similarly, broader review of the literature revealed that outside of the assessment of differences in genotype frequency, very little is known regarding racial differences in CYP3A4 activity. Results presented in Chapter III demonstrate that race is a potential source of variability in CYP3A4 exposure as significantly higher midazolam clearance was observed in healthy age matched males of South Asian compared to Caucasian ancestry that was not explained by differences in the frequency of CYP3A genotypes. This variability has important implications

for the regulatory approval of KIs as clinical trials are often performed in homogenous Caucasian cohorts, and it is likely that bridging studies would be necessary to define the effective concentration of KIs in non-Caucasian cohorts in order to avoid systemic sub-therapeutic dosing. Taken together the results presented in Chapters II and III provide important new insights regarding sources of variability in KI exposure and describe the development and verification of a novel strategy to characterise such variability. These results have direct application in terms of prospectively optimising KI dosing. They also provide broader translation though future research efforts to more extensively assess alternate potential sources of variability in KI exposure such as age and gender using the approach employed here to assess race.

In order to translate the findings regarding the value of prospectively characterising variability in CYP3A4 novel strategies are required. Current methods to assess variability in CYP3A activity have notable limitations and there remains a need for a minimally-invasive clinically translatable biomarker to define CYP3A activity. Results in Chapter IV demonstrate that CYP3A4 activity may be accounted for using the caffeine/TMU ratio as a dietary marker of activity. The strength of correlations was retained post-rifampin dosing and appreciably weaker correlations were observed between the change in midazolam AUC and change in caffeine/TMU ratios post-/pre- rifampin dosing. BSV in CYP3A activity was well described by caffeine/TMU ratios pre- and post- induction. However, WSV caused by induction was poorly described. A dietary caffeine/TMU ratio may be a convenient tool to assess BSV in CYP3A activity, but assessment of caffeine/TMU ratio alone is unlikely to account for all sources of variability in CYP3A activity.

In addition to developing novel strategies to complement KI TDM there is also considerable scope to help facilitate clinical translation by addressing the technical inefficiencies of existing

analytical approaches used to underpin this strategy. Improving the efficiency of the analytical platform underpinning TDM assists pathology providers in justifying the investment in assays to quantify patient samples for drugs that individually are used in limited populations. Specifically, the development of a common platform to assess all KIs is important in this regard. Chapter V describes a novel approach for the quantification of 18 KIs in plasma, providing a platform that is unparalleled in terms of scope for the assessment of KI TDM and facilitating pharmacokinetic studies with KIs. This approach was developed, validated and reported in accordance with the 2015 version of the FDA guidance for industry on ‘analytical procedures and methods validation for drugs and biologics’ facilitating direct application as a clinical trials platform. The application of this approach was explored in Chapter VI.

Overall this thesis has contributed to a greater understanding of KI dosing. The results presented here have identified a number of sources of variability in KI exposure and have demonstrated the development, verification and application of these strategies to improve KI dosing and patient outcomes. This is highlighted by the 9 month additional survival benefit achieved by the patient described in Chapter VI, which was directly attributed to the work undertaken in this thesis. In conclusion this thesis contributed to better understand developing pathways to investigate/establish variability, thereby unmasking opportunities for optimised KI dosing.

---

# REFERENCES

---

1. Robb KA, Simon AE, Miles A, Wardle J. Public perceptions of cancer: a qualitative study of the balance of positive and negative beliefs. *BMJ open*. 2014;4(7):e005434.
2. Cancer in Australia 2017. In: Welfare AIOHa, editor. Number 101 ed. Canberra: AIHW; 2017.
3. Torre LA, Bray F, Siegel RL, Ferlay J, Lortet-Tieulent J, Jemal A. Global cancer statistics, 2012. *CA: A Cancer Journal for Clinicians*. 2015;65(2):87-108.
4. Patafio FM, Brooks SC, Wei X, Peng Y, Biagi J, Booth CM. Research output and the public health burden of cancer: is there any relationship? *Current Oncology*. 2016;23(2):75-80.
5. Hanahan D, Weinberg Robert A. Hallmarks of Cancer: The Next Generation. *Cell*. 2011;144(5):646-74.
6. Lemmon MA, Schlessinger J. Cell signaling by receptor tyrosine kinases. *Cell*. 2010;141(7):1117-34.
7. Burkhart DL, Sage J. Cellular mechanisms of tumour suppression by the retinoblastoma gene. *Nature reviews Cancer*. 2008;8(9):671-82.
8. Law ME, Corsino PE, Narayan S, Law BK. Cyclin-Dependent Kinase Inhibitors as Anticancer Therapeutics. *Molecular pharmacology*. 2015;88(5):846-52.
9. Hydbring P, Bahram F, Su Y, Tronnorsjö S, Högstrand K, von der Lehr N, et al. Phosphorylation by Cdk2 is required for Myc to repress Ras-induced senescence in cotransformation. *Proceedings of the National Academy of Sciences of the United States of America*. 2010;107(1):58-63.
10. Grivennikov SI, Greten FR, Karin M. Immunity, inflammation, and cancer. *Cell*. 2010;140(6):883-99.
11. Adams JM, Cory S. The Bcl-2 apoptotic switch in cancer development and therapy. *Oncogene*. 2007;26(9):1324-37.
12. Delbridge AR, Strasser A. The BCL-2 protein family, BH3-mimetics and cancer therapy. *Cell death and differentiation*. 2015;22(7):1071-80.
13. Carter BZ, Mak PY, Mu H, Zhou H, Mak DH, Schober W, et al. Combined Targeting of BCL-2 and BCR-ABL Tyrosine Kinase Eradicates Chronic Myeloid Leukemia Stem Cells. *Science translational medicine*. 2016;8(355):355ra117-355ra117.
14. Blasco MA. Telomeres and human disease: ageing, cancer and beyond. *Nature reviews Genetics*. 2005;6(8):611-22.
15. Park JI, Venteicher AS, Hong JY, Choi J, Jun S, Shkreli M, et al. Telomerase modulates Wnt signalling by association with target gene chromatin. *Nature*. 2009;460(7251):66-72.
16. Cunningham AP, Love WK, Zhang RW, Andrews LG, Tollefsbol TO. Telomerase Inhibition in Cancer Therapeutics: Molecular-Based Approaches. *Current medicinal chemistry*. 2006;13(24):2875-88.
17. Baeriswyl V, Christofori G. The angiogenic switch in carcinogenesis. *Seminars in cancer biology*. 2009;19(5):329-37.
18. Kazerounian S, Yee KO, Lawler J. Thrombospondins in cancer. *Cellular and molecular life sciences : CMLS*. 2008;65(5):700-12.
19. Olive KP, Jacobetz MA, Davidson CJ, Gopinathan A, McIntyre D, Honess D, et al. Inhibition of Hedgehog signaling enhances delivery of chemotherapy in a mouse model of pancreatic cancer. *Science (New York, NY)*. 2009;324(5933):1457-61.
20. Zee YK, O'Connor JP, Parker GJ, Jackson A, Clamp AR, Taylor MB, et al. Imaging angiogenesis of genitourinary tumors. *Nature reviews Urology*. 2010;7(2):69-82.

21. Klymkowsky MW, Savagner P. Epithelial-mesenchymal transition: a cancer researcher's conceptual friend and foe. *The American journal of pathology*. 2009;174(5):1588-93.
22. Karnoub AE, Dash AB, Vo AP, Sullivan A, Brooks MW, Bell GW, et al. Mesenchymal stem cells within tumour stroma promote breast cancer metastasis. *Nature*. 2007;449(7162):557-63.
23. Gocheva V, Wang HW, Gadea BB, Shree T, Hunter KE, Garfall AL, et al. IL-4 induces cathepsin protease activity in tumor-associated macrophages to promote cancer growth and invasion. *Genes & development*. 2010;24(3):241-55.
24. Hugo H, Ackland ML, Blick T, Lawrence MG, Clements JA, Williams ED, et al. Epithelial-mesenchymal and mesenchymal-epithelial transitions in carcinoma progression. *Journal of cellular physiology*. 2007;213(2):374-83.
25. Madsen CD, Sahai E. Cancer dissemination--lessons from leukocytes. *Developmental cell*. 2010;19(1):13-26.
26. Kessenbrock K, Plaks V, Werb Z. Matrix metalloproteinases: regulators of the tumor microenvironment. *Cell*. 2010;141(1):52-67.
27. Naumov GN, Folkman J, Straume O, Akslen LA. Tumor-vascular interactions and tumor dormancy. *APMIS : acta pathologica, microbiologica, et immunologica Scandinavica*. 2008;116(7-8):569-85.
28. Barkan D, Green JE, Chambers AF. Extracellular matrix: a gatekeeper in the transition from dormancy to metastatic growth. *European journal of cancer (Oxford, England : 1990)*. 2010;46(7):1181-8.
29. Teng MW, Swann JB, Koebel CM, Schreiber RD, Smyth MJ. Immune-mediated dormancy: an equilibrium with cancer. *Journal of leukocyte biology*. 2008;84(4):988-93.
30. Demicheli R, Retsky MW, Hrushesky WJ, Baum M, Gukas ID. The effects of surgery on tumor growth: a century of investigations. *Annals of oncology : official journal of the European Society for Medical Oncology*. 2008;19(11):1821-8.
31. Kim K-H, Kim H. Progress of antibody-based inhibitors of the HGF-cMET axis in cancer therapy. *Experimental & Molecular Medicine*. 2017;49(3):e307.
32. Kinzler KW, Vogelstein B. Cancer-susceptibility genes. Gatekeepers and caretakers. *Nature*. 1997;386(6627):761, 3.
33. Negrini S, Gorgoulis VG, Halazonetis TD. Genomic instability--an evolving hallmark of cancer. *Nature reviews Molecular cell biology*. 2010;11(3):220-8.
34. Jackson SP, Bartek J. The DNA-damage response in human biology and disease. *Nature*. 2009;461(7267):1071-8.
35. Artandi SE, DePinho RA. Telomeres and telomerase in cancer. *Carcinogenesis*. 2010;31(1):9-18.
36. Dziadkowiec KN, Gąsiorowska E, Nowak-Markwitz E, Jankowska A. PARP inhibitors: review of mechanisms of action and BRCA1/2 mutation targeting. *Przegląd Menopauzalny = Menopause Review*. 2016;15(4):215-9.
37. Sunada S, Nakanishi A, Miki Y. Crosstalk of DNA double-strand break repair pathways in poly(ADP-ribose) polymerase inhibitor treatment of breast cancer susceptibility gene 1/2-mutated cancer. *Cancer science*. 2018.
38. de Visser KE, Eichten A, Coussens LM. Paradoxical roles of the immune system during cancer development. *Nature reviews Cancer*. 2006;6(1):24-37.
39. DeNardo DG, Andreu P, Coussens LM. Interactions between lymphocytes and myeloid cells regulate pro- versus anti-tumor immunity. *Cancer metastasis reviews*. 2010;29(2):309-16.
40. Jones RG, Thompson CB. Tumor suppressors and cell metabolism: a recipe for cancer growth. *Genes & development*. 2009;23(5):537-48.
41. Fantin VR, St-Pierre J, Leder P. Attenuation of LDH-A expression uncovers a link between glycolysis, mitochondrial physiology, and tumor maintenance. *Cancer cell*. 2006;9(6):425-34.

42. DeBerardinis RJ, Lum JJ, Hatzivassiliou G, Thompson CB. The biology of cancer: metabolic reprogramming fuels cell growth and proliferation. *Cell metabolism*. 2008;7(1):11-20.
43. Savoia P, Astrua C, Fava P. Ipilimumab (Anti-Ctla-4 Mab) in the treatment of metastatic melanoma: Effectiveness and toxicity management. *Human Vaccines & Immunotherapeutics*. 2016;12(5):1092-101.
44. Drenberg CD, Baker SD, Sparreboom A. Integrating clinical pharmacology concepts in individualized therapy with tyrosine kinase inhibitors. *Clin Pharmacol Ther*. 2013;93(3):215-9.
45. Humphrey R, Brockway-Lunardi L, Bonk D, Dohoney KM, Doroshow JH, Meech SJ, et al. Opportunities and Challenges in the Development of Experimental Drug Combinations for Cancer. *Journal of the National Cancer Institute*. 2011;103(16):1222-6.
46. Eckstein N, Roper L, Haas B, Potthast H, Hermes U, Unkrig C, et al. Clinical pharmacology of tyrosine kinase inhibitors becoming generic drugs: the regulatory perspective. *Journal of Experimental & Clinical Cancer Research*. 2014;33(1):15.
47. Arora A, Scholar EM. Role of Tyrosine Kinase Inhibitors in Cancer Therapy. *J Pharmacol Exp Ther*. 2005;315(3):971-9.
48. Krause DS, Van Etten RA. Tyrosine Kinases as Targets for Cancer Therapy. *New England Journal of Medicine*. 2005;353(2):172-87.
49. McTigue M, Murray BW, Chen JH, Deng YL, Solowiej J, Kania RS. Molecular conformations, interactions, and properties associated with drug efficiency and clinical performance among VEGFR TK inhibitors. *Proc Natl Acad Sci*. 2012;109(45):18281-9.
50. Ladanyi M, Pao W. Lung adenocarcinoma: guiding EGFR-targeted therapy and beyond. *Modern pathology : an official journal of the United States and Canadian Academy of Pathology, Inc*. 2008;21 Suppl 2:S16-22.
51. He M, Capelletti M, Nafa K, Yun C-H, Arcila ME, Miller VA, et al. EGFR Exon 19 Insertions: A New Family of Sensitizing EGFR Mutations in Lung Adenocarcinoma. *Clin Cancer Res*. 2012;18(6):1790-7.
52. Rosell R, Carcereny E, Gervais R, Vergnenegre A, Massuti B, Felip E, et al. Erlotinib versus standard chemotherapy as first-line treatment for European patients with advanced EGFR mutation-positive non-small-cell lung cancer (EURTAC): a multicentre, open-label, randomised phase 3 trial. *Lancet Oncol*. 2012;13(3):239-46.
53. Yang JJ, Zhang XC, Su J, Xu CR, Zhou Q, Tian HX, et al. Lung cancers with concomitant EGFR mutations and ALK rearrangements: diverse responses to EGFR-TKI and crizotinib in relation to diverse receptors phosphorylation. *Clin Cancer Res*. 2014;20(5):1383-92.
54. Stewart EL, Tan SZ, Liu G, Tsao MS. Known and putative mechanisms of resistance to EGFR targeted therapies in NSCLC patients with EGFR mutations-a review. *Translational lung cancer research*. 2015;4(1):67-81.
55. Chen Y, Tortorici MA, Garrett M, Hee B, Klamerus KJ, Pithavala YK. Clinical pharmacology of axitinib. *Clin Pharmacokinet*. 2013;52(9):713-25.
56. Tortorici MA, Cohen EE, Pithavala YK, Garrett M, Ruiz-Garcia A, Kim S, et al. Pharmacokinetics of single-agent axitinib across multiple solid tumor types. *Cancer Chemother Pharmacol*. 2014;74(6):1279-89.
57. Nguyen L, Holland J, Miles D, Engel C, Benrimoh N, O'Reilly T, et al. Pharmacokinetic (PK) drug interaction studies of cabozantinib: Effect of CYP3A inducer rifampin and inhibitor ketoconazole on cabozantinib plasma PK and effect of cabozantinib on CYP2C8 probe substrate rosiglitazone plasma PK. *J Clin Pharmacol*. 2015;55(9):1012-23.
58. Nair A, Lemery SJ, Yang J, Marathe A, Zhao L, Zhao H, et al. FDA Approval Summary: Lenvatinib for Progressive, Radio-iodine-Refractory Differentiated Thyroid Cancer. *Clinical cancer research : an official journal of the American Association for Cancer Research*.

2015;21(23):5205-8.

59. Deng Y, Sychterz C, Suttle AB, Dar MM, Bershas D, Negash K, et al. Bioavailability, metabolism and disposition of oral pazopanib in patients with advanced cancer. *Xenobiotica; the fate of foreign compounds in biological systems*. 2013;43(5):443-53.

60. Imbs DC, Negrier S, Cassier P, Hollebecque A, Varga A, Blanc E, et al. Pharmacokinetics of pazopanib administered in combination with bevacizumab. *Cancer Chemother Pharmacol*. 2014;73(6):1189-96.

61. Bruix J, Tak WY, Gasbarrini A, Santoro A, Colombo M, Lim HY, et al. Regorafenib as second-line therapy for intermediate or advanced hepatocellular carcinoma: multicentre, open-label, phase II safety study. *European journal of cancer (Oxford, England : 1990)*. 2013;49(16):3412-9.

62. Strumberg D, Richly H, Hilger RA, Schleucher N, Korfee S, Tewes M, et al. Phase I clinical and pharmacokinetic study of the Novel Raf kinase and vascular endothelial growth factor receptor inhibitor BAY 43-9006 in patients with advanced refractory solid tumors. *J Clin Oncol*. 2005;23(5):965-72.

63. Kane RC, Farrell AT, Saber H, Tang S, Williams G, Jee JM, et al. Sorafenib for the Treatment of Advanced Renal Cell Carcinoma. *Clinical Cancer Research*. 2006;12(24):7271-8.

64. Goodman VL, Rock EP, Dagher R, Ramchandani RP, Abraham S, Gobburu JV, et al. Approval summary: sunitinib for the treatment of imatinib refractory or intolerant gastrointestinal stromal tumors and advanced renal cell carcinoma. *Clinical cancer research : an official journal of the American Association for Cancer Research*. 2007;13(5):1367-73.

65. Faivre S, Delbaldo C, Vera K, Robert C, Lozahic S, Lassau N, et al. Safety, pharmacokinetic, and antitumor activity of SU11248, a novel oral multitarget tyrosine kinase inhibitor, in patients with cancer. *J Clin Oncol*. 2006;24(1):25-35.

66. Martin P, Oliver S, Kennedy SJ, Partridge E, Hutchison M, Clarke D, et al. Pharmacokinetics of vandetanib: three phase I studies in healthy subjects. *Clin Ther*. 2012;34(1):221-37.

67. Stopfer P, Marzin K, Narjes H, Gansser D, Shahidi M, Uttereuther-Fischer M, et al. Afatinib pharmacokinetics and metabolism after oral administration to healthy male volunteers. *Cancer Chemotherapy & Pharmacology*. 2012;69(4):1051-61.

68. Wind S, Schmid M, Erhardt J, Goeldner RG, Stopfer P. Pharmacokinetics of afatinib, a selective irreversible ErbB family blocker, in patients with advanced solid tumours. *Clin Pharmacokinet*. 2013;52(12):1101-9.

69. Johnson JR, Cohen M, Sridhara R, Chen YF, Williams GM, Duan J, et al. Approval summary for erlotinib for treatment of patients with locally advanced or metastatic non-small cell lung cancer after failure of at least one prior chemotherapy regimen. *Clinical cancer research : an official journal of the American Association for Cancer Research*. 2005;11(18):6414-21.

70. Frohna P, Lu J, Eppler S, Hamilton M, Wolf J, Rakhit A, et al. Evaluation of the absolute oral bioavailability and bioequivalence of erlotinib, an inhibitor of the epidermal growth factor receptor tyrosine kinase, in a randomized, crossover study in healthy subjects. *J Clin Pharmacol*. 2006;46(3):282-90.

71. Swaisland HC, Smith RP, Laight A, Kerr DJ, Ranson M, Wilder-Smith CH, et al. Single-dose clinical pharmacokinetic studies of gefitinib. *Clin Pharmacokinet*. 2005;44(11):1165-77.

72. Ranson M, Wardell S. Gefitinib, a novel, orally administered agent for the treatment of cancer. *Journal of Clinical Pharmacy & Therapeutics*. 2004;29(2):95-103.

73. Burris HA, 3rd, Hurwitz HI, Dees EC, Dowlati A, Blackwell KL, O'Neil B, et al. Phase I safety, pharmacokinetics, and clinical activity study of lapatinib (GW572016), a reversible dual inhibitor of epidermal growth factor receptor tyrosine kinases, in heavily pretreated patients

with metastatic carcinomas. *J Clin Oncol*. 2005;23(23):5305-13.

74. LoRusso PM, Jones SF, Koch KM, Arya N, Fleming RA, Loftiss J, et al. Phase I and pharmacokinetic study of lapatinib and docetaxel in patients with advanced cancer. *Journal of clinical oncology : official journal of the American Society of Clinical Oncology*. 2008;26(18):3051-6.

75. Lau YY, Gu W, Lin T, Song D, Yu R, Scott J. Effects of meal type on the oral bioavailability of the ALK inhibitor, ceritinib, in healthy adult subjects. *J Clin Pharmacol*. 2015.

76. Ou SH. Crizotinib: a novel and first-in-class multitargeted tyrosine kinase inhibitor for the treatment of anaplastic lymphoma kinase rearranged non-small cell lung cancer and beyond. *Drug Des Devel Ther*. 2011;5:471-85.

77. Yamazaki S, Johnson TR, Smith BJ. Prediction of Drug-Drug Interactions with Crizotinib as the CYP3A Substrate Using a Physiologically Based Pharmacokinetic Model. *Drug Metab Dispos*. 2015;43(10):1417-29.

78. Takahashi RH, Choo EF, Ma S, Wong S, Halladay J, Deng Y, et al. Absorption, Metabolism, Excretion, and the Contribution of Intestinal Metabolism to the Oral Disposition of [14C]Cobimetinib, a MEK Inhibitor, in Humans. *Drug metabolism and disposition: the biological fate of chemicals*. 2016;44(1):28-39.

79. Falchook GS, Long GV, Kurzrock R, Kim KB, Arkenau HT, Brown MP, et al. Dose selection, pharmacokinetics, and pharmacodynamics of BRAF inhibitor dabrafenib (GSK2118436). *Clinical cancer research : an official journal of the American Association for Cancer Research*. 2014;20(17):4449-58.

80. Infante JR, Fecher LA, Falchook GS, Nallapareddy S, Gordon MS, Becerra C, et al. Safety, pharmacokinetic, pharmacodynamic, and efficacy data for the oral MEK inhibitor trametinib: a phase 1 dose-escalation trial. *Lancet Oncol*. 2012;13(8):773-81.

81. Kim G, McKee AE, Ning YM, Hazarika M, Theoret M, Johnson JR, et al. FDA approval summary: vemurafenib for treatment of unresectable or metastatic melanoma with the BRAFV600E mutation. *Clinical cancer research : an official journal of the American Association for Cancer Research*. 2014;20(19):4994-5000.

82. Solimando DA, Waddell JA. Drug Monographs: Bosutinib and Regorafenib. *Hosp Pharm*. 2013;48(3):190-4.

83. Brave M, Goodman V, Kaminskas E, Farrell A, Timmer W, Pope S, et al. Sprycel for chronic myeloid leukemia and Philadelphia chromosome-positive acute lymphoblastic leukemia resistant to or intolerant of imatinib mesylate. *Clinical cancer research : an official journal of the American Association for Cancer Research*. 2008;14(2):352-9.

84. Peng B, Hayes M, Resta D, Racine-Poon A, Druker BJ, Talpaz M, et al. Pharmacokinetics and pharmacodynamics of imatinib in a phase I trial with chronic myeloid leukemia patients. *J Clin Oncol*. 2004;22(5):935-42.

85. Hazarika M, Jiang X, Liu Q, Lee SL, Ramchandani R, Garnett C, et al. Tassigna for chronic and accelerated phase Philadelphia chromosome--positive chronic myelogenous leukemia resistant to or intolerant of imatinib. *Clinical cancer research : an official journal of the American Association for Cancer Research*. 2008;14(17):5325-31.

86. Narasimhan NI, Dorer DJ, Davis J, Turner CD, Marbury TC, Sonnichsen D. Evaluation of pharmacokinetics and safety of ponatinib in subjects with chronic hepatic impairment and matched healthy subjects. *Cancer Chemother Pharmacol*. 2014;74(2):341-8.

87. de Jong J, Sukbuntherng J, Skee D, Murphy J, O'Brien S, Byrd JC, et al. The effect of food on the pharmacokinetics of oral ibrutinib in healthy participants and patients with chronic lymphocytic leukemia. *Cancer Chemother Pharmacol*. 2015;75(5):907-16.

88. Jin F, Robeson M, Zhou H, Hisoire G, Ramanathan S. The pharmacokinetics and safety of idelalisib in subjects with moderate or severe hepatic impairment. *J Clin Pharmacol*.

2015;55(8):944-52.

89. Dowty ME, Lin J, Ryder TF, Wang W, Walker GS, Vaz A, et al. The pharmacokinetics, metabolism, and clearance mechanisms of tofacitinib, a janus kinase inhibitor, in humans. *Drug metabolism and disposition: the biological fate of chemicals*. 2014;42(4):759-73.

90. van Erp NP, Gelderblom H, Guchelaar HJ. Clinical pharmacokinetics of tyrosine kinase inhibitors. *Cancer Treat Rev*. 2009;35(8):692-706.

91. FDA. OFEV (nintedanib) prescribing information 2014 [Available from: [http://www.accessdata.fda.gov/drugsatfda\\_docs/label/2014/205832s0001bl.pdf](http://www.accessdata.fda.gov/drugsatfda_docs/label/2014/205832s0001bl.pdf)].

92. Hurwitz HI, Dowlati A, Saini S, Savage S, Suttle AB, Gibson DM, et al. Phase I Trial of Pazopanib in Patients with Advanced Cancer. *Clinical Cancer Research*. 2009;15(12):4220-7.

93. FDA. Afatinib (GILOTRIF) clinical pharmacology and biopharmaceutics review. Center for Drug Evaluation and Research. 2014; Application ID 201292Orig1s000:1-96.

94. FDA. TAGRISSO (osimertinib) prescribing information 2015 [Available from: [http://www.accessdata.fda.gov/drugsatfda\\_docs/label/2015/208065s0001bl.pdf](http://www.accessdata.fda.gov/drugsatfda_docs/label/2015/208065s0001bl.pdf)].

95. FDA. ALECENSA (alectinib) prescribing information 2015 [Available from: [http://www.accessdata.fda.gov/drugsatfda\\_docs/label/2015/208434s0001bl.pdf](http://www.accessdata.fda.gov/drugsatfda_docs/label/2015/208434s0001bl.pdf)].

96. Kazandjian D, Blumenthal GM, Chen HY, He K, Patel M, Justice R, et al. FDA approval summary: crizotinib for the treatment of metastatic non-small cell lung cancer with anaplastic lymphoma kinase rearrangements. *Oncologist*. 2014;19(10):e5-11.

97. FDA. Dabrafenib (TAFINLAR) clinical pharmacology and biopharmaceutics review. Center for Drug Evaluation and Research; 2014. p. 1-83.

98. Scheers E, Leclercq L, de Jong J, Bode N, Bockx M, Laenen A, et al. Absorption, Metabolism, and Excretion of Oral <sup>14</sup>C Radiolabeled Ibrutinib: An Open-Label, Phase I, Single-Dose Study in Healthy Men. *Drug Metabolism and Disposition*. 2015;43(2):289-97.

99. FDA. JAKAFI (ruxolitinib) prescribing information 2014 [Available from: [http://www.accessdata.fda.gov/drugsatfda\\_docs/label/2014/202192s0091bl.pdf](http://www.accessdata.fda.gov/drugsatfda_docs/label/2014/202192s0091bl.pdf)].

100. FDA. IBRANCE (palbociclib) prescribing information 2015 [Available from: [http://www.accessdata.fda.gov/drugsatfda\\_docs/label/2015/207103s0001bl.pdf](http://www.accessdata.fda.gov/drugsatfda_docs/label/2015/207103s0001bl.pdf)].

101. Di Gion P, Kanefendt F, Lindauer A, Scheffler M, Doroshyenko O, Fuhr U, et al. Clinical pharmacokinetics of tyrosine kinase inhibitors: focus on pyrimidines, pyridines and pyrroles. *Clin Pharmacokinet*. 2011;50(9):551-603.

102. Scheffler M, Di Gion P, Doroshyenko O, Wolf J, Fuhr U. Clinical pharmacokinetics of tyrosine kinase inhibitors: focus on 4-anilinoquinazolines. *Clin Pharmacokinet*. 2011;50(6):371-403.

103. van Leeuwen RWF, van Gelder T, Mathijssen RHJ, Jansman FGA. Drug-drug interactions with tyrosine-kinase inhibitors: a clinical perspective. *The Lancet Oncology*. 2013;15(8):e315-e26.

104. Polasek TM, Lin FPY, Miners JO, Doogue MP. Perpetrators of pharmacokinetic drug-drug interactions arising from altered cytochrome P450 activity: a criteria-based assessment. *British journal of clinical pharmacology*. 2011;71(5):727-36.

105. Budha NR, Frymoyer A, Smelick GS, Jin JY, Yago MR, Dresser MJ, et al. Drug absorption interactions between oral targeted anticancer agents and PPIs: is pH-dependent solubility the Achilles heel of targeted therapy? *Clin Pharmacol Ther*. 2012;92(2):203-13.

106. Scripture CD, Figg WD. Drug interactions in cancer therapy. *Nat Rev Cancer*. 2006;6(7):546-58.

107. Wang Y, Wang M, Qi H, Pan P, Hou T, Li J, et al. Pathway-Dependent Inhibition of Paclitaxel Hydroxylation by Kinase Inhibitors and Assessment of Drug-Drug Interaction Potentials. *Drug Metabolism and Disposition*. 2014;42(4):782-95.

108. Filppula AM, Neuvonen M, Laitila J, Neuvonen PJ, Backman JT. Autoinhibition of CYP3A4 leads to important role of CYP2C8 in imatinib metabolism: variability in CYP2C8

activity may alter plasma concentrations and response. *Drug metabolism and disposition: the biological fate of chemicals.* 2013;41(1):50-9.

109. van Erp NP, Gelderblom H, Karlsson MO, Li J, Zhao M, Ouwerkerk J, et al. Influence of CYP3A4 inhibition on the steady-state pharmacokinetics of imatinib. *Clinical cancer research : an official journal of the American Association for Cancer Research.* 2007;13(24):7394-400.

110. Khan MS, Barratt DT, Somogyi AA. Impact of CYP2C8\*3 polymorphism on in vitro metabolism of imatinib to N-desmethyl imatinib. *Xenobiotica.* 2016;46(3):278-87.

111. Burns K, Nair PC, Rowland A, Mackenzie PI, Knights KM, Miners JO. The Nonspecific Binding of Tyrosine Kinase Inhibitors to Human Liver Microsomes. *Drug Metab Dispos.* 2015;43(12):1934-7.

112. Reyner EL, Sevidal S, West MA, Clouser-Roche A, Freiwald S, Fenner K, et al. In Vitro Characterization of Axitinib Interactions with Human Efflux and Hepatic Uptake Transporters: Implications for Disposition and Drug Interactions. *Drug Metabolism and Disposition.* 2013;41(8):1575-83.

113. van Leeuwen RWF, Peric R, Hussaarts KGAM, Kienhuis E, IJzerman NS, de Bruijn P, et al. Influence of the Acidic Beverage Cola on the Absorption of Erlotinib in Patients With Non-Small-Cell Lung Cancer. *J Clin Oncol.* 2016.

114. Singh BN. Effects of food on clinical pharmacokinetics. *Clin pharmacokinet.* 1999;37(3):213-55.

115. Jain RK, Brar SS, Lesko LJ. Food and oral antineoplastics: more than meets the eye. *Clinical cancer research : an official journal of the American Association for Cancer Research.* 2010;16(17):4305-7.

116. Ling J, Fettner S, Lum BL, Riek M, Rakhit A. Effect of food on the pharmacokinetics of erlotinib, an orally active epidermal growth factor receptor tyrosine-kinase inhibitor, in healthy individuals. *Anti-Cancer Drugs.* 2008;19(2):209-16.

117. Bello CL, Sherman L, Zhou J, Verkh L, Smeraglia J, Mount J, et al. Effect of food on the pharmacokinetics of sunitinib malate (SU11248), a multi-targeted receptor tyrosine kinase inhibitor: results from a phase I study in healthy subjects. *Anti-Cancer Drugs.* 2006;17(3):353-8.

118. Koch KM, Reddy NJ, Cohen RB, Lewis NL, Whitehead B, Mackay K, et al. Effects of food on the relative bioavailability of lapatinib in cancer patients. *Journal of Clinical Oncology.* 2009;27(8):1191-6.

119. Ieiri I, Tsunemitsu S, Maeda K, Ando Y, Izumi N, Kimura M, et al. Mechanisms of Pharmacokinetic Enhancement Between Ritonavir and Saquinavir; Micro/Small Dosing Tests Using Midazolam (CYP3A4), Fexofenadine (p-Glycoprotein), and Pravastatin (OATP1B1) as Probe Drugs. *The Journal of Clinical Pharmacology.* 2013;53(6):654-61.

120. Ulvestad M, Skottheim IB, Jakobsen GS, Bremer S, Molden E, Asberg A, et al. Impact of OATP1B1, MDR1, and CYP3A4 expression in liver and intestine on interpatient pharmacokinetic variability of atorvastatin in obese subjects. *Clin Pharmacol Ther.* 2013;93(3):275-82.

121. Kirn R, Wandel C, Leake B, Cvetkovic M, Fromm M, Dempsey P, et al. Interrelationship Between Substrates and Inhibitors of Human CYP3A and P-Glycoprotein. *Pharm Res.* 1999;16(3):408-14.

122. Shao J, Markowitz JS, Bei D, An G. Enzyme- and Transporter-Mediated Drug Interactions with Small Molecule Tyrosine Kinase Inhibitors. *J Pharm Sci.* 2014;103(12):3810-33.

123. Lees J, Chan A. Polypharmacy in elderly patients with cancer: clinical implications and management. *The Lancet Oncology.* 2011;12(13):1249-57.

124. Eskens F, Verweij J. The clinical toxicity profile of vascular endothelial growth factor

(VEGF) and vascular endothelial growth factor receptor (VEGFR) targeting angiogenesis inhibitors; A review. *European Journal of Cancer*. 2006;42(18):3127-39.

125. de Wit D, Guchelaar HJ, den Hartigh J, Gelderblom H, van Erp NP. Individualized dosing of tyrosine kinase inhibitors: are we there yet? *Drug Discov Today*. 2015;20(1):18-36.

126. Demetri GD, Wang Y, Wehrle E, Racine A, Nikolova Z, Blanke CD, et al. Imatinib Plasma Levels Are Correlated With Clinical Benefit in Patients With Unresectable/Metastatic Gastrointestinal Stromal Tumors. *Journal of Clinical Oncology*. 2009;27(19):3141-7.

127. Widmer N, Decosterd LA, Leyvraz S, Duchosal MA, Rosselet A, Debiec-Rychter M, et al. Relationship of imatinib-free plasma levels and target genotype with efficacy and tolerability. *British Journal of Cancer*. 2008;98(10):1633-40.

128. Rini BI, Garrett M, Poland B, Dutcher JP, Rixe O, Wilding G, et al. Axitinib in Metastatic Renal Cell Carcinoma: Results of a Pharmacokinetic and Pharmacodynamic Analysis. *The Journal of Clinical Pharmacology*. 2013;53(5):491-504.

129. Gouloze SC, Galettis P, Boddy AV, Martin JH. Monte Carlo simulations of the clinical benefits from therapeutic drug monitoring of sunitinib *Cancer chemotherapy and pharmacology*. 2016;78(1):209-16.

130. Rixe O, Dutcher J, Motzer R, Wilding G, Stadler W, Garrett M, et al. Diastolic blood pressure (dbP) and pharmacokinetics (PK) as predictors of axitinib efficacy in metastatic renal cell cancer (mRCC). 2009;27:abstr 5045.

131. Tiseo M, Andreoli R, Gelsomino F, Mozzoni P, Azzoni C, Bartolotti M, et al. Correlation between erlotinib pharmacokinetics, cutaneous toxicity and clinical outcomes in patients with advanced non-small cell lung cancer (NSCLC). *Lung cancer*. 2014;83(2):265-71.

132. Zhao YY, Li S, Zhang Y, Zhao HY, Liao H, Guo Y, et al. The relationship between drug exposure and clinical outcomes of non-small cell lung cancer patients treated with gefitinib. *Med Oncol*. 2011;28(3):697-702.

133. Picard S, Titier K, Etienne G, Teilhet E, Ducint D, Bernard MA, et al. Trough imatinib plasma levels are associated with both cytogenetic and molecular responses to standard-dose imatinib in chronic myeloid leukemia. *Blood*. 2007;109(8):3496-9.

134. Larson RA, Druker BJ, Guilhot F, O'Brien SG, Riviere GJ, Krahnke T, et al. Imatinib pharmacokinetics and its correlation with response and safety in chronic-phase chronic myeloid leukemia: a subanalysis of the IRIS study. *Blood*. 2008;111(8):4022-8.

135. Takahashi N, Miura M, Kuroki J, Mitani K, Kitabayashi A, Sasaki O, et al. Multicenter phase II clinical trial of nilotinib for patients with imatinib-resistant or -intolerant chronic myeloid leukemia from the East Japan CML study group evaluation of molecular response and the efficacy and safety of nilotinib. *Biomarker Res*. 2014;2:6.

136. Larson RA, Yin OQ, Hochhaus A, Saglio G, Clark RE, Nakamae H, et al. Population pharmacokinetic and exposure-response analysis of nilotinib in patients with newly diagnosed Ph+ chronic myeloid leukemia in chronic phase. *European journal of clinical pharmacology*. 2012;68(5):723-33.

137. Suttle AB, Ball HA, Molimard M, Hutson TE, Carpenter C, Rajagopalan D, et al. Relationships between pazopanib exposure and clinical safety and efficacy in patients with advanced renal cell carcinoma. *Br J Cancer*. 2014;111(10):1909-16.

138. Yau T, Chen PJ, Chan P, Curtis CM, Murphy PS, Suttle AB, et al. Phase I dose-finding study of pazopanib in hepatocellular carcinoma: evaluation of early efficacy, pharmacokinetics, and pharmacodynamics. *Clinical cancer research: an official journal of the American Association for Cancer Research*. 2011;17(21):6914-23.

139. Fukudo M, Ito T, Mizuno T, Shinsako K, Hatano E, Uemoto S, et al. Exposure-toxicity relationship of sorafenib in Japanese patients with renal cell carcinoma and hepatocellular carcinoma. *Clin pharmacokinet*. 2014;53(2):185-96.

140. Houk BE, Bello CL, Poland B, Rosen LS, Demetri GD, Motzer RJ. Relationship

between exposure to sunitinib and efficacy and tolerability endpoints in patients with cancer: results of a pharmacokinetic/pharmacodynamic meta-analysis. *Cancer Chemother Pharmacol*. 2010;66(2):357-71.

141. Lankheet NA, Kloth JS, Gadellaa-van Hooijdonk CG, Cirkel GA, Mathijssen RH, Lolkema MP, et al. Pharmacokinetically guided sunitinib dosing: a feasibility study in patients with advanced solid tumours. *British Journal of Cancer*. 2014;110(10):2441-9.

142. Zhang A, Fox P, Coulter S, Balakrishnar B, Liddle C, Gurney H. Effect of toxicity-adjusted dose (TAD) of sunitinib on intra-patient variation of trough levels: A longitudinal study in metastatic renal cell cancer (mRCC). *Journal of clinical oncology : official journal of the American Society of Clinical Oncology*. 2014;32(5s).

143. Mangoni A, Woodman R, Kichenadasse G, Rowland A, Sorich M. Anti-VEGF-induced hypertension and cancer outcomes: translating research into clinical practice. *Exp Rev Prec Med Drug Devel*. 2016.

144. Shah DR, Shah RR, Morganroth J. Tyrosine kinase inhibitors: their on-target toxicities as potential indicators of efficacy. *Drug Saf*. 2013;36(6):413-26.

145. Steeghs N, Gelderblom H, Roodt JO, Christensen O, Rajagopalan P, Hovens M, et al. Hypertension and rarefaction during treatment with telatinib, a small molecule angiogenesis inhibitor. *Clinical cancer research : an official journal of the American Association for Cancer Research*. 2008;14(11):3470-6.

146. Sorich M, Rowland A, Kichenadasse G, Woodman R, Mangoni A. Risk factors of proteinuria in renal cell carcinoma patients treated with VEGF inhibitors. *Br J Cancer*. 2016;114:1313-7.

147. Riesenbeck LM, Bierer S, Hoffmeister I, Kopke T, Papavassilis P, Hertle L, et al. Hypothyroidism correlates with a better prognosis in metastatic renal cancer patients treated with sorafenib or sunitinib. *World journal of urology*. 2011;29(6):807-13.

148. Daimon M, Kato T, Kaino W, Takase K, Karasawa S, Wada K, et al. Thyroid dysfunction in patients treated with tyrosine kinase inhibitors, sunitinib, sorafenib and axitinib, for metastatic renal cell carcinoma. *Jpn J Clin Oncol*. 2012;42(8):742-7.

149. Clemons J, Gao D, Naam M, Breaker K, Garfield D, Flaig TW. Thyroid dysfunction in patients treated with sunitinib or sorafenib. *Clin Genitourin Cancer*. 2012;10(4):225-31.

150. Perez-Soler R. Can rash associated with HER1/EGFR inhibition be used as a marker of treatment outcome? *Oncology (Williston Park)*. 2003;17(11 Suppl 12):23-8.

151. Perez-Soler R. Rash as a surrogate marker for efficacy of epidermal growth factor receptor inhibitors in lung cancer. *Clin Lung Cancer*. 2006;8 Suppl 1:S7-14.

152. Wacker B, Nagrani T, Weinberg J, Witt K, Clark G, Cagnoni PJ. Correlation between development of rash and efficacy in patients treated with the epidermal growth factor receptor tyrosine kinase inhibitor erlotinib in two large phase III studies. *Clinical cancer research : an official journal of the American Association for Cancer Research*. 2007;13(13):3913-21.

153. Vincenzi B, Santini D, Russo A, Addeo R, Giuliani F, Montella L, et al. Early skin toxicity as a predictive factor for tumor control in hepatocellular carcinoma patients treated with sorafenib. *Oncologist*. 2010;15(1):85-92.

154. Petrelli F, Borgonovo K, Cabiddu M, Lonati V, Barni S. Relationship between skin rash and outcome in non-small-cell lung cancer patients treated with anti-EGFR tyrosine kinase inhibitors: a literature-based meta-analysis of 24 trials. *Lung Cancer*. 2012;78(1):8-15.

155. Mita AC, Papadopoulos K, de Jonge MJ, Schwartz G, Verweij J, Mita MM, et al. Erlotinib 'dosing-to-rash': a phase II inpatient dose escalation and pharmacologic study of erlotinib in previously treated advanced non-small cell lung cancer. *Br J Cancer*. 2011;105(7):938-44.

156. Lyman GH. Impact of chemotherapy dose intensity on cancer patient outcomes. *Journal of the National Comprehensive Cancer Network : JNCCN*. 2009;7(1):99-108.

157. Calvo E, Malik SN, Siu LL, Baillargeon GM, Irish J, Chin SF, et al. Assessment of erlotinib pharmacodynamics in tumors and skin of patients with head and neck cancer. *Annals of oncology : official journal of the European Society for Medical Oncology / ESMO*. 2007;18(4):761-7.
158. Mantyh PW. Cancer pain and its impact on diagnosis, survival and quality of life. *Nature reviews Neuroscience*. 2006;7(10):797-809.
159. Santos FP, Kantarjian H, Fava C, O'Brien S, Garcia-Manero G, Ravandi F, et al. Clinical impact of dose reductions and interruptions of second-generation tyrosine kinase inhibitors in patients with chronic myeloid leukaemia. *British journal of haematology*. 2010;150(3):303-12.
160. Khosravan R, Huang X, Wiltshire R, Lechuga M, Motze R. A retrospective analysis of data from two trials of sunitinib in patients with advanced renal cell carcinoma (RCC): Pitfalls of efficacy subgroup analyses based on dose-reduction status. *Journal of clinical oncology : official journal of the American Society of Clinical Oncology*. 2012(30):suppl 5; abstr 363.
161. Bjarnason GA, Khalil B, Hudson JM, Williams R, Milot LM, Atri M, et al. Outcomes in patients with metastatic renal cell cancer treated with individualized sunitinib therapy: Correlation with dynamic microbubble ultrasound data and review of the literature. *Urologic Oncology: Seminars and Original Investigations*. 2014;32(4):480-7.
162. Najjar YG, Mittal K, Elson P, Wood L, Garcia JA, Dreicer R, et al. A 2 weeks on and 1 week off schedule of sunitinib is associated with decreased toxicity in metastatic renal cell carcinoma. *European journal of cancer (Oxford, England : 1990)*. 2014;50(6):1084-9.
163. Foulon V, Schoffski P, Wolter P. Patient adherence to oral anticancer drugs: an emerging issue in modern oncology. *Acta Clin Belg*. 2011;66(2):85-96.
164. Gandhi S, Day L, Paramsothy T, Giotis A, Ford M, Boudreau A, et al. Oral Anticancer Medication Adherence, Toxicity Reporting, and Counseling: A Study Comparing Health Care Providers and Patients. *J Oncol Prac*. 2015.
165. Saleem M, Dimeski G, Kirkpatrick CM, Taylor PJ, Martin JH. Target concentration intervention in oncology: where are we at? *Therapeutic drug monitoring*. 2012;34(3):257-65.
166. Sorich MJ, Wiese MD, Rowland A, Kichenadasse G, McKinnon RA, Karapetis CS. Extended RAS mutations and anti-EGFR monoclonal antibody survival benefit in metastatic colorectal cancer. *Ann Oncol*. 2015;26(1):13-21.
167. Rowland A, Dias MM, Wiese MD, Kichenadasse G, McKinnon RA, Karapetis CS, et al. Meta-analysis of BRAF mutation as a predictive biomarker of benefit from anti-EGFR monoclonal antibody therapy for RAS wild-type metastatic colorectal cancer. *Br J Cancer*. 2015;112(12):1888-94.
168. Rowland A, Dias MM, Wiese MD, Kichenadasse G, McKinnon RA, Karapetis CS, et al. Meta-analysis comparing the efficacy of anti-EGFR monoclonal antibody therapy between KRAS G13D and other KRAS mutant metastatic colorectal cancer tumours. *European journal of cancer (Oxford, England : 1990)*. 2016;55:122-30.
169. Elens L, van Gelder T, Hesselink DA, Haufroid V, van Schaik RH. CYP3A4\*22: promising newly identified CYP3A4 variant allele for personalizing pharmacotherapy. *Pharmacogenomics*. 2013;14(1):47-62.
170. Wang D, Sadee W. The Making of a CYP3A Biomarker Panel for Guiding Drug Therapy. *J Personal Med*. 2012;2(4):175-91.
171. Kloth JS, Klumpen HJ, Yu H, Eechoute K, Samer CF, Kam BL, et al. Predictive value of CYP3A and ABCB1 phenotyping probes for the pharmacokinetics of sunitinib: the ClearSun study. *Clin Pharmacokinet*. 2014;53(3):261-9.
172. Snyder BD, Rowland A, Polasek TM, Miners JO, Doogue MP. Evaluation of felodipine as a potential perpetrator of pharmacokinetic drug-drug interactions. *European journal of clinical pharmacology*. 2014;70:1115-22.

173. Mårde Arrhén Y, Nylén H, Lövgren-Sandblom A, Kanebratt KP, Wide K, Diczfalusy U. A comparison of 4 $\beta$ -hydroxycholesterol:cholesterol and 6 $\beta$ -hydroxycortisol:cortisol as markers of CYP3A4 induction. *British Journal of Clinical Pharmacology*. 2013;75(6):1536-40.
174. Shen H, Dai J, Liu T, Cheng Y, Chen W, Freedden C, et al. Coproporphyrins I and III as Functional Markers of OATP1B Activity: In Vitro and In Vivo Evaluation in Preclinical Species. *The Journal of pharmacology and experimental therapeutics*. 2016.
175. Chmielecki J, Foo J, Oxnard GR, Hutchinson K, Ohashi K, Somwar R, et al. Optimization of dosing for EGFR-mutant non-small cell lung cancer with evolutionary cancer modeling. *Sci Trans Med*. 2011;3(90):90ra59.
176. Shah NT, Kris MG, Pao W, Tyson LB, Pizzo BM, Heinemann MH, et al. Practical management of patients with non-small-cell lung cancer treated with gefitinib. *J Clinical Oncol*. 2005;23(1):165-74.
177. Rowland A, Van Dyk M, Mangoni A, Miners J, McKinnon R, Wiese M, et al. Kinase inhibitor pharmacokinetics. *Exp Opin Drug Metab Toxicol*. 2017;13:31-49.
178. Scheffler M, Di Gion P, Doroshenko O, Wolf J, Fuhr U. Clinical Pharmacokinetics of Tyrosine Kinase Inhibitors. *Clin Pharmacokinet*. 2011;50(6):371-403.
179. Di Gion P, Kanefendt F, Lindauer A, Scheffler M, Doroshenko O, Fuhr U, et al. Clinical Pharmacokinetics of Tyrosine Kinase Inhibitors. *Clin Pharmacokinet*. 2011;50(9):551-603.
180. Emoto C, Murayama N, Rostami-Hodjegan A, Yamazaki H. Methodologies for investigating drug metabolism at the early drug discovery stage: prediction of hepatic drug clearance and P450 contribution. *Current drug metabolism*. 2010;11(8):678-85.
181. Rowland Yeo K, Jamei M, Yang J, Tucker GT, Rostami-Hodjegan A. Physiologically based mechanistic modelling to predict complex drug-drug interactions involving simultaneous competitive and time-dependent enzyme inhibition by parent compound and its metabolite in both liver and gut - the effect of diltiazem on the time-course of exposure to triazolam. *Eur J Pharm Sci*. 2010;39(5):298-309.
182. Rostami-Hodjegan A, Tucker GT. Simulation and prediction of in vivo drug metabolism in human populations from in vitro data. *Nat Rev Drug Discov*. 2007;6(2):140-8.
183. Bowalgaha K, Elliot DJ, Mackenzie PI, Knights KM, Swedmark S, Miners JO. S-Naproxen and desmethylnaproxen glucuronidation by human liver microsomes and recombinant human UDP-glucuronosyltransferases (UGT): role of UGT2B7 in the elimination of naproxen. *Br J Clin Pharmacol*. 2005;60(4):423-33.
184. Boase S, Miners JO. In vitro-in vivo correlations for drugs eliminated by glucuronidation: Investigations with the model substrate zidovudine. *Br J Clin Pharmacol*. 2002;54(5):493-503.
185. Lowry OH, Rosebrough NJ, Farr AL, Randall RJ. Protein measurement with the Folin phenol reagent. *J Biol Chem*. 1951;193(1):265-75.
186. Rowland A, Elliot DJ, Knights KM, Mackenzie PI, Miners JO. The "albumin effect" and in vitro-in vivo extrapolation. *Drug Metab Dispos*. 2008;36(5):870-7.
187. Korprasertthaworn P, Rowland A, Lewis BC, Mackenzie PI, Yoovathaworn K, Miners JO. Effects of amino acid substitutions at positions 33 and 37 on UDP-glucuronosyltransferase 1A9 (UGT1A9) activity and substrate selectivity. *Biochemical pharmacology*. 2012;84(11):1511-21.
188. Jones HM, Houston JB. Substrate depletion approach for determining in vitro metabolic clearance: time dependencies in hepatocyte and microsomal incubations. *Drug Metab Dispos*. 2004;32(9):973-82.
189. Jamei M, Marciniak S, Feng K, Barnett A, Tucker G, Rostami-Hodjegan A. The Simcyp® Population-based ADME Simulator. *Exp Opin Drug Metab Toxicol*. 2009;5(2):211-23.

190. Dong JQ, Chen B, Gibbs MA, Emery M, Gibbs JP. Applications of Computer-Aided Pharmacokinetic and Pharmacodynamic Methods from Drug Discovery Through Registration. *Curr Comput Aided Drug Des.* 2008;4(1):54-66.
191. Howgate EM, Rowland Yeo K, Proctor NJ, Tucker GT, Rostami-Hodjegan A. Prediction of in vivo drug clearance from in vitro data. I: impact of inter-individual variability. *Xenobiotica; the fate of foreign compounds in biological systems.* 2006;36(6):473-97.
192. Polasek TM, Polak S, Doogue MP, Rostami-Hodjegan A, Miners JO. Assessment of inter-individual variability in predicted phenytoin clearance. *Eur J Clin Pharmacol.* 2009;65(12):1203-10.
193. Wattanachai N, Polasek TM, Heath TM, Uchaipichat V, Tassaneeyakul W, Tassaneeyakul W, et al. In vitro-in vivo extrapolation of CYP2C8-catalyzed paclitaxel 6 $\alpha$ -hydroxylation: effects of albumin on in vitro kinetic parameters and assessment of interindividual variability in predicted clearance. *Eur J Clin Pharmacol.* 2011;67(8):815-24.
194. Cheeti S, Budha NR, Rajan S, Dresser MJ, Jin JY. A physiologically based pharmacokinetic (PBPK) approach to evaluate pharmacokinetics in patients with cancer. *Biopharmaceutics & drug disposition.* 2013;34(3):141-54.
195. van Dyk M, Miners J, Kichenadasse G, McKinnon R, Rowland A. A novel approach for the simultaneous quantification of 18 small molecule kinase inhibitors in human plasma. *J Chromatogr B.* 2016;1033:17-26.
196. Wind S, Schnell D, Ebner T, Freiwald M, Stopfer P. Clinical Pharmacokinetics and Pharmacodynamics of Afatinib. *Clin Pharmacokinet.* 2017;56(3):235-50.
197. Hamilton M, Wolf JL, Rusk J, Beard SE, Clark GM, Witt K, et al. Effects of smoking on the pharmacokinetics of erlotinib. *Clin Cancer Res.* 2006;12(7 Pt 1):2166-71.
198. Wind S, Giessmann T, Jungnik A, Brand T, Marzin K, Bertulis J, et al. Pharmacokinetic drug interactions of afatinib with rifampicin and ritonavir. *Clinical drug investigation.* 2014;34(3):173-82.
199. Hamilton M, Wolf JL, Drolet DW, Fettner SH, Rakhit AK, Witt K, et al. The effect of rifampicin, a prototypical CYP3A4 inducer, on erlotinib pharmacokinetics in healthy subjects. *Cancer Chemo Pharmacol.* 2014;73(3):613-21.
200. Gao B, Yeap S, Clements A, Balakrishnar B, Wong M, Gurney H. Evidence for therapeutic drug monitoring of targeted anticancer therapies. *J Clin Oncol.* 2012;30(32):4017-25.
201. Klumpen HJ, Samer CF, Mathijssen RH, Schellens JH, Gurney H. Moving towards dose individualization of tyrosine kinase inhibitors. *Cancer Treat Rev.* 2011;37(4):251-60.
202. Rakhit A, Pantze MP, Fettner S, Jones HM, Charoin JE, Riek M, et al. The effects of CYP3A4 inhibition on erlotinib pharmacokinetics: computer-based simulation (SimCYP) predicts in vivo metabolic inhibition. *Eur J Clin Pharmacol.* 2008;64(1):31-41.
203. Deeken JF, Beumer JH, Anders NM, Wanjiku T, Rusnak M, Rudek MA. Preclinical assessment of the interactions between the antiretroviral drugs, ritonavir and efavirenz, and the tyrosine kinase inhibitor erlotinib. *Cancer Chemother Pharmacol.* 2015;76(4):813-9.
204. Enzi G, Gasparo M, Biondetti PR, Fiore D, Semisa M, Zurlo F. Subcutaneous and visceral fat distribution according to sex, age, and overweight, evaluated by computed tomography. *The American journal of clinical nutrition.* 1986;44(6):739-46.
205. Wilkinson GR. Drug metabolism and variability among patients in drug response. *N Engl J Med.* 2005;352(21):2211-21.
206. Perera V, Gross AS, McLachlan AJ. Influence of environmental and genetic factors on CYP1A2 activity in individuals of South Asian and European ancestry. *Clinical pharmacology and therapeutics.* 2012;92(4):511-9.
207. McGraw J, Waller D. Cytochrome P450 variations in different ethnic populations. *Expert opinion on drug metabolism & toxicology.* 2012;8(3):371-82.

208. Thorn CF, Aklillu E, Klein TE, Altman RB. PharmGKB summary: very important pharmacogene information for CYP1A2. *Pharmacogenetics and Genomics*. 2012;22(1):73-7.
209. Perera V, Gross AS, McLachlan AJ. Diurnal variation in CYP1A2 enzyme activity in South Asians and Europeans. *J Pharm Pharmacol*. 2013;65(2):264-70.
210. Zanger U, Schwab M. Cytochrome P450 enzymes in drug metabolism. *Pharmacology & therapeutics*. 2013;138(1):103-41.
211. Wilkinson GR. Cytochrome P4503A (CYP3A) metabolism: prediction of in vivo activity in humans. *Journal of pharmacokinetics and biopharmaceutics*. 1996;24(5):475-90.
212. Westlind A, Lofberg L, Tindberg N, Andersson TB, Ingelman-Sundberg M. Interindividual differences in hepatic expression of CYP3A4: relationship to genetic polymorphism in the 5'-upstream regulatory region. *Biochem Biophys Res Commun*. 1999;259(1):201-5.
213. Rowland A, van Dyk M, Warncken D, Mangoni A, Sorich M, Rowland A. Evaluation of modafinil as a perpetrator of metabolic drug-drug interactions *British journal of clinical pharmacology*. 2018;84:501-9.
214. Yamaori S, Yamazaki H, Iwano S, Kiyotani K, Matsumura K, Saito T, et al. Ethnic differences between Japanese and Caucasians in the expression levels of mRNAs for CYP3A4, CYP3A5 and CYP3A7. *Xenobiotica; the fate of foreign compounds in biological systems*. 2005;35(1):69-83.
215. He P, Court MH, Greenblatt DJ, Von Moltke LL. Genotype-phenotype associations of cytochrome P450 3A4 and 3A5 polymorphism with midazolam clearance in vivo. *Clinical pharmacology and therapeutics*. 2005;77(5):373-87.
216. Floyd MD, Gervasini G, Masica AL, Mayo G, George ALJ, Bhat K, et al. Genotype-phenotype associations for common CYP3A4 and CYP3A5 variants in the basal and induced metabolism of midazolam in European- and African-American men and women. *Pharmacogenetics and Genomics*. 2003;13(10):595-606.
217. Roach M, De Silvio M, Rebbick T, Grignon D, Rotman M, Wolkov H, et al. Racial Differences in CYP3A4 Genotype and Survival Among Men Treated on Radiation Therapy Oncology Group (RTOG) 9202: A Phase III Randomized Trial. *International Journal of Radiation Oncology\*Biography\*Physics*. 2007;69(1):79-87.
218. Lakhman SS, Ma Q, Morse GD. Pharmacogenomics of CYP3A: considerations for HIV treatment. *Pharmacogenomics*. 2009;10(8):1323-39.
219. Xie HG, Wood AJ, Kim RB, Stein CM, Wilkinson GR. Genetic variability in CYP3A5 and its possible consequences. *Pharmacogenomics*. 2004;5(3):243-72.
220. Mizutani T. PM frequencies of major CYPs in Asians and Caucasians. *Drug Metab Rev*. 2003;35(2-3):99-106.
221. Shih P-S, Huang J-D. Pharmacokinetics of Midazolam and 1'-Hydroxymidazolam in Chinese with Different CYP3A5 Genotypes. *Drug Metabolism and Disposition*. 2002;30(12):1491-6.
222. Mirghani RA, Sayi J, Aklillu E, Allqvist A, Jande M, Wennerholm A, et al. CYP3A5 genotype has significant effect on quinine 3-hydroxylation in Tanzanians, who have lower total CYP3A activity than a Swedish population. *Pharmacogenet Genomics*. 2006;16(9):637-45.
223. Ferrareso M, Turolo S, Belingheri M, Tirelli AS, Cortinovis I, Milani S, et al. Relationship between mRNA expression levels of CYP3A4, CYP3A5 and SXR in peripheral mononuclear blood cells and aging in young kidney transplant recipients under tacrolimus treatment. *Pharmacogenomics*. 2015;16(5):483-91.
224. Gashaw I, Kirchheiner J, Goldammer M, Bauer S, Seidemann J, Zoller K, et al. Cytochrome p450 3A4 ribonucleic acid induction by rifampin in peripheral blood mononuclear cells. *Clinical pharmacology and therapeutics*. 2003;74(5):448-57.
225. Haas CE, Brazeau D, Cloen D, Booker BM, Frerichs V, Zaranek C, et al. Cytochrome

- P450 mRNA expression in peripheral blood lymphocytes as a predictor of enzyme induction. *European journal of clinical pharmacology*. 2005;61(8):583-93.
226. Flexner C. HIV-Protease Inhibitors. *New England Journal of Medicine*. 1998;338(18):1281-93.
227. Jamei M, Dickinson GL, Rostami-Hodjegan A. A framework for assessing inter-individual variability in pharmacokinetics using virtual human populations and integrating general knowledge of physical chemistry, biology, anatomy, physiology and genetics: A tale of 'bottom-up' vs 'top-down' recognition of covariates. *Drug metab*. 2009;24(1):53-75.
228. van Dyk M, Rowland A. PBPK modeling as an approach to evaluate the effect of covariates and DDIs on variability in EGFR kinase inhibitor exposure. *Transl Cancer Res*. 2017;6:1600-12.
229. Zanger UM, Schwab M. Cytochrome P450 enzymes in drug metabolism: regulation of gene expression, enzyme activities, and impact of genetic variation. *Pharmacology & therapeutics*. 2013;138(1):103-41.
230. Hohmann N, Kocheise F, Carls A, Burhenne J, Haefeli WE, Mikus G. Midazolam microdose to determine systemic and pre-systemic metabolic CYP3A activity in humans. *British Journal of Clinical Pharmacology*. 2015;79(2):278-85.
231. Smith B, Pithavala Y, Zientek M, Goosen T, Marshall J. Across the continuum: DMPK experiences from preclinical to market. *Proc 2015 APSA-ASCEPT JSM*. 2015;O112.
232. Kim HY, Martin JH, Mclachlan AJ, Boddy AV. Precision dosing of targeted anticancer drugs—challenges in the real world. *Translational Cancer Research*. 2017:S1500-S11.
233. Jurica J, Sulcova A. Determination of Cytochrome P450 Metabolic Activity Using Selective Markers. In: Paxton J, editor. *Topics on Drug Metabolism*. Rijeka: InTech; 2012. p. Ch. 8.
234. M Bosilkovska CFS, J Déglon, M Rebsamen, C Staub, P Dayer, B Walder, J A Desmeules, and Y Daali. Geneva Cocktail for Cytochrome P450 and P-Glycoprotein Activity Assessment Using Dried Blood Spots. *Clinical Pharmacology & Therapeutics*. 2014;96(3):10.
235. Streetman DS, Bertino JS, Jr., Nafziger AN. Phenotyping of drug-metabolizing enzymes in adults: a review of in-vivo cytochrome P450 phenotyping probes. *Pharmacogenetics*. 2000;10(3):187-216.
236. Paine MF, Hart HL, Ludington SS, Haining RL, Rettie AE, Zeldin DC. The human intestinal cytochrome P450 "pie". *Drug metabolism and disposition: the biological fate of chemicals*. 2006;34(5):880-6.
237. Shin KH, Choi MH, Lim KS, Yu KS, Jang IJ, Cho JY. Evaluation of endogenous metabolic markers of hepatic CYP3A activity using metabolic profiling and midazolam clearance. *Clin Pharmacol Ther*. 2013;94(5):601-9.
238. Fuhr U, Jetter A, Kirchheiner J. Appropriate phenotyping procedures for drug metabolizing enzymes and transporters in humans and their simultaneous use in the "cocktail" approach. *Clinical pharmacology and therapeutics*. 2007;81(2):270-83.
239. Galteau MM, Shamsa F. Urinary 6beta-hydroxycortisol: a validated test for evaluating drug induction or drug inhibition mediated through CYP3A in humans and in animals. *European journal of clinical pharmacology*. 2003;59(10):713-33.
240. Chen Y-C, Gotzkowsky SK, Nafziger AN, Kulawy RW, Rocci ML, Bertino JS, et al. Poor correlation between 6 $\beta$ -hydroxycortisol:cortisol molar ratios and midazolam clearance as measure of hepatic CYP3A activity. *British journal of clinical pharmacology*. 2006;62(2):187-95.
241. Diczfalusy U, Kanebratt KP, Bredberg E, Andersson TB, Böttiger Y, Bertilsson L. 4 $\beta$ -Hydroxycholesterol as an endogenous marker for CYP3A4/5 activity. Stability and half-life of elimination after induction with rifampicin. *British journal of clinical pharmacology*. 2009;67(1):38-43.

242. Miners JO, Birkett DJ. The use of caffeine as a metabolic probe for human drug metabolizing enzymes. *Gen Pharmacol Vasc S.* 1996;27(2):245-9.
243. Tassaneeyakul W, Birkett DJ, McManus ME, Tassaneeyakul W, Veronese ME, Andersson T, et al. Caffeine metabolism by human hepatic cytochromes P450: contributions of 1A2, 2E1 and 3A isoforms. *Biochem Pharmacol.* 1994;47(10):1767-76.
244. Kinirons MT, O'Shea D, Downing TE, Fitzwilliam AT, Joellenbeck L, Groopman JD, et al. Absence of correlations among three putative in vivo probes of human cytochrome P4503A activity in young healthy men. *Clinical pharmacology and therapeutics.* 1993;54(6):621-9.
245. Diczfalusy U, Nylen H, Elander P, Bertilsson L. 4beta-Hydroxycholesterol, an endogenous marker of CYP3A4/5 activity in humans. *British journal of clinical pharmacology.* 2011;71(2):183-9.
246. Bjorkhem-Bergman L, Backstrom T, Nylen H, Ronquist-Nii Y, Bredberg E, Andersson TB, et al. Comparison of endogenous 4beta-hydroxycholesterol with midazolam as markers for CYP3A4 induction by rifampicin. *Drug metabolism and disposition: the biological fate of chemicals.* 2013;41(8):1488-93.
247. Ged C, Rouillon JM, Pichard L, Combalbert J, Bressot N, Bories P, et al. The increase in urinary excretion of 6 beta-hydroxycortisol as a marker of human hepatic cytochrome P450III<sub>A</sub> induction. *British journal of clinical pharmacology.* 1989;28(4):373-87.
248. Tassaneeyakul W, Birkett DJ, McManus ME, Tassaneeyakul W, Veronese ME, Andersson T, et al. Caffeine metabolism by human hepatic cytochromes p450: Contributions of 1A2, 2E1 and 3A isoforms. *Biochemical Pharmacology.* 1994;47(10):1767-76.
249. Shao J, Markowitz JS, Bei D, An G. Enzyme- and Transporter-Mediated Drug Interactions with Small Molecule Tyrosine Kinase Inhibitors. *J Pharm Sci.* 2014;103(12):3810-33.
250. Klumpen HJ, Samer CF, Mathijssen RHJ, Schellens JHM, Gurney H. Moving towards dose individualization of tyrosine kinase inhibitors. *Cancer Treat Rev.* 2011;37(4):251-60.
251. Haouala A, Zanolari B, Rochat B, Montemurro M, Zaman K, Duchosal MA, et al. Therapeutic Drug Monitoring of the new targeted anticancer agents imatinib, nilotinib, dasatinib, sunitinib, sorafenib and lapatinib by LC tandem mass spectrometry. *Journal of chromatography B, Analytical technologies in the biomedical and life sciences.* 2009;877(22):1982-96.
252. Yu H, Steeghs N, Nijenhuis CM, Schellens JH, Beijnen JH, Huitema AD. Practical guidelines for therapeutic drug monitoring of anticancer tyrosine kinase inhibitors: focus on the pharmacokinetic targets. *Clin pharmacokinet.* 2014;53(4):305-25.
253. Chahbouni A, den Burger JC, Vos RM, Sinjewel A, Wilhelm AJ. Simultaneous quantification of erlotinib, gefitinib, and imatinib in human plasma by liquid chromatography tandem mass spectrometry. *Ther Drug Monit.* 2009;31(6):683-7.
254. De Francia S, D'Avolio A, De Martino F, Pirro E, Baietto L, Siccardi M, et al. New HPLC-MS method for the simultaneous quantification of the antileukemia drugs imatinib, dasatinib, and nilotinib in human plasma. *Journal of chromatography B, Analytical technologies in the biomedical and life sciences.* 2009;877(18-19):1721-6.
255. Honeywell R, Yazdadah K, Giovannetti E, Losekoot N, Smit EF, Walraven M, et al. Simple and selective method for the determination of various tyrosine kinase inhibitors used in the clinical setting by liquid chromatography tandem mass spectrometry. *Journal of chromatography B, Analytical technologies in the biomedical and life sciences.* 2010;878(15-16):1059-68.
256. Gotze L, Hegele A, Metzelder SK, Renz H, Nockher WA. Development and clinical application of a LC-MS/MS method for simultaneous determination of various tyrosine kinase inhibitors in human plasma. *Clinica chimica acta; international journal of clinical chemistry.*

2012;413(1-2):143-9.

257. van Erp NP, de Wit D, Guchelaar HJ, Gelderblom H, Hessing TJ, Hartigh J. A validated assay for the simultaneous quantification of six tyrosine kinase inhibitors and two active metabolites in human serum using liquid chromatography coupled with tandem mass spectrometry. *Journal of chromatography B, Analytical technologies in the biomedical and life sciences*. 2013;937:33-43.

258. Lankheet NA, Hillebrand MJ, Rosing H, Schellens JH, Beijnen JH, Huitema AD. Method development and validation for the quantification of dasatinib, erlotinib, gefitinib, imatinib, lapatinib, nilotinib, sorafenib and sunitinib in human plasma by liquid chromatography coupled with tandem mass spectrometry. *Biomedical chromatography : BMC*. 2013;27(4):466-76.

259. Couchman L, Birch M, Ireland R, Corrigan A, Wickramasinghe S, Josephs D, et al. An automated method for the measurement of a range of tyrosine kinase inhibitors in human plasma or serum using turbulent flow liquid chromatography-tandem mass spectrometry. *Anal Bioanal Chem*. 2012;403(6):1685-95.

260. Bouchet S, Chauzit E, Ducint D, Castaing N, Canal-Raffin M, Moore N, et al. Simultaneous determination of nine tyrosine kinase inhibitors by 96-well solid-phase extraction and ultra performance LC/MS-MS. *Clinica chimica acta; international journal of clinical chemistry*. 2011;412(11-12):1060-7.

261. Ismaiel OA, Halquist MS, Elmamly MY, Shalaby A, Thomas Karnes H. Monitoring phospholipids for assessment of ion enhancement and ion suppression in ESI and APCI LC/MS/MS for chlorpheniramine in human plasma and the importance of multiple source matrix effect evaluations. *J Chromatogr B*. 2008;875(2):333-43.

262. Ismaiel OA, Zhang T, Jenkins RG, Karnes HT. Investigation of endogenous blood plasma phospholipids, cholesterol and glycerides that contribute to matrix effects in bioanalysis by liquid chromatography/mass spectrometry. *J Chromatogr B*. 2010;878(31):3303-16.

263. Mano N, Nozawa M, Sato M, Mori M, Yamaguchi H, Kanda K, et al. Identification and elimination of ion suppression in the quantitative analysis of sirolimus in human blood by LC/ESI-MS/MS. *J Chromatogr B*. 2011;879(13-14):968-74.

264. Ismaiel OA, Halquist MS, Elmamly MY, Shalaby A, Karnes HT. Monitoring phospholipids for assessment of matrix effects in a liquid chromatography-tandem mass spectrometry method for hydrocodone and pseudoephedrine in human plasma. *Journal of Chromatography B*. 2007;859(1):84-93.

265. Tuck MK, Chan DW, Chia D, Godwin AK, Grizzle WE, Krueger KE, et al. Standard Operating Procedures for Serum and Plasma Collection: Early Detection Research Network Consensus Statement Standard Operating Procedure Integration Working Group. *J Proteome Res*. 2009;8(1):113-7.

266. Vaught JB. Blood Collection, Shipment, Processing, and Storage. *Cancer Epidemiol Biomarkers Prev*. 2006;15(9):1582-4.

267. Vennepureddy A, Thumallapally N, Motilal Nehru V, Atallah JP, Terjanian T. Novel Drugs and Combination Therapies for the Treatment of Metastatic Melanoma. *J Clin Med Res*. 2016;8(2):63-75.

268. Rowland A, Van Dyk M, Mangoni A, Miners J, McKinnon R, Wiese M, et al. Kinase inhibitor pharmacokinetics: Comprehensive summary and roadmap for addressing inter-individual variability in exposure *Exp Opin Drug Metab Toxicol*. 2017;13:31-49.

269. Rousset M, Dutriaux C, Bosco-Levy P, Prey S, Pham-Ledard A, Dousset L, et al. Trough dabrafenib plasma concentrations can predict occurrence of adverse events requiring dose reduction. *Clin Chim Acta*. 2017;472:26-9.

270. Rowland M, Peck C, Tucker G. Physiologically-Based Pharmacokinetics in Drug Development and Regulatory Science. *Ann Rev Pharmacol Toxicol*. 2011;51(1):45-73.

271. Rostami-Hodjegan A. Physiologically based pharmacokinetics joined with in vitro-in vivo extrapolation of ADME: a marriage under the arch of systems pharmacology. *Clin Pharmacol Ther.* 2012;92(1):50-61.
272. Zhao P, Zhang L, Grillo JA, Liu Q, Bullock JM, Moon YJ, et al. Applications of Physiologically Based Pharmacokinetic (PBPK) Modeling and Simulation During Regulatory Review. *Clinical pharmacology and therapeutics.* 2011;89(2):259-67.
273. Zhao P, Rowland M, Huang SM. Best practice in the use of physiologically based pharmacokinetic modeling and simulation to address clinical pharmacology regulatory questions. *Clin Pharmacol Ther.* 2012;92(1):17-20.
274. Darwich A, Ogungbenro K, Hatley O, Rostami-Hodjegan A. Role of pharmacokinetic modeling and simulation in precision dosing of anticancer drugs. *Transl Cancer Res.* 2017;doi: 10.21037/tcr.2017.09.14.
275. Wagner C, Zhao P, Pan Y, Hsu V, Grillo J, Huang SM, et al. Application of Physiologically Based Pharmacokinetic (PBPK) Modeling to Support Dose Selection: Report of an FDA Public Workshop on PBPK. *CPT: Pharmacomet Syst Pharmacol.* 2015;4(4):226-30.
276. Luzon E, Blake K, Cole S, Nordmark A, Versantvoort C, Berglund EG. Physiologically based pharmacokinetic modeling in regulatory decision-making at the European Medicines Agency. *Clin Pharmacol Ther.* 2016;doi: 10.1002/cpt.539.
277. Jamei M, Marciniak S, Edwards D, Wragg K, Feng K, Barnett A, et al. The Simcyp Population Based Simulator: Architecture, Implementation, and Quality Assurance. *In Silico Pharmacology.* 2013;1:9.
278. Bershas DA, Ouellet D, Mamaril-Fishman DB, Nebot N, Carson SW, Blackman SC, et al. Metabolism and Disposition of Oral Dabrafenib in Cancer Patients: Proposed Participation of Aryl Nitrogen in Carbon-Carbon Bond Cleavage via Decarboxylation following Enzymatic Oxidation. *Drug Metab Dispos.* 2013;41(12):2215-24.
279. Patel N, Wiśniowska B, Jamei M, Polak S. Real Patient and its Virtual Twin: Application of Quantitative Systems Toxicology Modelling in the Cardiac Safety Assessment of Citalopram. *The AAPS Journal.* 2017;20(1):6.
280. Polasek T, Tucker G, Sorich M, Wiese M, Mohan T, Rostami-Hodjegan A, et al. Prediction of olanzapine exposure in individual patients using PBPK modelling and simulation. *British journal of clinical pharmacology.* 2018;84:462-76.
281. Gallant JE, Koenig E, Andrade-Villanueva J, Chetchotisakd P, DeJesus E, Antunes F, et al. Cobicistat Versus Ritonavir as a Pharmacoenhancer of Atazanavir Plus Emtricitabine/Tenofovir Disoproxil Fumarate in Treatment-Naive HIV Type 1–Infected Patients: Week 48 Results. *The Journal of Infectious Diseases.* 2013;208(1):32-9.
282. Eechoute K, Fransson MN, Reyners AK, de Jong FA, Sparreboom A, van der Graaf WTA, et al. A Long-term Prospective Population Pharmacokinetic Study on Imatinib Plasma Concentrations in GIST Patients. *Clinical Cancer Research.* 2012;18(20):5780-7.

---

# APPENDICES

---

## **Appendix 1 – Appendix Table 1**

## Appendix 1: Appendix Table 1

TKI	BCT	Serum Z Gel	K3 EDTA	Lithium Heparin	Lithium Heparin Gel	Glass	Plastic
Axitinib	Serum Z Gel	1.000	0.367	1.000	0.182	0.020	0.000
	K3 EDTA		1.000	0.445	0.995	0.475	0.009
	Lithium Heparin			1.000	0.464	0.026	0.000
	Lithium Heparin Gel				1.000	0.755	0.021
	Glass					1.000	0.191
	Plastic						1.000
Dabrafenib	Serum Z Gel	1.000	0.999	0.975	0.036	0.053	0.000
	K3 EDTA		1.000	0.999	0.064	0.094	0.001
	Lithium Heparin			1.000	0.119	0.172	0.001
	Lithium Heparin Gel				1.000	1.000	0.128
	Glass					1.000	0.088
	Plastic						1.000
Dasatinib	Serum Z Gel	1.000	0.995	0.584	0.998	0.999	0.999

	K3 EDTA		1.000	0.851	0.932	0.953	0.944
	Lithium Heparin			1.000	0.359	0.398	0.380
	Lithium Heparin Gel				1.000	1.000	1.000
	Glass					1.000	1.000
	Plastic						1.000
Erlotinib	Serum Z Gel	1.000	0.006	0.117	0.048	0.511	0.388
	K3 EDTA		1.000	0.504	0.805	0.115	0.166
	Lithium Heparin			1.000	0.993	0.888	0.957
	Lithium Heparin Gel				1.000	0.611	0.743
	Glass					1.000	1.000
	Plastic						1.000
Gefitinib	Serum Z Gel	1.000	0.001	0.987	1.000	0.988	0.310
	K3 EDTA		1.000	0.003	0.001	0.000	0.000
	Lithium Heparin			1.000	0.993	0.810	0.123
	Lithium Heparin Gel				1.000	0.978	0.277
	Glass					1.000	0.631
	Plastic						1.000

Imatinib	Serum Z Gel	1.000	0.200	0.006	0.000	0.000	0.000
	K3 EDTA		1.000	0.355	0.018	0.025	0.020
	Lithium Heparin			1.000	0.464	0.563	0.498
	Lithium Heparin Gel				1.000	1.000	1.000
	Glass					1.000	1.000
	Plastic						1.000
Lapatinib	Serum Z Gel	1.000	0.657	0.274	0.003	0.002	0.000
	K3 EDTA		1.000	0.970	0.036	0.024	0.002
	Lithium Heparin			1.000	0.126	0.086	0.566
	Lithium Heparin Gel				1.000	1.000	0.566
	Glass					1.000	0.702
	Plastic						1.000
Nilotinib	Serum Z Gel	1.000	0.410	0.992	0.541	0.243	0.007
	K3 EDTA		1.000	0.719	1.000	0.999	0.183
	Lithium Heparin			1.000	0.843	0.498	0.018
	Lithium Heparin Gel				1.000	0.986	0.125
	Glass					1.000	0.319

	Plastic						1.000
Pazopanib	Serum Z Gel	1.000	0.537	0.663	0.240	0.089	0.080
	K3 EDTA		1.000	1.000	0.986	0.792	0.756
	Lithium Heparin			1.000	0.950	0.673	0.633
	Lithium Heparin Gel				1.000	0.986	0.977
	Glass					1.000	1.000
	Plastic						1.000
Regorafenib	Serum Z Gel	1.000	0.008	1.000	0.778	0.291	0.976
	K3 EDTA		1.000	0.006	0.001	0.000	0.002
	Lithium Heparin			1.000	0.896	0.376	0.994
	Lithium Heparin Gel				1.000	0.930	0.990
	Glass					1.000	0.661
	Plastic						1.000
Ruxolitinib	Serum Z Gel	1.000	0.000	0.008	0.210	0.394	0.015
	K3 EDTA		1.000	0.000	0.000	0.000	0.000
	Lithium Heparin			1.000	0.991	0.213	0.998
	Lithium Heparin Gel				1.000	0.459	1.000

	Glass					1.000	0.367
	Plastic						1.000
Sorafenib	Serum Z Gel	1.000	0.110	0.213	0.490	0.031	0.000
	K3 EDTA		1.000	0.509	0.949	0.989	0.177
	Lithium Heparin			1.000	0.935	0.834	0.009
	Lithium Heparin Gel				1.000	1.000	0.043
	Glass					1.000	0.068
	Plastic						1.000
Sunitinib	Serum Z Gel	1.000	0.443	0.949	0.105	0.151	0.283
	K3 EDTA		1.000	0.893	0.908	0.967	0.999
	Lithium Heparin			1.000	0.372	0.490	0.730
	Lithium Heparin Gel				1.000	1.000	0.984
	Glass					1.000	0.998
	Plastic						1.000
N-desethyl Sunitinib	Serum Z Gel	1.000	0.224	0.988	0.992	0.999	1.000
	K3 EDTA		1.000	0.086	0.468	0.361	0.190
	Lithium Heparin			1.000	0.842	0.923	0.995

	Lithium Heparin Gel				1.000	1.000	0.982
	Glass					1.000	0.997
	Plastic						1.000
Vemurafenib	Serum Z Gel	1.000	0.850	0.286	0.112	0.185	0.023
	K3 EDTA		1.000	0.875	0.548	0.730	0.155
	Lithium Heparin			1.000	0.987	1.000	0.632
	Lithium Heparin Gel				1.000	0.999	0.926
	Glass					1.000	0.796
	Plastic						1.000
Trametinib	Serum Z Gel	1.000	0.583	0.940	0.938	1.000	0.453
	K3 EDTA		1.000	0.970	0.971	0.712	1.000
	Lithium Heparin			1.000	1.000	0.982	0.912
	Lithium Heparin Gel				11.000	0.981	0.915
	Glass					1.000	0.578
	Plastic						1.000